Measurement of Hydrogen Gas Concentration Using Ultrasound

マハジャビン, タスキン

https://doi.org/10.15017/2534508

出版情報：Kyushu University, 2019, 博士（工学）, 課程博士
バージョン：
権利関係：

Measurement of Hydrogen Gas Concentration Using Ultrasound

A Thesis Submitted

In Partial Fulfillment of the Requirements

For the Degree of

Doctor of Engineering

By

Mahjabin Taskin

To the

DEPARTMENT OF AUTOMOTIVE SCIENCES

GRADUATE SCHOOL OF INTEGRATED FRONTIER SCIENCES

KYUSHU UNIVERSITY

FUKUOKA, JAPAN

SEPTEMBER 2019

DEDICATED TO
MY
BELOVED PARENTS

ABSTRACT

Hydrogen (H_2) gas has been attracted more attention all over the world to reduce the production of carbon dioxide from the traditional fossil fuel-based energy sources (petroleum oil, coal, and natural gasoline). Recently, H_2 gas is widely employed for fuel cells used in transportation or generating electricity and heat in factories and residential buildings. For these usages, H_2 is transported by pipeline. Since H_2 is an explosive gas, it is important to measure the H_2 gas concentration without making a hole on the pipe surface. This dissertation focuses on the measurement of the H_2 gas concentration using ultrasound from the exterior of the pipe. The concentration of the gas can be measured based on the speed of variation of the ultrasound traveling inside the pipe. Drilling a hole in the pipe to extract the gas is not required for the gas concentration measurement, which is a unique advantage of ultrasonic method.

Therefore, the first attempt was to measure the non-flowing H_2 gas concentration from the exterior of the stainless steel (SUS) pipe. Since the noise signal was circling inside the SUS pipe itself, the main challenge of this measurement was observing the airborne signal from the exterior of the SUS pipe. Noise signal was reduced by pasting sound absorbing material (SAM) on the SUS pipe surface and the airborne signal was observed from the exterior of the SUS pipe. As a result, the concentration of H_2 gas was successfully measured. The propagation of ultrasound wave in the SUS pipe was simulated by the finite-difference-time-domain (FDTD) method that could explain the ultrasound propagation signals in the SUS pipe. The reduction of noise signal using two transmitters was simulated by FDTD method.

Next attempt was to measure the flowing H_2 gas concentration from the exterior of the pipe, which was more challenging than the measurement of non-flowing gas concentration. The concentration of H_2 gas was able to be measured accurately up to 39 m/s. Due to the fluctuation of waveform, the maximum error in the H_2 gas concentration at 39 m/s flow was calculated about 0.32%. The response time of measuring the gas concentration was fast as less than 0.1 s. Since longitudinal and transverse waves can propagate through the solid, the limit speeds of flow were calculated as 30 m/s and 60 m/s for longitudinal and transverse wave, respectively.

Finally, the ultrasonic signal propagation in two-layer gas flow was studied. In the above experiment, the intensity degradation of signal was observed while the signal was propagating through the non-uniform H_2 and air mixed gas flowing system. An experiment was conducted using different concentrations of H_2 gas and it was proved that the intensity loss did not depend simply on the concentration of H_2 gas. To investigate the reason of intensity loss, Schlieren photography was taken to visualize the H_2 gas motion after the injection into the flowing air of 2 m/s. It was observed that high concentration H_2 gas was flowing in the middle of the airflow without quick diffusion in to the air. A 2D air-H_2-air gas flow model was considered where 100% H_2 was flowing in the middle of the airflow, and the gas layers were separated by two fluctuated interfaces. According to the calculation using this model, only limited conditions of the signals can reach to the receiver due to the refraction at the fluctuating air-H_2-air gas interfaces while propagating. It was found that the receiver could hardly detect the signals; hence, the intensity of the signal looked degraded due to the refraction on the interfaces while propagation through more than two-layer gas system.

In conclusion, the findings of this study showed that the ultrasonic gas sensor could be effectively applied for the measurement of H_2 gas concentration in a pipeline from exterior of a pipe.

TABLE OF CONTENTS

LIST OF FIGURES

LIST OF TABLES

LIST OF NOTATIONS

γ	**Specific heat ratio**
R	**Gas constant**
M	**Molar mass**
T	**Absolute temperature**
ρ	**Volume concentration of gas**
γ_{mix}	**Specific heat ratio of the mixed gas**
M_{mix}	**Molecular mass of mixed gas.**
v	**Speed of sound**
n	**Number of moles of gas**
v_a	**Speed of airflow**
v_{mix}	**Speed of sound in mixed gas**
t	**Ultrasound traveling time**
t_{mix}	**Ultrasound traveling time in mixed gas**
Δt	**Difference of sound traveling time**
Z	**Acoustic impedance**
D	**Density of the medium**
P	**Pressure amplitude**
p	**Sound pressure**
T_A	**Transmission coefficient**
R_A	**Reflection coefficient**
T_p	**Transmittance**
R_p	**Reflectance**
u_x, u_y, u_z	**Particle velocity**
V	**Volume of the particle**
K_e	**Volume modulus of elasticity**
T_s	**Stress tensor**
$[C]$	**Stiffness tensor**
$[U]$	**Velocity of the particle**
Δh	**Spatial discrete width**

ΔT_F	**Discrete time interval**
a	**Time step**
β	**Divergence angle**
f	**Frequency of the transmitter**
v_{avg}	**Average speed of flow**
v_{max}	**Maximum speed of flow**
v	**Kinematic viscosity**
μ	**Dynamic viscosity**
Re	**Reynolds number**
A	**Amplitude of sound wave**
I	**Intensity of sound wave**
α	**Absorption coefficient**
α_{vis}	**Absorption coefficient due to viscosity**
α_{hc}	**Absorption due to heat conductivity**
$\alpha_{classical}$	**Classical absorption coefficient**
η	**Viscosity**
C_p	**Specific heat at constant pressure**
χ	**Coefficient of heat conductivity**
l_o	**Inner diameter**
d_o	**Thickness of the PVC pipe**
l	**Propagation length of the ultrasonic wave in airborne of the pipe**
d	**Propagation length inside of the PVC pipe**
v_a	**Air flow velocity in the pipe**
v	**Speed of sound in the air**
θ_1	**Angle between the axis along a pipe diameter and the ultrasound propagation direction flowing downstream**
θ_2	**Refracted angle from air to PVC pipe**
θ_3	**Refracted angle from PVC to the transducer**
Z_a,	**Acoustic impedances of air**
Z_p	**Acoustic impedances of PVC**
Z_t	**acoustic impedances of transducer ceramic**

α_p	**Attenuation coefficients of the PVC**
α_a	**Attenuation coefficients of the air**
d_a	**Average thicknesses of the air layer**
l_H	**Average thicknesses of H_2 gas layer**
L_o	**Distance between position of transducer and H_2 injection hole**
x_1	**Distance between first and second refraction points**
x_2	**Distance between the second and third refraction points**
x_t	**Distance between the center of receiver and the signal arrival position**
δ	**Angle between the first refracted wave and *y*-axis.**
ξ	**Angle between the second refracted wave and *y*-axis at second refraction point**
ϕ_1	**Incident angle towards the fluctuated interface from air**
ϕ_2	**Refracted angle at H_2**
ϕ_3	**Incident angle towards the fluctuated interface from H_2**
ϕ_4	**Refracted angle at air**

LIST OF ABBREVIATIONS

SUS	**S**tainless **S**teel
SAM	**S**ound **A**bsorption **M**aterial
AS	**A**irborne **S**ignal
NS	**N**oise **S**ignal
FDTD	**F**inite-**D**ifference-**T**ime-**D**omain
PVC	**P**oly**v**inyl **C**hloride

CHAPTER 1

GENERAL INTRODUCTION

1.1. INTRODUCTION

Since the beginning of the industrial revolution in the 18th century, the energy carrier that has been used to accommodate our extensive daily activities is based mainly on fossil fuels, such as coal, petroleum and natural gas. To shape our human civilization, the exploitation of fossil fuel to produce energy becomes an important factor. The rapid progress in the industrial and scientific revolution has brought about a drastic advancement in many aspects from transportation, communication even to medical technology. However, there are significant drawbacks to using fossil fuels for primary energy. Fossil fuels are limited in supply [1]. If we run out of fossil fuels without a backup plan, our energy demands will be unmet. Furthermore, fossil fuel use is also unsustainable for our health and the safety of the environment. Since the combustion of fossil fuel emits large volumes of carbon dioxide (CO_2), which accounted as one of the greenhouse gases [2]. Human fossil fuel use also affects the energy balance on earth, which could force the global climate to change [3].

Increasing concern and interest about finding an alternative energy carrier is also stemmed from the strong demand for fuel to support this ever-increasing energy consumption [4]. Replacement of fossil fuel with a sustainable alternative is important to reduce and manage the emission of greenhouse gases, which keep on rising. Of all the existing alternative energy sources and carrier, hydrogen (H_2) has been praised and proposed as one of the most sustainable energy carriers. H_2 can be produced from the abundant source such as water [5]. H_2 has favorable characteristics because combustion of H_2 does not emit CO_2 because it contains no carbon. It only produces water (H_2O) which can be decomposed again into H_2 and oxygen (O_2) [6]. More importantly, as a gas, H_2 has a relatively higher (specific) energy content, when compared with other fuels **(Table 1.1)** [7], which makes H_2 becoming more attractive than other energy sources. Moreover, the renewable energy sources such as wind or solar, cannot produce energy all the time made H_2 advantageous over these alternative energy sources since H_2 production does not rely

heavily on nature course. Although H_2 gas is currently used primarily for manufacturing chemicals [8], a bright future is predicted for it, as an alternative energy carrier to replace the dominant fossil fuel for transportation fuel. Fuel cells are being designed and implemented to run on hydrogen fuel. This application was already established in aerospace as hydrogen has been used in fuel cells since the 1950s for space applications [9]. By the year 2050, an ideal H_2 economy is planning to be fully implemented [10]; thus, H_2 will be used to fuel transportation or to generate electricity and heat for industrial and residential use. Since gaseous H_2 has a low energy content by volume (**Table 1.1**), H_2 is compressed and stored at high pressure.

Table 1.1 Comparison of energy per unit volume of several fuels [7].

Fuel type	Energy (specific) per unit mass (J/kg)	Energy density per unit volume (MJ/L)
H_2 liquid	141.90	10.044
H_2 gaseous	141.90	0.01188
Natural gas	50.00	0.0364
LNG	50.00	22.2
LPG	48.80	25.3
Gasoline	47.40	34.2
Jet fuel	46.50	35.00
Fuel oil	45.50	34.00
Biodiesel	37.00	33.00
Charcoal	30.00	34.00
Ethanol	29.90	24.00
Methanol	22.30	15.6

The expanding use of gaseous H_2 as an energy source means that H_2 storage and handling will have growing importance. Safety issues arise with any handling and storage applications for a flammable gas like H_2. The use of a combustible energy carrier first requires an understanding of its ignition, combustion, and potential detonation behavior [11]. H_2 has a larger window (4–75% v/v H_2) of flammability in comparison to natural gas, gasoline, propane, ethane, methane, propylene, etc. However, H_2 has low ignition energy (0.02 mJ), and the leakage of H_2 of about 4

vol. % (lower explosive limit/LEL) in the air could easily create a conflagration [12]. H_2 explosion incidents, such as the space-shuttle Challenger back in 1986 [13] or at Fukushima power plant in 2011 [14] is enough to create reservations regarding the safety aspect of H_2 handling. Therefore, gaining and ensuring public trust regarding the safety aspect of H_2 utilization is one of the most significant obstacles in the transition from fossil fuel-based to H_2 economy.

As a colorless, odorless and tasteless flammable gas, H_2 cannot be detected by human senses [15]. It is required to detect the presence and quantifying the concentration of H_2 gas. Measurement of rapid and accurate concentration of H_2 gas is essential to alert to the formation of potentially explosive mixtures with air and to help prevent the risk of an explosion. Besides the ability to detect H_2 rapidly, the sensor needs to be a fast response and to have features such as low maintenance cost and simple operation.

1.2. Conventional Approaches to H_2 Gas Sensing

Various mechanisms for H_2 gas sensing and detection have been studied so far. Some conventional sensing mechanisms that are still widely used in the industry including catalytic sensors, solid-state sensors, electrochemical sensors, gas chromatography, and metal oxide sensors are popular technologies. This part will introduce conventional H_2 gas sensors.

1.2.1. Catalytic Sensors

Jonson discovered the first gas sensor in 1923 [16], [17] and was used for detection of methane in mines. So far, Pellistor-type catalytic hydrogen sensors are a well-developed technology and a recent market survey of commercially available hydrogen sensors [18]. This type of hydrogen sensor is widely available and typically used for hydrogen concentrations up to 4.0%. The working principle of catalytic sensors is based on the oxidation of flammable gas. They work by burning the target gas and generating a specific combustion enthalpy, thus enabling the detection of low concentration analyses in a short response time [19], [20]. This principle can be applied to detect any combustible gas including hydrogen. A catalytic palletised resistor (or “Pellistor”) consists of

a very fine coil of platinum wire, embedded within a ceramic pellet as shown in Fig. 1.1. The surface of the pellet is activated with a suitable catalyst, which is usually a noble metal such as platinum or palladium. When the surface becomes hot, it acts as a catalyst to promote exothermic oxidation of flammable gases. In operation, the catalyst layer is heated by passing a current throughout the underlying coil. In the presence of flammable gas, the hot catalyst allows oxidation to occur in a similar chemical reaction to combustion. Just as in combustion, the reaction releases heat, which causes the temperature of the catalyst together with its underlying pellet and coil to rise. This rise in temperature results in a change in the electrical resistance, which constitutes the signal from the sensor. The catalytic gas sensor is a robust and stable gas sensor. It has a long lifetime, wide operating temperature range. The operation of these sensors is simple. It can measure the flammability of gases. It is a low-cost technology.

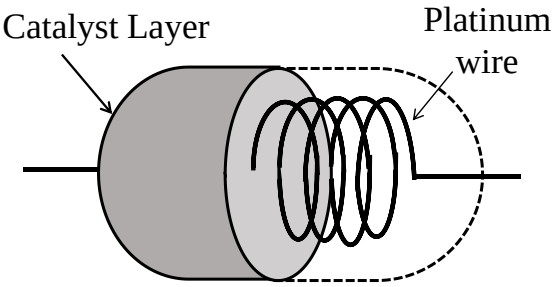

Fig. 1.1. Schematic diagram of the catalytic gas sensor [21].

However, the catalytic sensor has some drawbacks that it is not hydrogen-selective. Catalytic sensor can detect combustible gases such as methane and cannot differentiate between hydrogen and methane. If the sensor is exposed in extreme conditions such as very high humidity, high temperatures for a long period of time, sensor performance may be damaged. It consumes high power at least 5–10% O_2 to operate. This sensor can be poisoned by lead, chlorine, and silicones.

1.2.2. SOLID-STATE SENSORS

Solid-state sensors are the broad category of sensors comprising the bulk of hydrogen sensing technologies available. Solid-state semiconductors with a hydrogen sensitive layer are the most common of the chemisorbing hydrogen sensors. The basic principle on which this hydrogen

sensors function is that hydrogen concentration in a sample gas volume can be detected by monitoring the change in the physical properties of a chemisorbing film layer (Fig. 1.2). These sensors exhibit a change in electrical conductivity proportional to the amount of hydrogen adsorbed onto the surface layer at equilibrium [22]. Thin-film palladium has been the leading material investigated for sensing hydrogen due to its unique material response to hydrogen. The solid-state gas sensor is robust and able to detect a broad range of gases. It has a wide operating temperature range and a long operating life. This sensor is resistant to corrosive environments and low humidity.

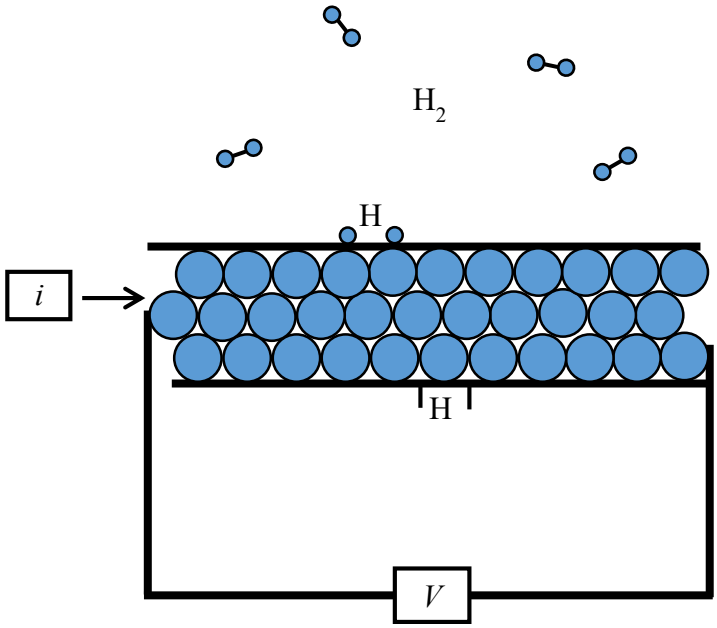

Fig. 1.2. Schematic diagram of palladium-based solid-state hydrogen sensor [23].

The main disadvantage of the solid-state gas sensor is the sensor is not commonly selective. It consumes high power.

1.2.3. ELECTROCHEMICAL SENSORS

In the 1970s, LaConti and Maget suggested the first electrochemical cell used in hydrogen detection [24]. Recently Korotcenkov et al. [25] have reviewed electrochemical hydrogen sensing. Electrochemical sensors represent the most commercially successful sensor type due to the simplicity of their operation, high sensitivity, and proven sensor mechanisms [26]. These sensors

work around the basic principle of oxidation and reduction which results in a flow of current. That current is measured by the internal circuitry of the sensor to decide the concentration. Hydrogen is detected using a specific electrochemical reaction between the anode and the cathode. The resulting signal is either a current or a voltage change in the external electrical circuit. Figure 1.3 shows the schematic diagram of an electrochemical gas sensor. The electrochemical gas sensor measures toxic gases in relatively low concentrations. It can detect a wide range of gases.

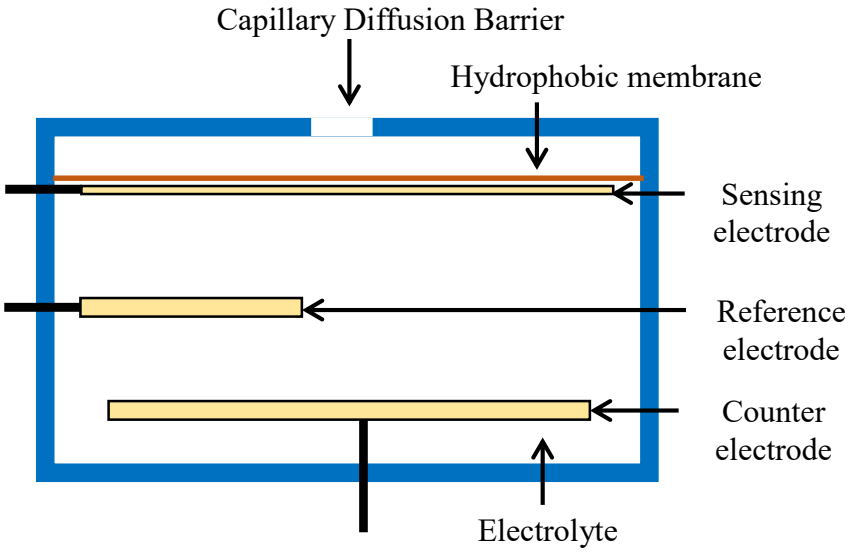

Fig. 1.3. Schematic diagram of an electrochemical gas sensor [27].

However, failures modes are unrevealed unless advanced monitoring technique used. This sensor requires air or oxygen to work.

1.2.4. GAS CHROMATOGRAPHY

Gas chromatography (GC) is also a common applied measuring principle for hydrogen detection. It is a typical laboratory analytical technique [28]. The principle of GC is the sample solution injected into the instrument enters a gas stream. It transports the sample into a separation tube known as the "column." The various components are separated inside the column. The detector measures the quantity of the components that exit the column (Fig. 1.4). A standard sample with known concentration is injected into the instrument. The unknown concentration is measured by comparing with the standard sample. The standard sample peak retention time

(appearance time) and area are compared to the test sample to calculate the concentration. It can measure other gases such as nitrogen, oxygen, and carbon dioxide in the presence of hydrogen. The separation performance of gas chromatography is excellent. It is highly sensitive and selective.

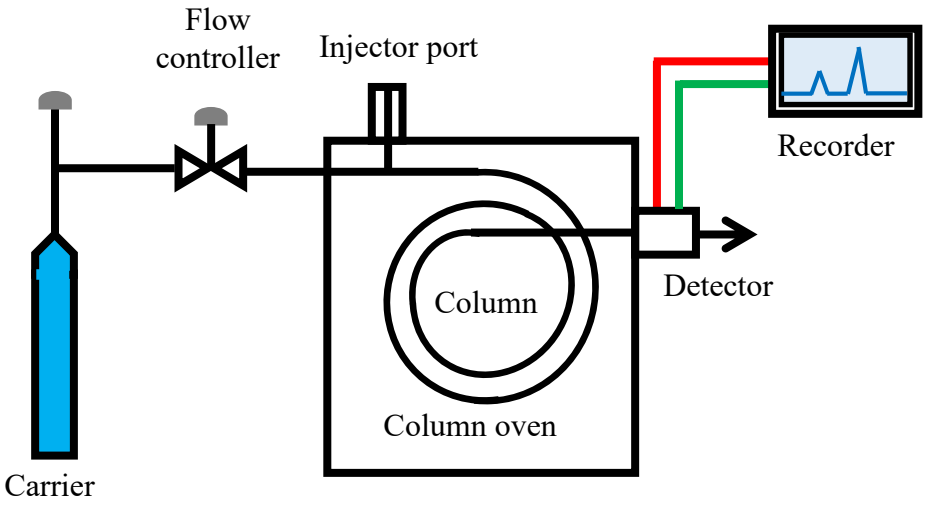

Fig. 1.4. Schematic diagram of gas chromatography [29].

However, gas chromatography is difficult in miniaturization for portable applications. Low sensitivity, long response times (minutes) due to the chromatography, time-intensive sample preparation, consumable (carrier and calibration gases), and labor-intensive handling procedures are the drawbacks of gas chromatography.

1.2.5. METAL OXIDE SENSORS

Metal oxide sensors are known as semiconductor-based sensors since they use a semiconducting film as the sensing element [30]. Since the 1950s, the electrical properties of metal oxides change when they are exposed to reducing gases [31]. In 1962 Seiyama was the first to apply this phenomenon to the detection of gases using a ZnO thin film [32]. In the same year, Taguchi [33] patented and subsequently marketed a SnO_2 based semiconductor device capable of detecting low concentrations of combustible and reducing gases using a simple electrical circuit. The most widely researched metal oxide used for sensing applications is a tin oxide (SnO_2). The principle of measuring the concentration of toxic gas in air is measured by the change in resistance inside the sensor. The reaction between the toxic gas and oxygen on the film surface varies,

depending on the reactivity of material and surrounding temperature. When gas enters into the sensor, it reacts with the film, which in turn triggers the device if the detected concentration is above a threshold value. Figure 1.5 shows the schematic diagram of a metal oxide based gas sensor. Metal oxide based gas sensor is a low-cost sensor. It has a short response time, a wide range of target gases, long lifetime, high sensitivity, short response time.

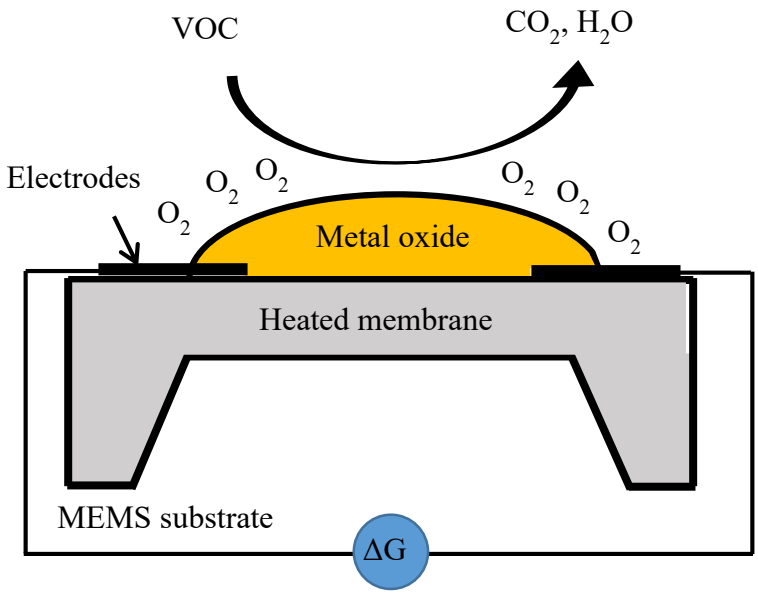

Fig. 1.5. Schematic diagram of metal oxide based gas sensor [34].

However, this sensor has relatively low sensitivity and selectivity. It is sensitive to environmental factors, and consume high-energy.

1.2.6. SURFACE ACOUSTIC SENSOR

A surface acoustic wave sensor (SAW) is an acoustic wave propagates along the surface of an elastic body and has an interesting feature that the energy of the wave is almost entirely contained in a thin layer within several wavelengths from the surface of a solid material. Because of this property, the propagation of a SAW is sensitive to the surface state and is easily influenced by the temperature change and mechanical change of the surface. Using this, a gas-sensitive film is formed on the SAW propagation path, and the gas concentration can be detected by using the change of the SAW due to H_2 adsorption, etc. as a signal [35], [36]. Figure 1.6 shows the basic

structure of the SAW-based H_2 gas sensor. By using the SAW element as a gas sensor, it was also developed as a sensor with much higher detection capability than the Pd resistance change sensor based on the principle of H_2 storage on metal. The first reported device measured H_2 gas using Pd thin film as a sensitive film and detected H_2 concentration from 100 ppm to several%. In this element, a comb-shaped electrode was formed on a substrate of $LiNbO_3$, a high-frequency surface wave was generated on the surface of the substrate from this electrode, and a change in phase difference measured from the opposite electrode was used as a gas concentration signal. Yamanaka et al. [37] describe a ball-shaped SAW sensor for H_2 in which the acoustic waves propagate multiple times around the same circular path, thereby amplifying the effect and increasing the sensitivity of the device. They report a short response time of <2 s and a measuring range of 10 ppm to 100%. SAW sensor is well known because of detecting nerve and blister agents. Since it is battery-less, it could be used for wireless applications. SAW sensor could be placed in harsh and rotating parts. However, due to its small size, it is difficult to handle during the fabrication process.

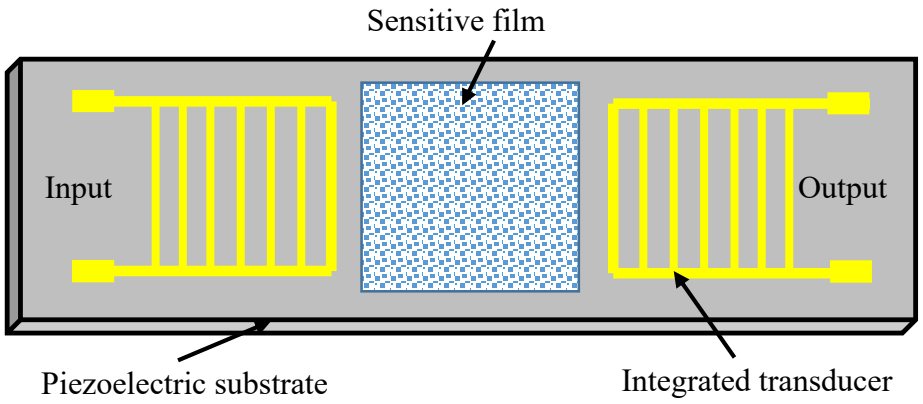

Fig. 1.6. Schematic diagram of a SAW sensor [38].

1.2.7. ULTRASONIC SENSORS

The ultrasonic sensor measures the concentration of H_2 gas based on the speed of sound variation in H_2 and other gases, particularly air. The central element of an ultrasonic gas sensor is the ultrasonic generator, the source that provides the electrical energy to the system's ultrasonic transducers. The job of ultrasonic generator is to receive and convert energy from the power source to the proper frequency, voltage, and amperage. The sensors supplied often take the form of a pair of eyes because there are two key parts. The transmitter emits a sound at a defined frequency, and

the receiver receives the signal after propagation through the gas. Piezoelectric and magnetostrictive are the two most commonly used transducers [39]. Figure 1.7 illustrates two gas chambers, which are precisely alike, respectively measuring ultrasonic propagation parameters (e.g., sound traveling time difference, Δt) in the H_2 gas and the mixture of H_2 and air. The gas concentration is determined by sound traveling time difference method [40], [41].

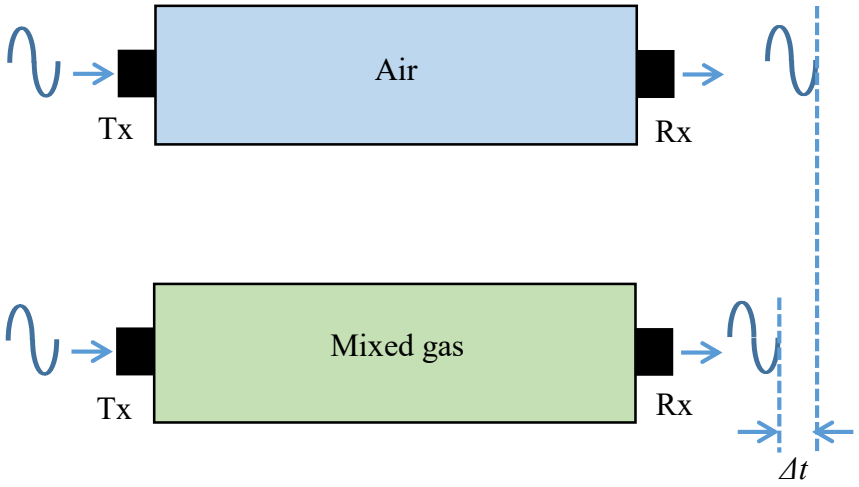

Fig. 1.7. Ultrasonic detection method [42].

1.3. Basic And Properties of Ultrasound

1.3.1. Ultrasound

The sound is a mechanical, elastic wave spreading through a physical medium in the form of longitudinal or compressional waves. The fundamental difference between sound and ultrasound is the wave frequency. Generally, sound waves are divided into three categories that depend on frequency ranges. (i) Audible waves lie within the range of sensitivity of the human ear (20 Hz – 20 kHz); (ii) Infrasonic waves are waves having frequencies below the audible range (<20 Hz), (iii) Ultrasonic waves are waves having frequencies above the audible range (>20 kHz) and less than microwave frequencies (up to 10 MHz) [43]. Figure 1.8 shows three categories of ultrasound depends on different frequency ranges. (i) power ultrasound (20 – 100 kHz); (ii) high frequency or extended range ultrasound (20 kHz – 2 MHz) and (iii) diagnostic ultrasound (>1 MHz). High-frequency ultrasound employs to measure gas concentration.

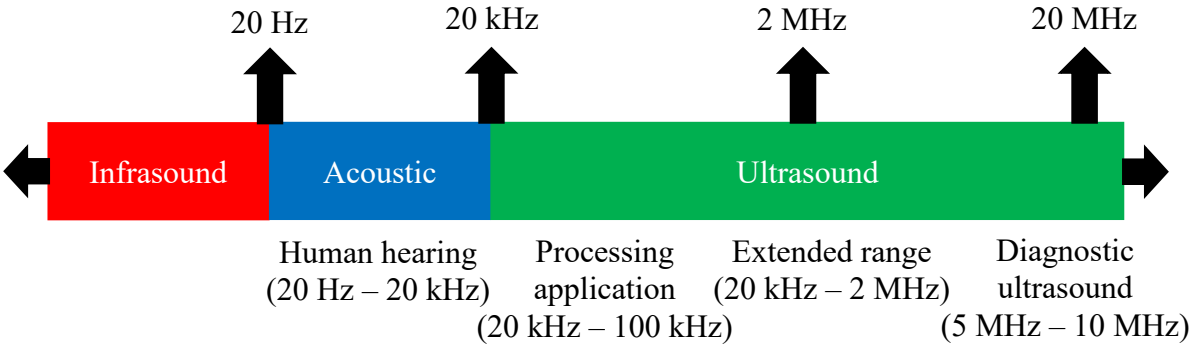

Fig. 1.8. Frequency range of sound.

1.3.2. ULTRASONIC WAVE PROPAGATION

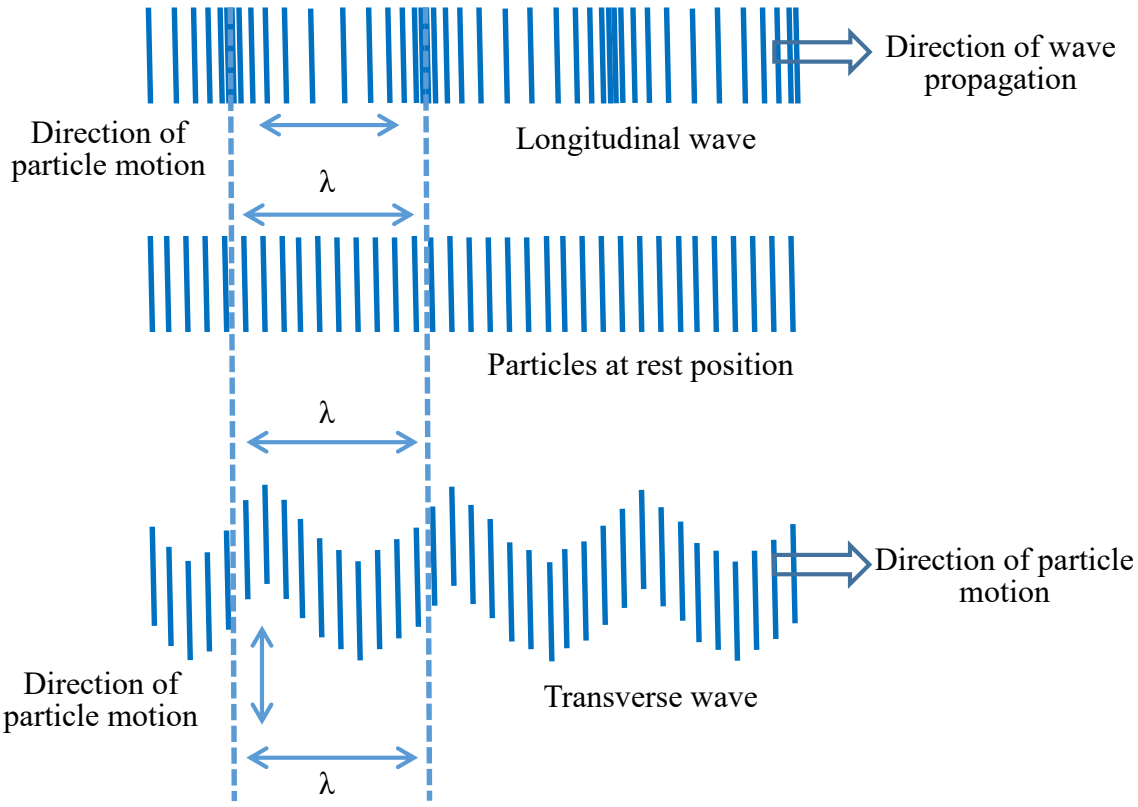

Fig. 1.9. Transverse and longitudinal wave.

In solids, two kinds of the wave can propagate with different velocities [44]. Ultrasonic wave can propagate in two principle modes that are based on the way the particles oscillate. Ultrasonic can propagate as longitudinal wave and transverse wave. In liquid and gas medium, an ultrasonic wave propagates as a longitudinal wave, in common with all sound waves [45]. Figure 1.9 shows the longitudinal and transverse wave oscillations.

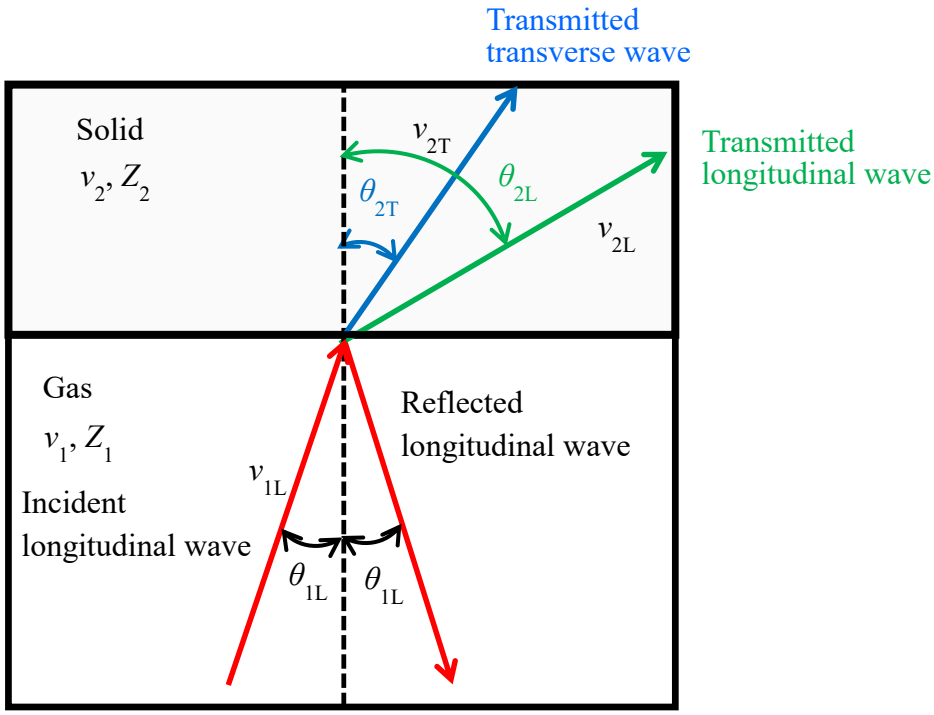

Fig. 1.10. Ultrasonic signal propagation at gas-solid interface.

When a longitudinal wave hits a gas-solid interface at θ_{1L}, both the longitudinal and transverse wave transmitted in the solid, as transverse wave can propagate in a solid material, as shown in the Fig. 1.10. As shown in Figure 1.10, Z_1 and Z_2 represent the acoustic impedance of gas and solid, respectively. Acoustic impedance is defined as the product of density of the medium and the speed of sound in that medium. The transverse wave does not refracted as much as the longitudinal wave. This occurs because transverse wave travel slower than longitudinal wave. The refracted transverse wave is refracted at a smaller angle than that of longitudinal wave. This is also due to the fact that the transverse wave velocity is less than the longitudinal wave velocity within a given material. Snell's Law holds true for transverse wave as well as longitudinal wave and can be written as follows:

$$\frac{\sin\theta_{1L}}{v_{1L}} = \frac{\sin\theta_{2L}}{v_{2L}} = \frac{\sin\theta_{2T}}{v_{2T}} \quad (1.1)$$

where, v_{1L} is the longitudinal wave velocity in gas medium, v_{2L} is the longitudinal wave velocity in solid medium, v_{2T} is the transverse wave velocity in solid medium. θ_{1L} is the incident angle of longitudinal wave at gas-solid interface. In solid, θ_{2L} and θ_{2T} are the refracted angles of longitudinal and transverse wave, respectively.

The values of the velocity of ultrasonic wave propagation, and other relevant physical constants of solids which important for ultrasonic technology, are given in **Table 1.2**. Constants of some gases at a temperature of 20°C are given in **Table 1.3**.

Table 1.2 Constants of some solid media at a temperature of 20°C [44].

Medium	**Density.10^3 (kg/m^3)**	**Speed of sound (m/s)**	
		Longitudinal	**Transverse**
Metals			
Tin	7.30	3320	1670
Aluminum	2.70	6320	3080
Magnesium	1.73	5780	3050
Cast iron	7.20	3500-5600	2200-3200
Brass	8.10	3830	2123
Nickel	8.80	3830	2960
Steel	7.80	5900-6000	3200
Non-metals			
Ice	1	3980	1990
Organic glass	1.18	2670	1121
Polystyrene	1.06	2350	1120
Quartz glass	2.60	5570	3515

Table 1.3 Speed of sound and temperature coefficient of the gases and vapors [46].

Gases and vapors	Speed of sound (m/s) at 20°C	Temperature coefficient (m/(s.°C))
Hydrogen	1310	2.2
Dry air	344	0.607
Nitrogen	349	0.85
Oxygen	327	0.57
Methane	442	0.62
Helium	1007	1.35

1.3.4. AMPLITUDE AND INTENSITY

The amplitude of the ultrasonic wave is the maximum increase (or decrease) in the pressure relative to ambient conditions in the absence of sound wave. Amplitude is used to discuss reflection, attenuation, and scattering. For example, sound waves in air are oscillations in atmospheric pressure and their amplitudes are proportional to the change in pressure during one oscillation. If a variable undergoes regular oscillations, and a graph of the system is drawn with the oscillating variable as the vertical axis and time as the horizontal axis, the amplitude is visually represented by the vertical distance between the extreme of the curve and the equilibrium value as shown in Fig. 1.11.

Intensity of sound, I is proportional to the square of the amplitude, A as given in eq. (1.1):

$$I \propto A^2 \tag{4.1}$$

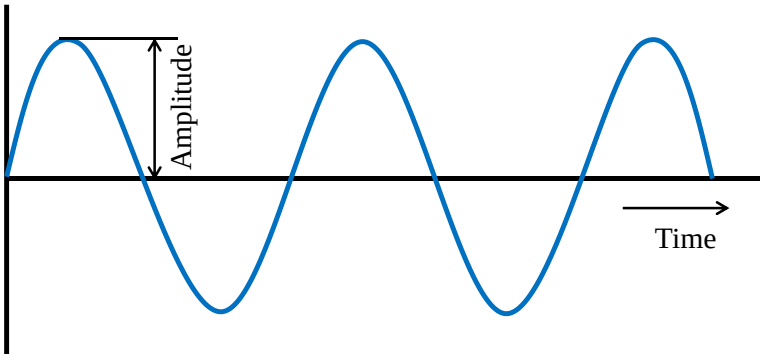

Fig. 1.11. Amplitude of sound wave.

1.3.5. ATTENUATION OF SOUND

When sound travels through a medium, its intensity decreases with distance. In an ideal material, the spreading of the wave only reduces sound pressure (signal amplitude). However, scattering and absorption of sound in other materials reduce the sound pressure. Scattering is the reflection of sound in directions other than its original direction of propagation. Absorption is the conversion of the sound energy to other forms of energy. The combined effect of scattering and absorption is called attenuation. In most cases, attenuation is nearly proportional to the distance.

1.4. APPLICATION OF ULTRASOUND

Ultrasound waves are used in many different fields. Medicine represents one of the widest areas of application for the ultrasound. The most common use of ultrasound in the medical department is its use in what is called an "ultrasound scan". This is used to project a moving image of a fetus inside a pregnant woman's body. Ultrasound is widely applied in medicine for therapy, diagnosis, and treatment as well [47]-[49]. Using the Doppler Effect in ultrasonic technology can be used to measure blood pressure and blood flow [50]. Applying ultrasound techniques using Doppler spectral simulation are used especially in the heart organs [51], [52]. It is also used in the study of infertility [53]. Ultrasound is also popular in the diagnosis of cancer, e.g.: liver (laparoscopy), thyroid [54], [55], or breast [56]; in brain diagnosis [57] and Transcranial [58] or osteoporosis [59]. Another application of ultrasound is Physiotherapy [60] as the treatment of cervical pain [61], [62]. It is used in surgical and medical instruments for fragmentation and removal of biological tissue [63], biopsies [64], activation of transplanted organs [65], orthodontics [66], in obstetrics [67] and ambulatory gynecology [68], [69], pediatric anesthesia [70], forensic examinations [71] or simply to disinfect medical instruments [72]. Ultrasound technology also extends to therapeutic applications [73], [74]. For example, as used in the treatment of dental [75], [76], chronic rhinosinusitis [77], ocular surgery [78], body contouring, kidney stone disruption and removal of blood clots as well in ultrasonic drugs [79].

A broad range of industrial applications of ultrasound has been in use for over 50 years from automotives to the textiles. Today, ultrasound is considered as one of the useful techniques, which

are important for various industrial processes like separation, crystallization and purification, etc. [80]. Ultrasonic cleaning is perhaps the oldest industrial application of power ultrasound. It continues to be used in numerous industries ranging from semiconductors to engine parts due to its low cost and efficient results [81]. For detecting, sizing and locating metal loss and cracks in transmission pipelines Ultrasonic In-Line Inspection Tools is used [82]. Nonlinear ultrasonics is used to assess damaged concrete in industrial applications like nuclear power plants, bridges, etc. [83]. Ultrasonic method is used to detect defects in welds and thick layers of steel, [84], in-situ sizing of fastener hole cracks in steel [85]. In the food industry, ultrasonic technology is used for freezing [86], and chilling [87]. By utilizing ultrasound technique, the clearing of pollutants from wastewater of agro-industry has become possible [88]. In the leather industry, several processes including cleaning, extraction, emulsification, homogenization, separation, preservation, diffusion and chemical reactions are produced by applying ultrasound [89]. Ultrasound methods and processes are used as a strong agent and recently they have got much attention, for treatment of wastewater, and in the purification of drinking water [90]. An ultrasonic flow meter is a type of flow meter that measures the velocity of a fluid with ultrasound to calculate volume flow [91]-[94].

1.4.1. LITERATURE REVIEW OF ULTRASONIC GAS SENSING

Measurement of gas concentration using ultrasonic wave is one of the latest applications of the ultrasonic method.

Joos et al. [95] developed an ultrasonic transmission sensor system based on piezoelectric transducers. This sensor can measure the concentration of gases in binary mixtures of known constituents, which is highly insensitive with respect to the influence of external parameters like total pressure or moisture. The ultrasonic transmission gas-analysis system is shown as in Fig. 1.12. There are numerous demands in industrial process control and monitoring where this technique can be applied favorably, including the control of mixtures of inert, aggressive or explosive gases, remote control of protective gas atmospheres and rapid mixing of gases. The short response time of this sensor with respect to gas composition (the order of several milliseconds) is beneficial. Other advantages are the accuracy, of the order of l-3% with respect to gas composition, its long-time stability and the small influence of moisture and gas pressure.

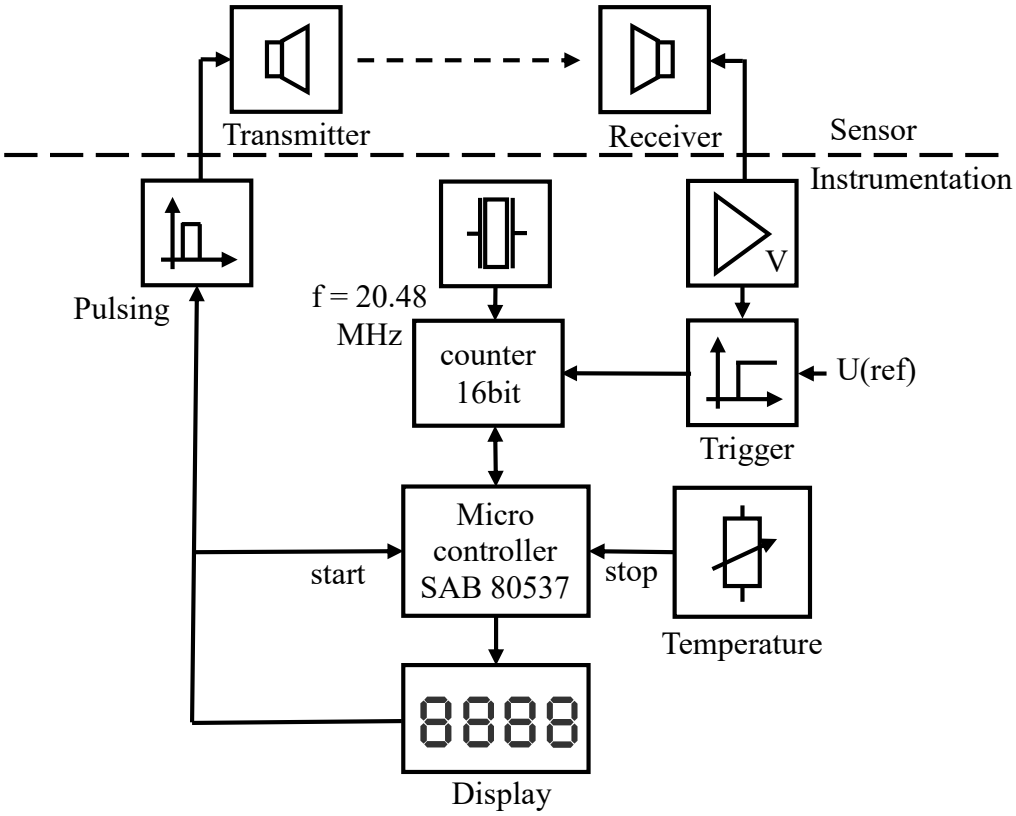

Fig. 1.12. Components and set-up of the ultrasonic transmission gas-analysis system [95].

However, a major restriction of this method is its very limited analytical power with respect to unknown or multicomponent gas mixtures. The principle of gas concentration measurement is complicated. Further improvements in the accuracy of the method, e.g., an error in concentration of less than 0.2 vol. % for CO_2-air mixtures in the range below 10% CO_2.

Sheen et al. [96] examined two ultrasonic techniques for use in a low-cost, fast-response portable helium leak detector. In one technique, a surface acoustic wave (SAW) device is used to detect helium gas through changes of thermal conductivity in helium/air mixtures. The second technique measures variations of sound speed (SS) in such mixtures. Both of the techniques can detect helium leaks as small as 10^{-4} and 10^{-5} cm^3/s, respectively. A prototype sound speed sensor for detecting He in air is showed as in Fig. 1.13. It is a low-cost, fast-response portable helium leak detector.

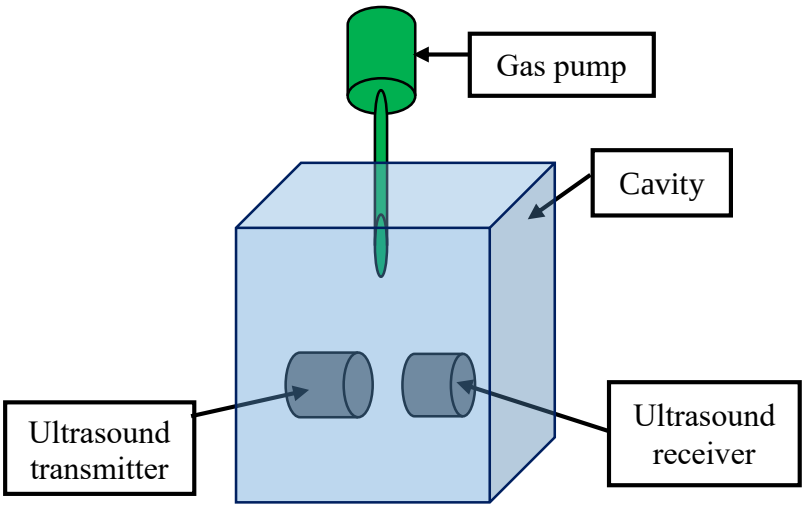

Fig. 1.13. Prototype sound speed sensor for detecting He in air [96].

Vyas et al. [97] fabricated a non-invasive gas sensor. It can measure the gas concentration of a specific gas in a binary mixture such as H_2, He, etc. mixed in the air based on time of flight (TOF) measurements of the ultrasonic signal. The method achieved reliability, and the sensor has a long life. The sensor is found to be suitable for the determination of CO_2 concentration in human exhaled air. A schematic diagram of the experimental setup used for unknown gas concentration measurement of test gases in a binary gas mixture is shown in Fig. 1.14.

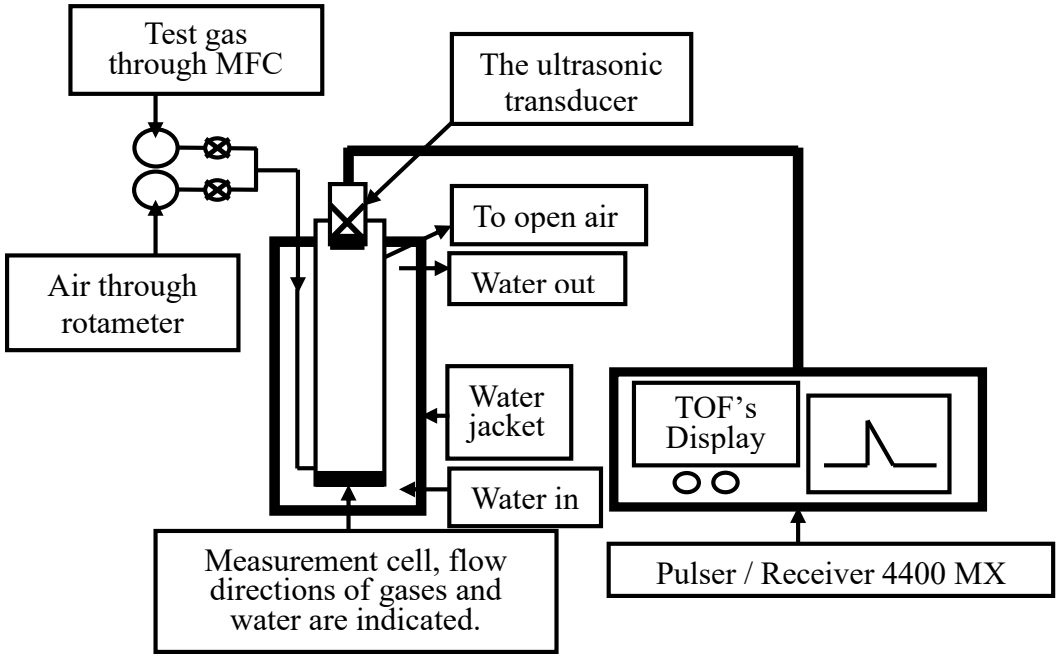

Fig. 1.14. Schematic diagram of the set up used for measurement of unknown concentrations of test gases in a binary gas mixture [97].

Toda et al. [98] described a detection method with a millisecond temporal resolution using ultrasound to determine the gas concentration. The amplitude pattern of an ultrasound signal shifts due to change in the gas concentration. Based on this principle, a high-speed gas concentration monitoring device was fabricated. This device can measure the rapid gas changes from pure nitrogen to a mixture of 5% oxygen and 95% nitrogen with a 45 dB signal-to-noise ratio. A schematic diagram of the ultrasound chamber having embedded transmitter and receiver is shown as in Fig. 1.15. The device can detect the gas concentration on a millisecond time scale. The device and the signal processing of this sensor is simple. It does not have the same gas selectivity as a GC. Therefore, this sensor is applicable when the variation of the flowing gases is fixed. Moreover, this sensor has a long life because this sensor does not employ chemical reactions. Additionally, it may work under severe conditions such as at high temperatures or with an erosion gas where ordinary reaction gas sensors breakdown. This sensor measures changes in gas concentrations by measuring the shift in the gap-dependent curve.

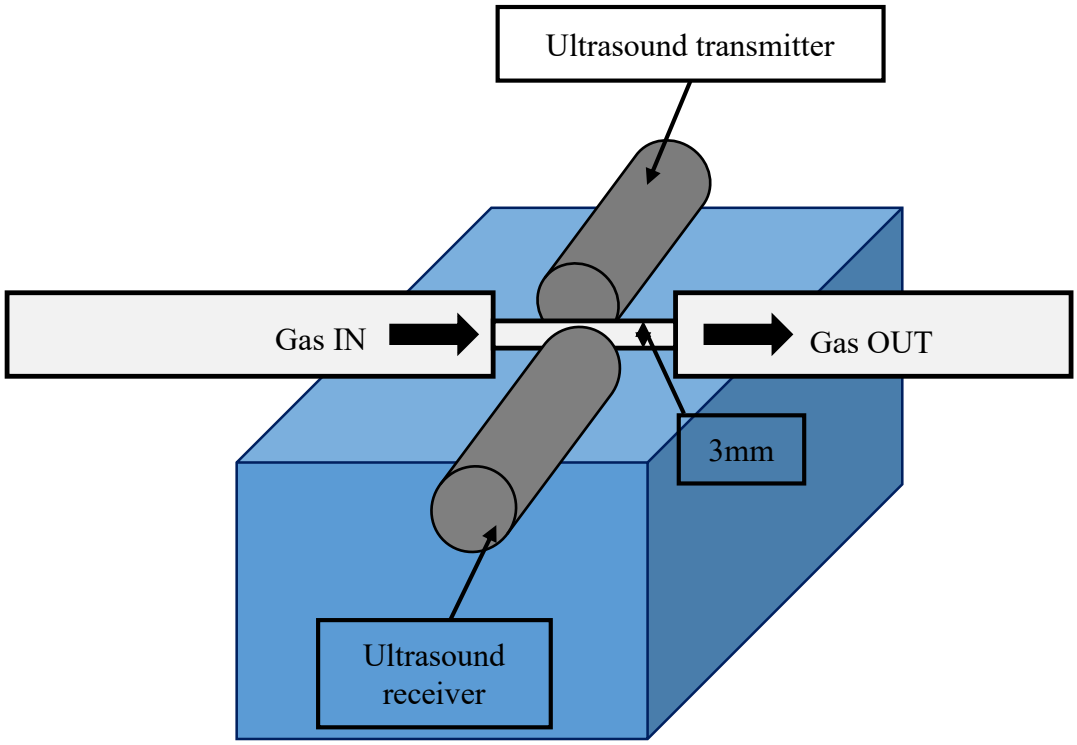

Fig. 1.15. Ultrasound transmitter and receiver units embedded in the chamber [98].

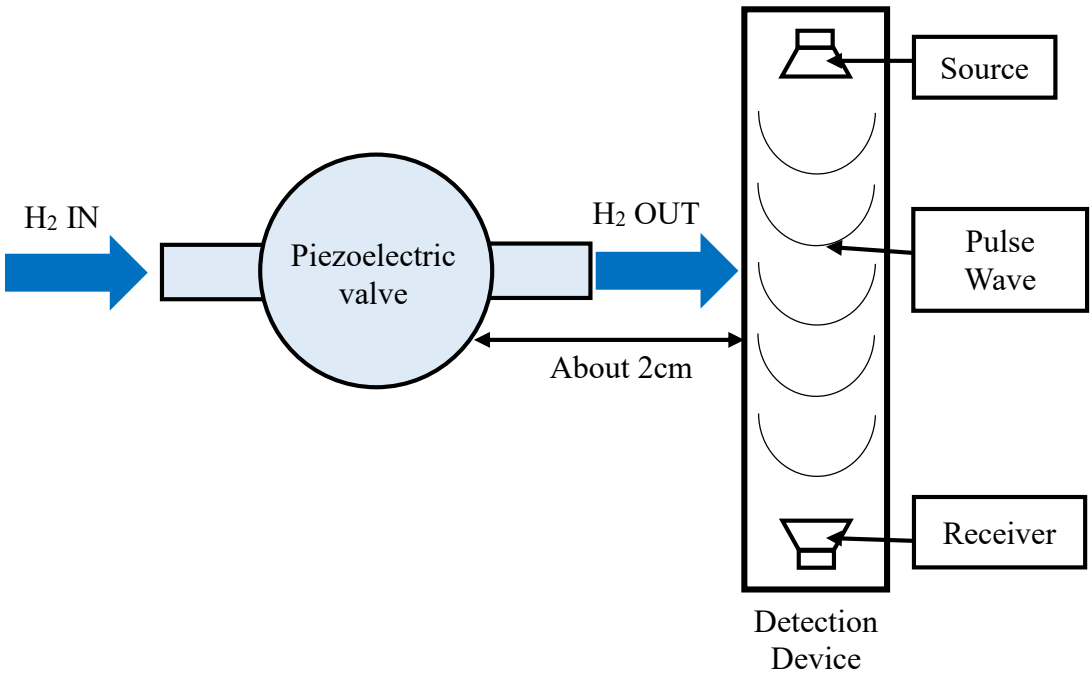

Fig. 1.16. A schematic diagram of the response time measurement method [99].

Sonoyama et al. [99] developed a prototype palm size hydrogen sensor having detection time around 1~2 millisecond. It uses the difference in sound velocity between hydrogen and the air. This sensor can detect hydrogen instantly and accurately (as low as 100ppm). Also, this sensor can be fabricated with low cost compare with other ones because it does not use precious metals as a catalyst. The change of temperature was compensated for the speed of sound, and the hydrogen concentration was obtained accurately even if the temperature varied [46], [100]. This ultrasonic sensor has sensing performance whether the gas is hydrogen or not. Figure 1.16 shows the schematic diagram of the response time measurement method. This sensor investigated the humidity characteristics of the ultrasonic sensor. The humidity characteristics of the ultrasonic hydrogen sensor were evaluated by comparing the theoretical value of the ultrasonic wave arrival time with the experimental value [99], [100]. The temperature was fixed to two patterns of -20°C and 40°C using a small environmental unit, and the relative humidity was changed from 40% to 90%. The ultrasound arrival time was measured each time the relative humidity changed by 10%. It was calculated and adjusted to be Δt=0 when the relative humidity is 50% at 40°C.

1.5. MOTIVATION

Recently, hydrogen transportation by pipeline has received much attention due to heat and energy provision. Pipelines are regarded as the most efficient method of transporting large quantities of hydrogen over long distances. Hydrogen transportation by pipeline is demonstrated in some of the leading industrial nations: 210 km in Germany, 400 km from France to Belgium, and over 720 km throughout the U.S. [101]. Europe and North America have already started using around 3000 km of high-pressure hydrogen pipelines for industrial processes [102]. In addition, Japan becomes the first country in the world to realize a hydrogen-based society. The Japanese government is planning to develop a H_2 energy society as part of its strategy for the Tokyo Olympic Games to be held in 2020. H_2 will be distributed to support the activities of some 17,000 athletes and other guests. Residential facilities, training centers, and buses will be powered by H_2. Tokyo has already started operating fuel cell buses and has proceeded with plans to use H_2 in the Olympic and Paralympic villages. After 2020, the Olympic Village will be converted to an H_2 based high-class residential area [103]. Figure 1.17 shows the proposed plan of futuristic 'Hydrogen town' in Tokyo where H_2 will be transported by pipeline to the fuel cell [104]. Thus, monitoring H_2 gas concentration in a pipe is an important issue for transportation through a pipeline. Furthermore, fuel cell technology using hydrogen are being popular in factories and commercial buildings. Fuel cell manufacturers are also developing compact and inexpensive cells for home use [105]. Japan has set a goal to install fuel cell in 5.3 million homes by 2030, about 10 percent of all households [106]. For the advancement of fuel cell and hydrogen technologies, many countries have different targets. The European roadmap for the deployment of hydrogen and fuel cell technologies has now set a goal of 0.4–1.8 million hydrogen vehicles sold per year by 2020 [107]. Hydrogen concentration monitoring that goes in and coming out from a cathode is required for hydrogen fuel cell [108]. For city gas, usage of carbon dioxide can be controlled by blending the natural gas with hydrogen gas through the existing gas networks [109]. To avoid sudden increase of hydrogen gas concentration in the natural gas, the concentration of hydrogen should be carefully controlled during hydrogen injection into the natural gas [110].

Fig. 1.17. The proposed plan of 'Hydrogen town' in Tokyo [104].

Conventional and present ultrasonic H_2 sensors are described in the previous section. However, none of these sensors meets the requirement of measuring gas concentration from the exterior of the pipe. They need to extract the gas by making a hole into the pipe for the gas concentration measurement. Since H_2 is a combustible gas, making a hole may cause danger such as leakage or explosion. Therefore, it is required to measure the H_2 gas concentration from the exterior of the pipe without making any hole. We have proposed an ultrasonic gas sensor, which can measure the gas concentration from the exterior of the pipe without making a hole. This sensor can measure both of flowing and non-flowing gas concentration from the exterior of different pipe materials. Currently, two principles are used to measure the flow velocity using the ultrasonic wave. One is the Doppler method in which the flow velocity is measured by the Doppler phase/frequency shift of reflected ultrasonic waves [111], [112]. The other often-used method is the transit-time method [113], [114]. In this research, the gas concentration measurement is similar to this transit-time method and different from the Doppler method. The concentration of the gas can be measured based on the speed variation of the ultrasound traveling inside the pipe. Drilling a hole in the pipe to extract the gases is not necessary for the gas concentration measurement.

The emerging hydrogen economy concept would make the development of a highly selective and sensitive H_2 sensor a great interest and highly important. In addition to this, insight into H_2

sensing mechanism will be useful not only people who work for the gas sensor but also for other researcher or practitioners who study various H_2 applications.

1.6. RESEARCH OBJECTIVES

The overall objective of this work is to measure non-flowing and flowing hydrogen gas concentration by using ultrasound from the exterior of the pipe. To achieve this general objective, the works encompassed in this thesis have been organized to fit the following specific objectives.

1. To observe the airborne signal from the exterior of stainless steel (SUS) pipe and measure the non-flowing hydrogen gas concentration from the exterior of a SUS pipe.

2. To measure the flowing hydrogen gas concentration from the exterior of polyvinyl chloride (PVC) pipe.
3. To study the ultrasound propagation through the air-H_2-air two layer gas system. Intensity degradation of ultrasound through the system was studied.

1.7. DISSERTATION LAYOUT

This thesis is organized as follows. It consists of five chapters. Each chapter has its own different topics to discuss. In the following, a glimpse of the topic has been pointed out.

CHAPTER 1 discusses the background and the research problem of this study in details. The detailed literature review on various topics related to the present work is also discussed. Moreover, research objectives and structure of the thesis are included in this chapter.

CHAPTER 2 highlights the measurement of non-flowing H_2 gas concentration from the exterior of a SUS pipe. A sound absorbing material (SAM) is proposed to reduce the noise signal circling in the SUS wall. The circulation of sound in the SUS pipe wall is explained by finite-difference time-domain (FDTD) simulation method. Different experimental conditions are applied

to understand the amplitude of the received ultrasonic signal. A two-transmitter condition is proposed to cancel the noise signal. The experimental setup, simulated and measured results are summarized and compared in this chapter.

CHAPTER 3 describes the measurement of flowing hydrogen gas concentration from the exterior of a PVC pipe. The noise error is measured for various flow rates. The effect of noise error on gas concentration is studied. Furthermore, the effect of humidity and temperature on Δt are investigated. Finally, the limit of flow is investigated, and an equation is developed to calculate the limit of flow. The experimental results are summarized in this chapter.

CHAPTER 4 reports propagation of ultrasound trough two-layer mixed gas. The intensity of ultrasonic signal degradation was observed while hydrogen was mixed into air. The concentration of hydrogen gas was measured from the exterior of an acrylic pipe and it was found that the intensity of ultrasound does not depend on the gas concentration. An acrylic pipe is chosen to visualize hydrogen by using Schlieren photography from the exterior of the pipe. Two fluctuated interfaces in air-H_2-air system is observed. An air-H_2-air system is proposed, and the loss of signal intensity in this system is described. The simulated results are summarized in this chapter.

CHAPTER 5 draws conclusions and recommendations. This chapter summarizes the whole research work and actual findings are briefly mentioned based on the objective of the thesis. Moreover, this chapter also incorporates some limitations and recommendations for future works.

REFERENCES

[1] S. Shafiee and E. Topal, "When will fossil fuel reserves be diminished?", Energy Policy, **vol. 37**, no. 1, pp. 181-189, 2009.

[2] L. Chiari and A. Zecca, "Constraints of fossil fuels depletion on global warming projections", Energy Policy, **vol. 39**, no. 9, pp. 5026-5034, 2011.

[3] T. J. Crowley, "Cause of climate change over the past 1000 years", Science, **vol. 289**, no. 5477, pp. 270-277, 2000.

[4] U.E.I.A. (EIA), International Energy Outlook 2013 with Projections to 2040, International Energy Outlook 2013.

[5] T. Nakamura, "Hydrogen production from water utilizing solar heat at high temperatures", Solar Energy, **vol. 19**, pp. 467-475, 1977.

[6] H. Kato, K. Asakura and A. Kudo, "Highly efficient water splitting into H_2 and O_2 over lanthanum-doped $NaTaO_3$ photocatalysts with high crystallinity and surface nanostructure", Journal of the American Chemical Society, **vol. 125**, pp. 3082-3089, 2003.

[7] A. Midilli, M. Ay and I. Dincer, "On hydrogen and hydrogen energy strategies: I: Current status and needs", Renewable and Sustainable Energy Reviews, **vol. 9**, no. 3, pp. 255-271, 2005.

[8] R. Ramachandran and R. K. Menon, "An overview of industrial uses of hydrogen", International Journal of Hydrogen Energy, **vol. 23**, no. 7, pp. 593-598, 1998.

[9] S. Dunn, "Hydrogen futures: toward a sustainable energy system", International Journal of Hydrogen Energy, **vol. 27**, no. 3, pp. 235-264, 2002.

[10] G. Marbán and T. Valdés-Solís, "Towards the hydrogen economy?", International Journal of Hydrogen Energy, **vol. 32**, pp. 1625-1637, 2007.

[11] M. Fischer and H. Eichert, "Safety aspects of hydrogen energy. Hydrogen as an energy carrier", C.J. Winter and J. Nitsch eds. Springer-Verlag. Berlin, 1988.

[12] T. Hübert, L. Boon-Brett, G. Black and U. Banach, "Hydrogen sensor-a review", Sensors and Actuators B: Chemical, **vol. 157**, pp. 329-352, 2011.

[13] T. Pinch, "How do we treat technical uncertainty in systems failure? The case of the space shuttle challenger 1", in: T. Porte (Ed.) Social responses to large technical systems, Springer Netherlands1991, pp. 143-158, 1991.

[14] K. Hirose, "2011 Fukushima Dai-ichi nuclear power plant accident: summary of regional radioactive deposition monitoring results", Journal of Environmental Radioactivity, **vol. 111**, pp. 13-17, 2012.

[15] Y.S.H. Najjar, "Hydrogen safety: The road toward green technology", International Journal of Hydrogen Energy, **vol. 38**, pp. 10716-10728, 2013.

[16] M.P. Brungs, C. Mauchausse, D. Stroescu and D. Trimm, "The evaluation of hydrogen detectors for use in coal mines", Journal of the Energy Institute, **vol. 65**, pp. 66-69, 1992.

[17] C.A. Grimes, K. G. Ong, O. K. Varghese, X. Yang, G. Mor, M. Paulose, E. C. Dickey, C. Ruan, M. V. Pishko, J. W. Kendig and A. J. Mason, "A sentinel sensor network for hydrogen sensing", Sensors, **vol. 3**, pp. 69-82, 2003.

[18] Retrieved from the link: http://www.hysafe.org/download/1200/BRHS.Chap5.V1p2.pdf, Accessed 15 December 2010.

[19] S. Kulinyi, D. Brandszájsz, H. Amine, M. Ádám, P. Fürjes, I. Bársony and C. Dücso, "Olfactory detection of methane, propane, butane and hexane using conventional transmitter norms", Sensors and Actuators B: Chemical, **vol. 111**, pp. 286-292, 2005.

[20] C. Caucheteur, M. Debliquy, D. Lahem and P. Megret, "Catalytic fiber bragg grating sensor for hydrogen leak detection in air", IEEE Photonics Technology Letters, **vol. 20**, pp. 96-98, 2008.

[21] L. Xu, T. Li, X. Gao and Y. Wang, "Behaviour of a catalytic combustion methane gas sensor working on pulse mode", in Proceeding of the IEEE International Conference on Sensors, Kona, HI, USA, 1-4 November 2010, pp. 391-394, 2010.

[22] K. Scharnagle1, M. Eriksson, A. Karthigeyan, M. Burgmair, M. Zimmer and I. Eisele, "Hydrogen detection at high concentration with stabilized palladium", Sensors and Actuators B: Chemical, **vol. 78**, pp. 138-143, 2001.

[23] S. Mourya, A. Kumar, J. Jaiswal, G. Malik and B. Kumar, "Development of Pd-Pt functionalized high performance H_2 gas sensor based on silicon carbide coated porous silicon for extreme environment application", Sensors and Actuators B: Chemical, **vol. 283**, pp. 373-383, 2019.

[24] A. B. LaConti and H. J. R. Maget, "Electrochemical detection of H_2, CO and hydrocarbons in inert or oxygen atmosphere", Journal of the Electrochemical Society, **vol. 118**, pp. 506, 1978.

[25] G. Korotcenkov, S. D. Han and J. R. Stetter, "Review of electrochemical hydrogen sensors", Chemical Review, **vol. 109**, pp. 1402-1433, 2009.

[26] A. J. Bard, M. Stratmann and P. R. Unwin, Eds., "Instrumentation and Electroanalytical Chemistry", Wiley-VCH: New Jersey, **vol. 3**, 2003.

[27] G. Mothé, M. Castro, M. Sthel, G. Lima, L. Brasil, L. Campos, A. Rocha and H. Vargas, "Detection of greenhouse gas precursors from diesel engines using electrochemical and photoacoustic sensors", Sensors, **vol. 10**, pp. 9726-9741, 2010.

[28] K. H. Kim, "Performance characterization of the GC/PFPD for H_2S, CH_3SH, CH_3SCH_3, and CH_3SSCH_3 in air", Atmospheric Environment, **vol. 39**, pp. 2235-2242, 2005.

[29] S. Wu, G. Lv and R. Lou, "Applications of chromatography hyphenated techniques in the field of lignin pyrolysis", Applications of Gas Chromatography, pp. 41-64, 2012

[30] G. E. Eranna, B. C. Joshi, D. P. Runthala and R. P. Gupta, "Oxide materials for development for integrated gas sensors—a comprehensive review", Critical Reviews in Solid State and Material Sciences, **vol. 29**, no. 3-4, pp. 111-188, 2004.

[31] C. Wagner, "The mechanism of the decomposition of nitrogen oxide on zinc oxide as catalyst", The Journal of Chemical Physics, **vol. 18**, pp. 69-71, 1950.

[32] T. Seiyama, A. Kato, K. Fujishi and M. Nagatani, "A new detector for gaseous components using semiconductive thin films", Analytical Chemistry, **vol. 34**, pp. 1502-1503, 1962.

[33] N. Taguchi, Japan. Pat. 45-38200 (1962), 4738840 (1963) 50-23317.

[34] M. C. Çakır, D. Çalışkan, B. Bütün and E. Özbay, "Planar indium tin oxide heater for improved thermal distribution for metal oxide micromachined gas sensors", Sensors, **vol. 16**, pp. 1612, 2016.

[35] A. Pohl, "A review of wireless SAW sensors", IEEE Transactions on Ultrasonics, Ferroelectrics, and frequency control, **vol. 47**, pp. 317, 2000.

[36] J. I. Samuel, K. Sasikaran, K. –Z. Kourosh, T. Adrian and W. Wojtek, "A layered surface acoustic Wave ZnO/$LiTaO_3$ structure with a WO_3 selective layer for hydrogen sensing", Sensor Letters, **vol. 1**, pp. 33, 2003.

[37] K. Yamanaka, N. Nakaso, D. Sim and T. Fukiura, "Principle and application of ball surface acoustic wave (SAW) sensor", Acoustical Science and Technology, **vol. 30**, pp. 2-6, 2009.

[38] W. P. Jakubik, M. W. Urbańczyk, S. Kochowski and J. Bodzenta, "Bilayer structure for hydrogen detection in a surface acoustic wave sensor system", Sensors and Actuators B: Chemical, **vol. 82**, pp. 265-271, 2002.

[39] T. J. Mason and J. P. Lorimer, "Applied sonochemistry. The uses of power ultrasound in chemistry and processing", Wiley-VCH, pp. 1-48, 2002.

[40] C. Zhu, M. Shan and S. He, "A precise sensor for SF_6 based on piezoelectric ultrasound", Rare Metal Materials and Engineering, **vol. 35**, pp. 157-158, 2006.

[41] C. Zhu, M. Shan, Y. Liu and H. Zhang, "Microconcentration detector for SF_6 based on CPLD", Chinese Journal of Scientific Instruments, **vol. 26**, pp. 448-449, 2005.

[42] S. Minglei, L. Xiang, Z. Changping and Z. Jiahua; "Gas concentration detection using ultrasonic based on wireless sensor networks", 2nd International Conference on Information Science and Engineering (ICISE), pp. 2101-2106, 2010.

[43] L. Bergmann, "Ultrasonics and their scientific and technical applications", London: G. Bell and Sons Ltd., 1938.

[44] S. Kocis and Z. Figura, "Ultrasonic measurements and technologies", London, U.K.: Chapman & Hall, 1996.

[45] R. Halmshaw, "Introduction to the non-destructive testing of welded joints", Cambridge: Abington Publishing, 1996.

[46] H. Fukuoka, J. Jung, M. Inoue, H. Fujita and Y. Kato, "Absolute concentration measurement for hydrogen", Energy Procedia, **vol. 29**, pp. 283-290, Jan. 2012.

[47] J. A. Jensen, "Medical ultrasound imaging," Progress in biophysics and molecular biology", **vol. 93**, no. 1-3, pp. 153-165, 2007.

[48] T. J. Mason, "Therapeutic ultrasound an overview", Ultrasonics Sonochemistry, **vol. 18**, no. 4, pp. 847-852, 2011.

[49] S. Paliwal and S. Mitragotri, "Therapeutic opportunities in biological responses of ultrasound", Ultrasonics, **vol. 48**, no. 4, pp. 271-278, 2008.

[50] J. A. Jensen, "Medical ultrasound imaging", Progress in Biophysics and Molecular Biology, **vol. 93**, no. 1, pp. 153-165, 2007.

[51] J. M. Evans, R. Skidmore, N. P. Luckman and P. N. Wells, "A new approach to the noninvasive measurement of cardiac output using an annular array doppler technique, I. Theoretical considerations and ultrasonic fields", Ultrasound in Medicine & Biology, **vol. 15**, no. 3, pp. 167-178, 1989.

[52] M. J. Hung and W. J. Chemg, "Clinical applications of transthoracic doppler echocardiographic coronary flow reserve measurements in the left anterior descending coronary artery", Journal of Medical Ultrasound, **vol. 19**, no. 4, pp. 115-121, 2011.

[53] C. K. Chen, H. M. Wu and Y. K. Soong, "Clinical application of ultrasound in infertility: from two-dimensional to three-dimensional", Journal of Medical Ultrasound, **vol. 15**, no. 2, pp. 126-133, 2007.

[54] A. Basarab, H. Liebgott, F. Morestin, A. Lyshchik, T. higashi, R. Asato and P. Delachartre, "A method for vector displacement estimation with ultrasound imaging and its application for thyroid nodular disease", Medical Image Analysis, **vol. 12**, no. 3, pp. 259-274, 2008.

[55] T. G. Kangelaris, T. B. Kim and L. A. Orloff, “Role of ultrasound in thyroid disorders”, Ultrasound Clinics, **vol. 7**, no. 2, pp. 197-210, 2012.

[56] A. Jalian, S. B. Mashorhor, H. R. Mahmud, M. I. Saripan, A. R. Ramli and B. Karasfi, “Computer-aided detection/diagnosis of breast cancer in mammography and ultrasound: a review”, Clinical Imaging, **vol. 37**, no. 3, pp. 420-426, 2013.

[57] J. Aarnio, G. T. Clement and K. Hynynen, “A new ultrasound method for determining the acoustic phase shifts caused by the skull bone”, Ultrasound in Medicine & Biology, **vol. 31**, no. 6, pp. 771-780, 2005.

[58] S. Behrens, K. Spengos, M. Daffertshofer, H. Schroeck, C. E. Demfle and M. Hennerici, “Transcranial ultrasound-improved thrombolysis: diagnostic vs. therapeutic ultrasound”, Ultrasound in Medicine & Biology, **vol. 27**, no. 2, pp. 1683-1689, 2001.

[59] G. Guglielmi, G. Scalzo, F. de Terlizzi and W. C. Pe, “Quantitative ultrasound in osteoporosis and bone metabolism pathologies”, Radiologic Clinics of North America, **vol. 48**, no. 3, pp. 577-588, 2010.

[60] S. McKiernan, P. Chiarelli and H. Warren-Forward, “Diagnostic ultrasound use in physiotherapy, emergency medicine, and anaesthesiology”, Radiography, **vol. 16**, no. 2, pp. 154-159, 2010.

[61] C. Alcázar and R. M. Rodriguez, “Aplicación de ultrasonidos en el dolor cervical de origen inespecífico”, Fisioterapia, **vol. 29**, no. 4, 2007.

[62] L. Ghamkhar, M. Emami, M. A. Mohseni-Bandpei and H. Behtash, “Application of rehabilitative ultrasound in the assessment of low back pain: A literature review”, Journal of Bodywork and Movement Therapies, **vol. 15**, no. 4, pp. 465-477, 2011.

[63] B. O'Daly, E. Morris, G. Gavin, J. O'Byrne and G. McGuinness, “High-power low-frequency ultrasound: a review of tissue dissection and ablation in medicine and surgery”, Journal of Materials Processing Technology, **vol. 200**, no. 1, pp. 35-58, 2008.

[64] A. Fenster, K. Surry, W. Smith, J. Gill and D. B. Downey, “3D ultrasound imaging: applications in image-guided therapy and biopsy”, Computers & Graphics, **vol. 26**, no. 4, pp. 557-568, 2002.

[65] S. Wang, Y. Li, Y. Ji, C.-M. Lin, C. Man and X.-X. Zheng, "Stem-cell-activated organ following ultrasound exposure: Better transplant option for organ transplantation", Medical Hypotheses, **vol. 74**, no. 1, pp. 147-149, 2010.

[66] T. El-Bialy, I. El-Shamy and T. M. Graber, "Repair of orthodontically induced root resorption by ultrasound in humans", American Journal of Orthodontics and Dentofacial Orthopedics, **vol. 126**, no. 2, pp. 186-193, 2009.

[67] S. H. Eik-Nes, "Chapter 1 Physics and instrumentation", de Ultrasound in obstetrics and gynaecology, Edinburgh, Elsevier, pp. 1-20, 2009.

[68] N. N. Amso and A. Griffiths, "The role and applications of ultrasound in ambulatory gynaecology", Best Practice & Research Clinical Obstetrics & Gynaecology, **vol. 19**, no. 5, pp. 693-711, 2005.

[69] L. Coyne and N. J. Raine-Fenning, "Ultrasound in gynaecology and early pregnancy", Obstetrics, Gynaecology & Reproductive Medicine, **vol. 20**, no. 6, pp. 181-189, 2010.

[70] J. G. McCormack and S. Malherbe, "Applications of ultrasound in paediatric anaesthesia", Current Anaesthesia & Critical Care, **vol. 19**, no. 5, pp. 302-308, 2008.

[71] S. Uchigasaki, L. Oesterhelweg, A. Gehl, J. Sperhake, S. Oshida and N. Nemoto, "Application of compact ultrasound imaging device to postmortem diagnosis", Forensic Science International, **vol. 140**, no. 1, pp. 33-41, 2004.

[72] L. Jatzawauk, H. Schöne and H. Pietsch, "How to improve instrument disinfection by ultrasound", Journal of Hospital Infection, **vol. 1**, pp. 80-83, 2001.

[73] L. Crum, M. Bailey, J. H. Hwang, V. Khokhlova and O. Sapozhnikov, "Therapeutic ultrasound: Recent trends and future perspectives", Physics Procedia, **vol. 3**, no. 1, pp. 25-34, 2010.

[74] G. ter Haar, "Therapeutic applications of ultrasound", Progress in Biophysics and Molecular Biology, **vol. 93**, no. 1, pp. 111-129, 2007.

[75] B. Scheven, R. Shelton, P. Cooper, A. Walmsley and A. Smith, "Therapeutic ultrasound for dental tissue repair", Medical Hypotheses, **vol. 73**, no. 4, pp. 591-593, 2009.

[76] A. Walmsley, "Applications of ultrasound in dentistry", Ultrasound in Medicine & Biology, **vol. 14**, no. 1, pp. 7-14, 1988.

[77] J. Bartley and D. Young, "Ultrasound as a treatment for chronic rhinosinusitis", Medical Hypotheses, **vol. 73**, no. 1, pp. 15-17, 2009.

[78] M. Nabili, H. Patel, S. P. Mahesh, J. Liu, C. Geist and V. Zderic, "Ultrasound-enhanced delivery of antibiotics and anti-inflammatory drugs into the eye", Ultrasound in Medicine & Biology, **vol. 39**, no. 4, pp. 638-646, 2013.

[79] F. Ahmadi, I. V. McLoughlin, S. Chauhan and G. ter Haar, "Bio-effects and safety of low-intensity, low-frequency ultrasonic exposure", Progress in Biophysics and Molecular Biology, **vol. 108**, no. 3, pp. 119-138, 2012.

[80] R. Singla, F. Grieser and M. Ashokkumar, "The mechanism of sonochemical degradation of a cationic surfactant in aqueous solution", Ultrasonics Sonochemistry, **vol. 18**, no. 2, pp. 484-488, 2011.

[81] A. Shoh, "Industrial applications of Ultrasound – A Review I. High Power Ultrasound", IEEE Transactions on Ultrasonics Ferroelectrics and Frequency Control, **vol 22**, pp. 60-71, 1975.

[82] K. Reber, M. Beller, H, Willems and O. Barbian, "A new generation of ultrasonic in-line inspection tools for detecting, sizing and locating metal loss and cracks in transmission pipelines", Ultrasonic Symposium (IEEE), **vol. 1**, pp. 665-671, 2002.

[83] A. A. Shah, Y. Ribakov and S. Hirose, "Nondestructive evaluation of damaged concrete using nonlinear ultrasonics", Materials and Design, **vol. 30**, pp. 775-782, 2009.

[84] M. Riahi and M. R. Abolhasany, "Substitution of the time-of-flight diffraction technique for nondestructive testing of welds and thick layers of steel: A comparative investigation", Russian Journal of Nondestructive Testing, **vol. 42**, no. 12, pp. 794-801, 2006.

[85] J. E. Michaels, T. E. Michaels and B. Mi, "An ultrasonic angle beam method for in situ sizing of fastener hole cracks", Journal of Nondestructive Evaluation, **vol. 25**, no. 1, pp. 2-15, 2006.

[86] P. W. Cains, P. D, Martin and C. J. Price, “The use of ultrasound in industrial chemical synthesis and crystallization. 1. Applications to synthetic chemistry”, Organic process research & development, **vol. 2**, no. 1, pp. 34-48, 1998.

[87] T.S. Awad, H. A. Moharram, O. E. Shaltout, D, Asker and M. M. Youssef, “Applications of ultrasound in analysis, processing and quality control of food: A review”, Food Research International, **vol. 48**, no. 2, pp. 410-427, 2012.

[88] H. E. Hajjouji, J. R. Bailly, P. Winterton, G. Merlina, J. C. Revel and M. Hafidi, “Chemical and spectroscopic analysis of olive mill waste water during a biological treatment”, Bioresource Technology, **vol. 99**, no. 11, pp. 4958-4965, 2008.

[89] V. Sivakumar and P. G. Rao, “Studies on the use of power ultrasound in leather dyeing”, Ultrasonics Sonochemistry, **vol. 10**, no. 2, pp. 85-94, 2003.

[90] M. Ren, Y. H. Song, S. Xiao, P. Zeng and J. Peng, “Treatment of berberine hydrochloride wastewater by using pulse electro - coagulation process with Fe electrode”, Chemical Engineering Journal, **vol. 169**, no. 1, pp. 84-90, 2011.

[91] Y. Koike, T. Tsuyoshi, H. Kikura, M. Aritomi and M. Mori, “Flow rate measurement using ultrasonic Doppler method with cavitation bubbles”, IEEE Ultrasonics Symposium, **vol. 1**, pp. 531-534, 2002.

[92] D.W. Baker, “Pulsed ultrasonic Doppler blood-flow sensing”, IEEE Transactions on Sonics and Ultrasonics, **vol. 17**, pp. 170-184, 1970.

[93] K. Koyano, Y. Usui, T. Ikawa and T Sugi, “Ultrasonic flow meter”, U.S. Patent: 6.055,868, 2000.

[94] M. Terao, H. Tanaka and Y. Tanaka, “Easy-setup clamp-on ultrasonic flowmeter”, Japanese Journal of Applied Physics, **vol. 53**, 07KC08, 2014.

[95] M. Joos, H. Miller and G. Lindner, “An ultrasonic sensor for the analysis of binary gas mixtures”, Sensors and Actuators B, **vol. 15-16**, pp. 413-419, 1993.

[96] S. H. Sheen, H. T. Chien and A. C. Raptis, “Ultrasonic techniques for detecting helium leaks”, Sensors and Actuators B, **vol. 71**, pp. 197-202, 2000.

[97] J. C. Vyas, V. R. Katti, S. K. Gupta and J. V. Yakhmi, "A non-invasive ultrasonic gas sensor for binary gas mixtures", Sensors and Atuators B, **vol. 115**, pp. 28-32, 2006.

[98] H. Toda and T. Kobatakawa, "High-speed gas concentration measurement using ultrasound", Sensors and Actuators A, **vol. 144**, pp. 1-6, 2008.

[99] M. Sonoyama, H. Fujita and Y. Kato, "Application of ultrasonic to a hydrogen sensor", in Proceeding IEEE Sensors, no. 3, pp. 2141-2144, 2010.

[100] J. Jung and M. Sonoyama, H. Fujita, M. Inoue and Y. Kato, "The novel hydrogen sensor using ultrasonic", International Conference on Hydrogen Production (ICH2P-11), 160 ELE 1-8, 2011.

[101] W. A. Amos, "Costs of storing and transporting hydrogen", National Renewable Energy Laboratory (NREL) Golden, CO, November 1998.

[102] D. Hart, J. Howes, F. Lehner, P. Dodds, N. Hughes, B. Fais, N. Sabio and M. Crowther, "Scenarios for deployment of hydrogen in contributing to meeting carbon budgets and the 2050 target", 2015.

[103] S. Watanabe, "Hydrogen infrastructure in Japan", 2014 Annual Merit Review Proceedings, Washington, 2014.

[104] Retrieved from the link https://www.olympic.org/tokyo-2020

[105] H. Aki, S. Yamamoto, J. Kondoh, T. Maeda, H Yamaguchi, A. Murata and I. Ishii, "Fuel cells and energy networks of electricity, heat, and hydrogen in residential areas", International Journal of Hydrogen Energy, **vol. 31**, pp. 967-980, 2006.

[106] N. Behling, M. C. Williams and S. Managi, "Fuel cells and the hydrogen revolution: analysis of a strategic plan in Japan", Economic. Analysis and Policy, **vol. 48**, pp. 204-221, 2015.

[107] P. P. Edwards, V. L. Kuznetsov, W. I. F. David and N. P. Brandon, "Hydrogen and fuel cells: Towards a sustainable energy future", Energy Policy, **vol. 36**, pp. 4356-4362, 2008.

[108] M. Watanabe, R. Inoue, D. Ichikawa and K. Furusaki, "Development of thermal conductivity type hydrogen sensor", Fuel Cells, **vol. 5**, pp. 111628-111628, 2008.

[109] P. E. Dodds and S. Demoullin, “Conversion of the UK gas system to transport hydrogen”, International Journal of Hydrogen Energy, **vol. 38**, pp. 7189-7200, 2013.

[110] K. Altfeld and D. Pinchbeck, “Admissible hydrogen concentrations in natural gas systems”, Gas Energy, pp. 1-16, 2013.

[111] Y. Koike, T. Tsuyoshi, H. Kikura, M. Aritomi and M. Mori, “Flow rate measurement using ultrasonic Doppler method with cavitation bubbles”, in Proceeding of IEEE Ultrasonic Symposium, **vol. 1**, Oct. 2002, pp. 531-534.

[112] D. W. Baker, “Pulsed ultrasonic Doppler blood-flow sensing”, IEEE Transactions on Sonics and Ultrasonics, **vol. 17**, pp. 170-184, 1970.

[113] K. Koyano, Y. Usui, T. Ikawa and T. Sugi, “Ultrasonic flow meter”, U.S. Patent 6 055 868, May 2, 2000.

[114] M. Terao, H. Tanaka and Y. Tanaka, “Easy-setup clamp-on ultrasonic flowmeter”, Japanese Journal of Applied Physics, **vol. 53**, 07KC08, 2014.

CHAPTER 2

MEASUREMENT OF NON-FLOWING GAS CONCENTRATION FROM THE EXTERIOR OF A PIPE

2.1. INTRODUCTION

This chapter mainly focuses on the measurement of non-flowing H_2 gas concentration from the exterior of a pipe. At first, the principle of gas concentration measurement by using ultrasound is described. The principle of gas concentration measurement is based on the variation of sound speed detected by ultrasound. Usually, carbon steel or stainless steel (SUS) is used as the material for the pipelines of H_2 gas transportation [1]. In this chapter, concentration of H_2 gas in a SUS pipe is measured from the exterior of the SUS pipe without making a hole on the pipe surface. However, observation of airborne ultrasonic wave traveling in the SUS pipe is difficult because the sound wave is also circling inside the SUS pipe itself [2]. A very basic theory of ultrasound propagation at boundary is described here. Longitudinal and transverse waves propagate in a solid with different velocities [3]. The propagation of longitudinal and transverse waves in solid were described in section. 1.3.2. of Chapter 1. Since both of these waves are considered in the finite-difference-time-domain (FDTD) method, sound propagation through the SUS pipe was visualized by using the FDTD method [4], [5]. Simulated and experimental results of ultrasound propagation in a SUS pipe are compared. In this chapter, two methods were tried to reduce the noise signal. At first sound absorbing material (SAM) was pasted on the surface of the SUS pipe and successfully reduced the noise signal. Therefore, the airborne signal was observed from the exterior of the SUS pipe. This is the first time that a sound absorbing material (SAM) was selected which can reduce the ultrasonic signal circling inside the SUS pipe material. Therefore, it is possible to measure the gas concentration from the exterior of the pipe. Secondly, two transmitters and one receiver method as tried to cancel the noise signal by interfering each other. According to the FDTD simulation method, it has been found that signal amplitude for the condition of using two transmitters where the ultrasonic waves interfere with each other and cancel out the noise sound signal. Therefore, it could be possible to reduce the noise signal by using two transmitters; however,

it is not possible in practice. The probable reasons of the mismatch in simulation and experimental results are also discussed in this chapter.

2.2. PRINCIPLE

2.2.1. GAS CONCENTRATION MEASUREMENT USING ULTRASOUND

This section is described the gas concentration measurement by using ultrasound. Figure 2.1 shows an image of the ultrasonic detection unit applied in this research. Suppose the distance between the ultrasonic transmitter and the receiver is 5 cm, and the time required for the ultrasonic wave reach to the receiver is called the sound traveling time.

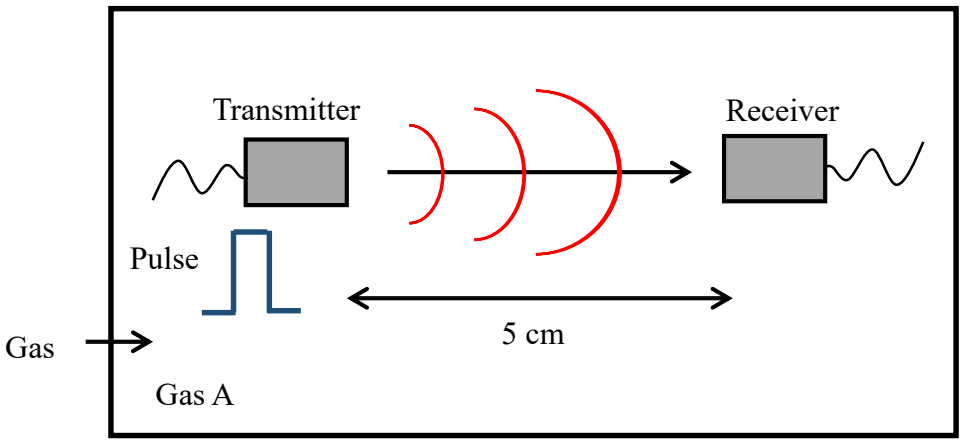

Fig. 2.1. Schematic diagram of the ultrasound detection system.

2.2.1.1. MIXED GASES MEASUREMENT FOR SAME γ AND T VALUES

The theoretical expression for the speed of sound in an ideal gas can be expressed as in eq. (2.1):

$$v = \sqrt{\frac{\gamma P}{D}} \tag{2.1}$$

where, P is the ambient pressure, D is the density of the medium and γ is the ratio of the specific heat of gas at constant pressure to that at constant volume.

The speed of sound is a unique value for each different types of gases. The principle of gas concentration measurement is based on the speed of sound variation of the ultrasound traveling inside the pipe [6], [7]. Substituting the ideal gas law ($PV=nRT$) and the definition of density, D (mass per unit volume), the velocity of sound in a gas can be expressed by eq. (2.2) [8], [9].

$$v = \sqrt{\frac{\gamma RT}{M}} \tag{2.2}$$

where, γ is the specific heat ratio, R is the gas constant 8.314 J/mol/K, T is the absolute temperature and M is the molar mass in kg/mol.

When gas B is mixed in gas A, the concentration of gas B can measure by measuring the sound velocity shift [10]. Both of gas A and gas B are considered as diatomic. Sound velocity formula for gas B mixed in gas A can be expressed as in eq. (2.3) [8].

$$v_{AB} = \sqrt{\frac{\gamma RT}{M_A(1-\rho)+M_B\rho}} \tag{2.3}$$

v_{AB} is the sound velocity of the mixed gas. M_A and M_B are molecular weights of gas A and B, respectively. ρ is the volume concentration ratio of gas B in gas A. γ, R and T are assumed to be the same for gas A and B.

When the speed of sound v, propagates a distance x, the traveling time can be expressed as $t = x/v$. If the sound velocity of gas B is faster than that of gas A, the sound velocity of mixed gas becomes faster for Δv. By using Δt, the difference of sound traveling time between gas A and mixture of gas A and B, the speed of sound v_{AB} for mixed gas can be expressed as in eq. (2.4):

$$v_{AB} = v + \Delta v = \frac{x}{t_A - \Delta t} = \frac{t_A v_A}{t_A - \Delta t} \tag{2.4}$$

By using eqs. (2.2) and (2.3), the concentration of gas B, ρ can be calculated as in eq. (2.5).

$$\rho = \frac{M_A}{M_A - M_B}\left\{1-\left(\frac{t_A-\Delta t}{t_A}\right)^2\right\} \tag{2.5}$$

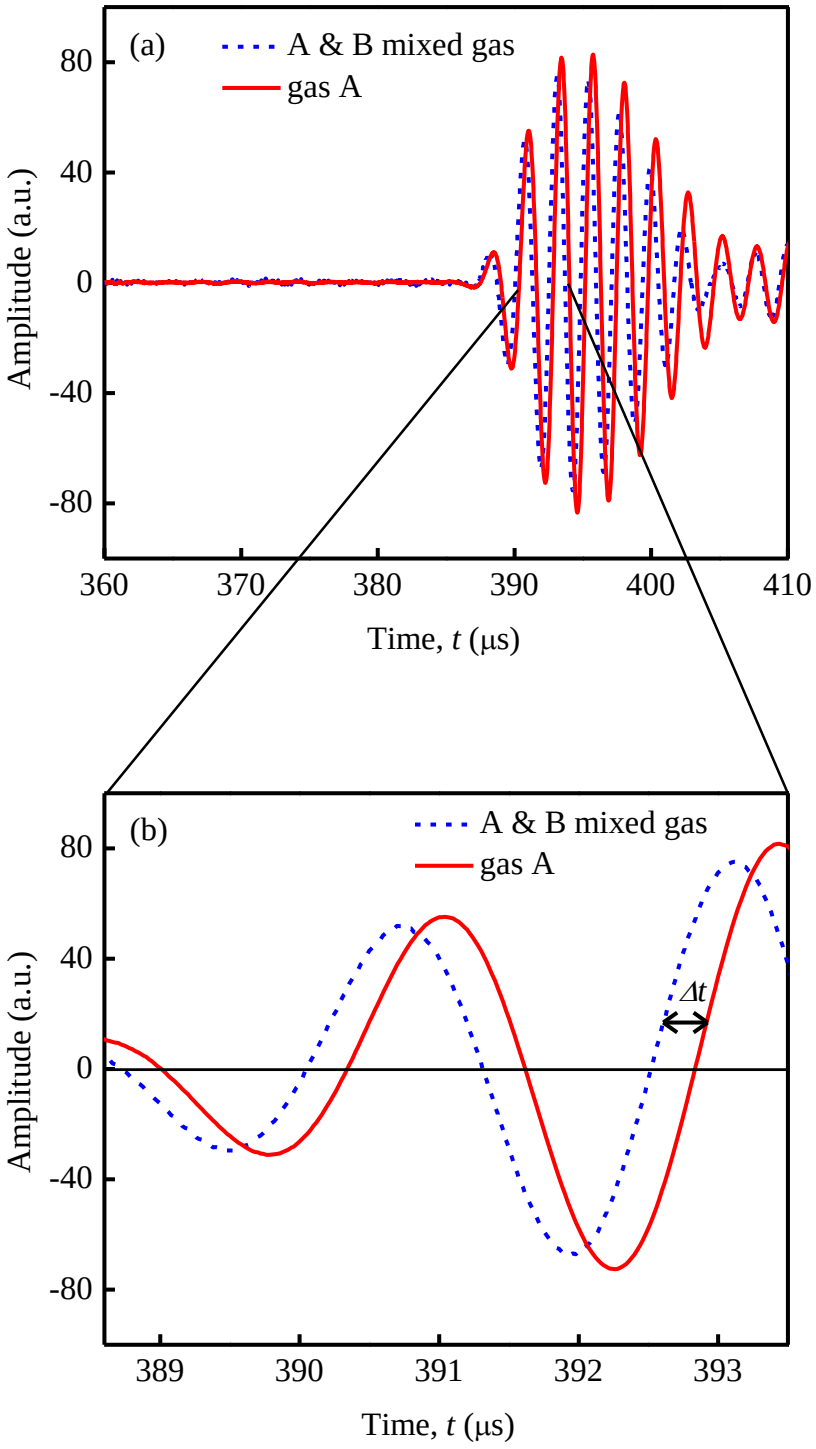

Fig. 2.2. The amplitude of the received ultrasonic signal in gas A and the mixture of gas A and gas B. Δt is the traveling time difference between gas A and the mixture of gas A and gas B [11].

Figure 2.2 shows an example of measuring sound traveling time difference, Δt. The specimen gases (assuming A= air and B= H_2) were flown in a PVC pipe that was placed horizontally. Length of the pipe was 880 mm with the inner diameter of 39 mm and PVC thickness of 2 mm. Two piezo ceramic transmitting and receiving probes were mounted on the pipe surface diagonally on the opposite sides of the pipe. The waveform of the ultrasonic signal was shifted after injecting H_2 gas. The solid line and dotted line show the waveforms of the ultrasonic wave for gas A (air) and the mixture of gas A (air) and gas B (H_2). The difference of sound traveling time between gas A (air) and mixed gas B (air) & B (H_2) is shown as Δt. Thus, the concentration of gas B (H_2), ρ can be calculated using the value of Δt as shown in eq. (2.5). Therefore, it is possible to measure and calculate the concentration of gas in a pipe using this ultrasonic method from the outside of the SUS pipe, and it does not require making any hole to extract the gases.

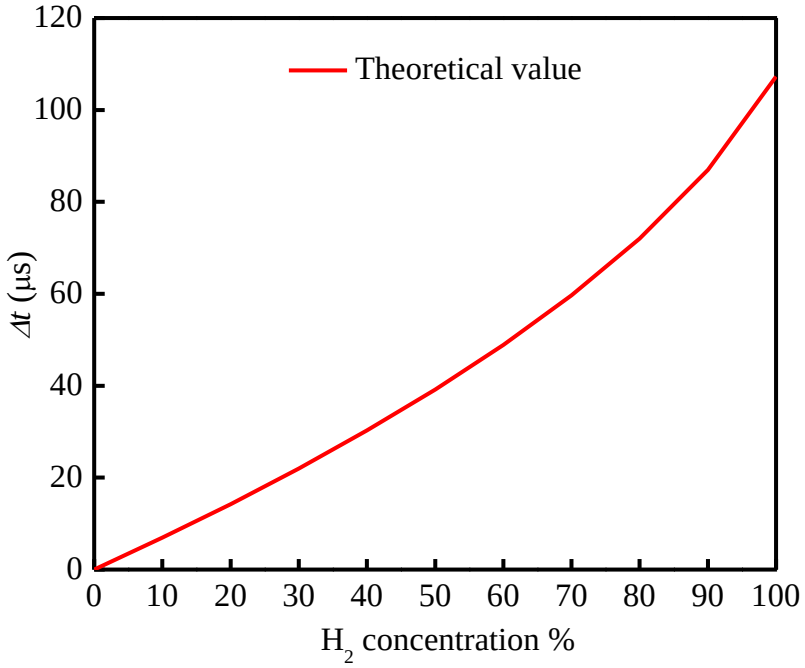

Fig. 2.3. The relation between H_2 concentration and sound traveling time difference, Δt.

Figure 2.3 shows the relation of H_2 concentration and sound traveling time, Δt difference. Red solid line shows the theoretical value of Δt according to H_2 concentration. Assuming that transducers are 50 mm apart from each other. From Fig. 2.3, it is observed that Δt is increased according to increase of H_2 concentration.

2.2.1.2. MIXED GASES MEASUREMENT FOR DIFFERENT γ AND T VALUES

In this section, γ and T are considered different for gas A and gas B where gas A and gas B are considered as diatomic and monoatomic or polyatomic gas, respectively. The sound velocity of the mixed gas of gas A and gas B is given by eq. (2.6).

$$v_{mix} = \sqrt{\frac{\gamma_{mix} RT}{M_{mix}}} \tag{2.6}$$

where, γ_{mix} is the specific heat ratio of the mixed gas, and M_{mix} is the molecular mass of mixed gas. γ_{mix} and M_{mix} are given by eqs. (2.7) and (2.8) [12], [13], respectively.

$$\gamma_{mix} = \gamma_A(1-\rho) + \gamma_B\rho \tag{2.7}$$

$$M_{mix} = M_A(1-\rho) + M_B\rho \tag{2.8}$$

where, γ_A and γ_B are the specific heat ratio of gas A and gas B, respectively. M_A and M_B are the molecular mass of gas A and gas B, respectively. ρ is the concentration (vol.%) of gas B in the mixed gas.

When the ultrasonic traveling distance is x, and the sound velocity is v, the ultrasonic traveling time is represented as $t=x/v$. Therefore, the difference of ultrasonic traveling time between gas A and the mixed gas is given by eq. (2.9) [13].

$$\Delta t = t_A - t_{mix} = \left(\frac{1}{v_A} - \frac{1}{v_{mix}} \right) x \tag{2.9}$$

Finally, the gas concentration ρ can be calculated by using eqs. (2.6) – (2.9). In this study, we made a program using the bisection method and performed concentration calculations. Specifically, first, assuming that ρ is 50%, Δt was calculated. Next, the calculated Δt was compared with the experimentally obtained Δt. From these results, the value of ρ can be assumed as a next value. This procedure was repeated to calculate the final concentration ρ.

2.2.2. ULTRASONIC WAVE PROPAGATION AT INTERFACE

The amplitude of the incident sound wave depends on the absorption and scattering effects, which is due to the variation in the speed of sound in an inhomogeneous medium. The interaction of the ultrasonic wave with the material is expressed as its acoustic impedance, which is comparable to the electrical impedance [14]. The acoustic impedance (Z) is expressed as in eq. (2.10)

$$Z = Dv \tag{2.10}$$

where Z is the acoustic impedance (kg/m^{2}s), D is the density of the medium (kg/m^3) and v is the sound velocity in the medium (m/s).

Whenever an ultrasound wave is incident on an interface formed by two materials having different acoustic impedances, some of the energy in the wave will be reflected and the remainder will be transmitted. The amplitude of the reflected wave depends on the difference between the acoustic impedances forming the interface. Consider the case of normal or perpendicular wave incidence on a flat interface as shown in Fig 2.4. Acoustic impedances of some materials and gases are given in **Table 2.1**.

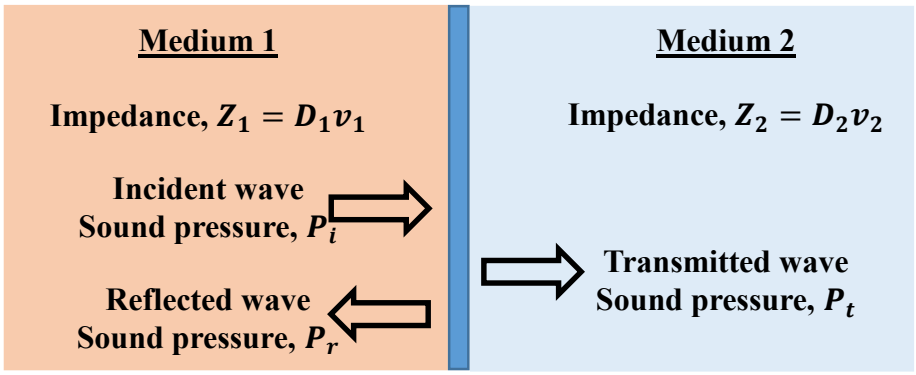

Fig. 2.4. Reflection and transmission at interface

Table 2.1. Acoustic impedances of some materials

Material	Speed of sound, c (m/s)	Density, D (kg/m^3)	Acoustic impedance, Z (kg/m^2/s)
Piezo ceramic	3880	7550	3×10^7
Stainless steel (SUS)	5900	7800	4.6×10^7
Polyvinyl chloride (PVC)	2350	1060	2.5×10^6
Air	340	1.225	4.16×10^2
Hydrogen	1310	0.089	1.16×10^2
Helium	1007	0.179	1.8×10^2
SAM	1700	2588	4.4×10^6

The ratio of the reflected pressure amplitude, P_r, to the incident pressure amplitude, P_i, is called the amplitude reflection coefficient as expressed in eq. (2.11):

$$\text{Reflection coefficient, } R_A = \frac{P_r}{P_i} = \left(\frac{Z_2 - Z_1}{Z_2 + Z_1} \right) \tag{2.11}$$

where Z_1 and Z_2 are acoustic impedances of medium 1, and 2, respectively.

The ratio of the transmitted pressure amplitude, P_t, to the incident pressure amplitude, P_i, is called the amplitude transmission coefficient as expressed in eq. (2.12):

$$\text{Transmission coefficient, } T_A = \frac{P_t}{P_i} = \frac{2Z_2}{Z_2 + Z_1} \tag{2.12}$$

The intensity is proportional to the square of the amplitude. Therefore, the intensities of the reflected (R_p) and transmitted (T_p) waves at an interface of two materials can be described as in eqs. (2.13), and (2.14), respectively [15]:

$$R_p = \left(\frac{Z_2 - Z_1}{Z_2 + Z_1} \right)^2 \tag{2.13}$$

$$T_p = \frac{4Z_1 Z_2}{\left(Z_2 + Z_1 \right)^2} \tag{2.14}$$

Therefore, the difference in acoustic impedance at the interface will control the amount of energy reflected. Conversely, if the impedances are similar, most of the energy will be transmitted. The reflectance and transmittance of sound between two medium are calculated using eqs. (2.13), and (2.14), respectively. The values are given in **Table 2.2**.

Table 2.2. Transmittance and reflectance of sound between two medium

Material	Reflectance, %	Transmittance, %
Piezo ceramic to SUS	2.19	97.80
Piezo ceramic to PVC	70.10	29.8
Piezo ceramic to air	99.99	0.004
Piezo ceramic to H_2	99.99	0.001
Piezo ceramic to SAM	59.87	40.12
SUS to air	99.99	0.003
SUS to SAM	68.40	31.59
SAM to air	99.96	0.03
Air to H_2	34.12	65.87

2.2.3. THE FINITE-DIFFERENCE-TIME-DOMAIN (FDTD) METHOD

The finite-difference time-domain (FDTD) method was first introduced by Yee in 1966 [16] for electromagnetic wave propagation and is hence sometimes referred to as the Yee scheme This simple and efficient method has been applied to a wide range of acoustic wave propagation problems [17]. The FDTD method includes an acoustic FDTD method and elastic FDTD method. The acoustic FDTD method is the combination of a continuous expression of sound pressure and an equation of motion. The elastic FDTD method is the combination of Hooke's law and equation of motion. When a force is applied to a particle, the particle moves by the force and the behavior can be described by the equation of motion. Figure 2.5 shows a particle having dimensions of ΔX, ΔY, ΔZ and D is the density [kg/m^3] of the medium. u_x, u_y, u_z are the particle velocities [m/s] in X, Y, Z directions, respectively and p is the sound pressure [Pa].

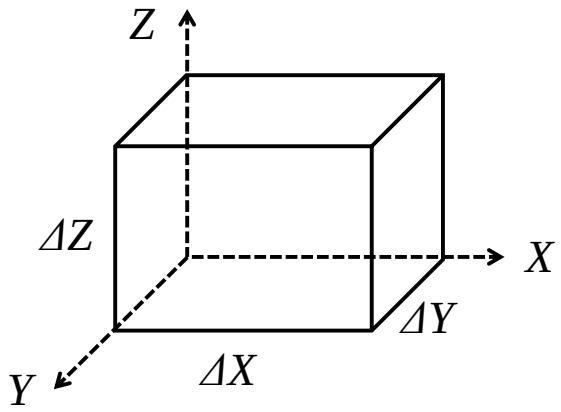

Fig. 2.5. Diagram of a particle.

Sound propagation in the SUS pipe is described by two kinds of differential equations, Euler's equation and the equation of continuity [18]. Euler's equation can be expressed as eqs. (2.15)-(2.17):

$$D\frac{\partial u_X}{\partial t}+\frac{\partial p}{\partial X}=0 \tag{2.15}$$

$$D\frac{\partial u_Y}{\partial t}+\frac{\partial p}{\partial Y}=0 \tag{2.16}$$

$$D\frac{\partial u_Z}{\partial t}+\frac{\partial p}{\partial Z}=0 \tag{2.17}$$

The change of volume, ΔV (m^3) of the particle can be expressed as eq. (2.18):

$$\Delta V=\left(\frac{\partial u_X}{\partial X}+\frac{\partial u_Y}{\partial Y}+\frac{\partial u_Z}{\partial Z}\right)\Delta Z\Delta Y\Delta Z \tag{2.18}$$

On the other hand, if V (m^3) is the volume before deformation and k_e is the volume modulus of elasticity [N/m^2], the sound pressure is determined from the definition formula of the bulk modulus can be expressed as eq. (2.19).

$$p=-k_e\frac{\Delta V}{V} \tag{2.19}$$

The equation of continuity can be expressed as eq. (2.20) by substituting eq. (2.18) into eq. (2.19):

$$\frac{\partial p}{\partial t}+k_e\left(\frac{\partial u_X}{\partial X}+\frac{\partial u_Y}{\partial Y}+\frac{\partial u_Z}{\partial Z}\right)=0 \tag{2.20}$$

The basic formula of elastic FDTD method are:

$$[C]\cdot\nabla_s[U]=-\frac{\partial}{\partial t}[-T] \tag{2.21}$$

$$D\cdot\frac{\partial}{\partial t}[U]=-\nabla\cdot[-T] \tag{2.22}$$

$$[T]=[T_1T_2T_3T_4T_5T_6]^t \tag{2.23}$$

$$\nabla\cdot=\begin{bmatrix}\frac{\partial}{\partial X} & 0 & 0 & 0 & \frac{\partial}{\partial Z} & \frac{\partial}{\partial Y}\\ 0 & \frac{\partial}{\partial Y} & 0 & \frac{\partial}{\partial Z} & 0 & \frac{\partial}{\partial X}\\ 0 & 0 & \frac{\partial}{\partial Z} & \frac{\partial}{\partial Y} & \frac{\partial}{\partial X} & 0\end{bmatrix} \tag{2.24}$$

$$\nabla\cdot=[\nabla\cdot]^t \tag{2.25}$$

Here, [-*T*] is a negative stress vector, [*C*] is the stiffness tensor, and [*U*] is the velocity of the particle. Stress is originally 3 × 3 tensor quantity, but considering the balance of moments, stress tensor is represented by a vector of T_1 to T_6 because the independent element of stress tensor is only 6 components. T_1 to T_3 are normal stress and T_4 to T_6 are shear stress. Both the longitudinal and transverse waves propagate in solid, whereas only longitudinal wave propagate in gas. Therefore, there is a term of stress tensor in the elastic FDTD. However, only longitudinal wave is considered here for the FDTD simulation. The sound pressure and the particle velocity continuously change with respect to space and time. For the finite difference approximation, a central difference approximation can be expressed as in eq. (2.26).

$$\frac{\partial f(X)}{\partial X}\approx\frac{f\left(X+\frac{\Delta X}{2}\right)-f\left(X-\frac{\Delta X}{2}\right)}{\Delta X} \tag{2.26}$$

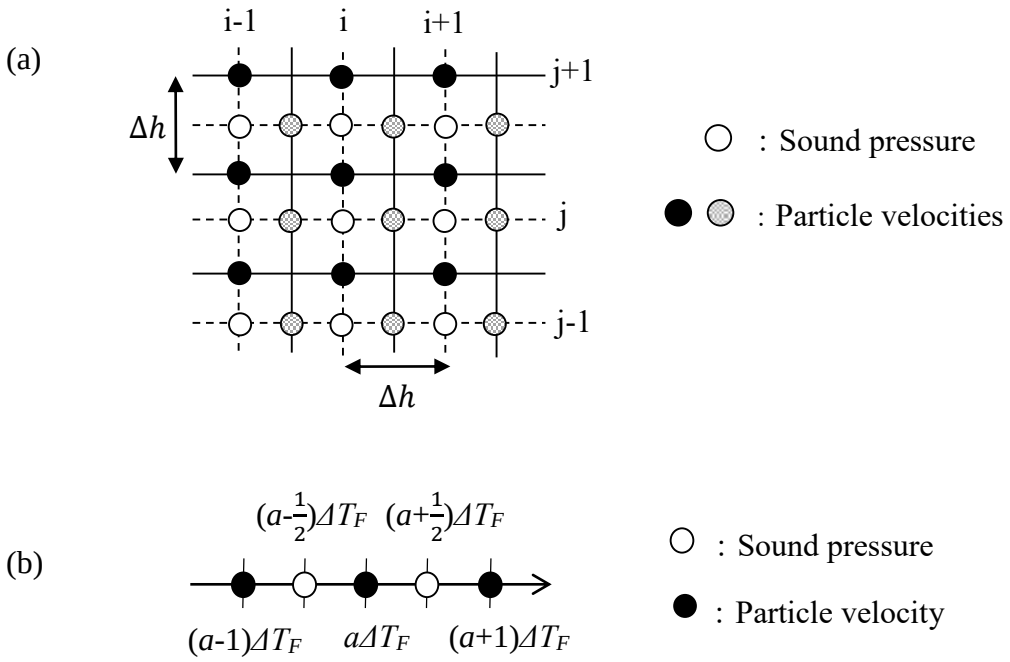

Fig. 2.6. Modeling of particles for different finite-difference-time-domain (FDTD) method. (a) The 2-D spatial arrangement of sound pressure and particle velocities. (b) Temporal arrangement of sound pressure and particle velocities [19].

For example, Fig. 2.5 shows the sound propagation directions in the particle. As shown in Fig. 2.5, sound is propagating to the *X*-axis and *Y*-axis. However, assuming that sound is not propagating to the *Z*-axis of the SUS pipe that is the vertical direction as shown in Fig. 2.5. Figure 2.6(a) shows the sound pressures are defined in the middle of each cell and the particle velocities on the faces in their respective coordinate direction. Considering i and j are the spatial step and the spatial discrete width, Δh, which is the same in *X* and *Y* directions. Spatial definition points of sound pressure and particle velocities are set at a half grid apart from each other. As shown in Fig. 2.6(b) their temporal definition points are also a half time step apart from each other. Here a discrete time interval is ΔT_F and a is the time step, which usually keeps the half grid. When a physical quantity is expressed as q on a spatial grid point $(X, Y, Z) = (ih, jh, kh)$ at time $a\Delta T_F$, this

is described as $q_{i,j}^{a}$. Thus, the particle velocities and sound pressure can be expressed as $u_{X}{}^{a}_{i+\frac{1}{2},j}, u_{Y}{}^{a}_{i,j+\frac{1}{2}}, p_{i,j}^{a+\frac{1}{2}}$.

$$u_{X}{}^{a+1}_{i+\frac{1}{2},j} = u_{X}{}^{a}_{i+\frac{1}{2},j} - \frac{\Delta T_F}{D\Delta h}\left(p_{i+1,j}^{a+\frac{1}{2}} - p_{i,j}^{a+\frac{1}{2}} \right) \tag{2.27}$$

$$u_{Y}{}^{a+1}_{i,j+\frac{1}{2}} = u_{Y}{}^{a}_{i,j+\frac{1}{2}} - \frac{\Delta T_F}{D\Delta h}\left(p_{i,j+1}^{a+\frac{1}{2}} - p_{i,j}^{a+\frac{1}{2}} \right) \tag{2.28}$$

$$p_{i,j}^{a+\frac{1}{2}} = p_{i,j}^{a-\frac{1}{2}} - \frac{k_e \Delta T_F}{\Delta h}\left[\left(u_{X}{}^{a}_{i+\frac{1}{2},j} - u_{X}{}^{a}_{i-\frac{1}{2},j} \right)\left(u_{Y}{}^{a}_{i,j+\frac{1}{2}} - u_{Y}{}^{a}_{i,j-\frac{1}{2}} \right) \right] \tag{2.29}$$

From (2.27)-(2.29), features of the FDTD method can be found. The particle velocity can be calculated from past particle velocity and sound pressure, while sound pressure can be calculated from past sound pressure and particle velocity. Therefore, it is necessary to store only a one-time step of each field by updating the pressure first and then the velocity.

2.3. Experimental Setup for the Measurement of Non-flowing H_2 Gas Concentration

This experimental setup is to measure the H_2 gas concentration by using ultrasound from the exterior of the SUS pipe. Figure 2.7(a) shows a schematic diagram of the experimental setup. The length of a cut SUS pipe was 130 mm with an inner diameter of 267 mm and a thickness of 4 mm. Figure 2.7(b) shows the photograph of the experimental SUS pipe. Two piezo ceramic transmitting and receiving probes (Japan Probe Co. LTD) having the surface area of 20 mm x 15 mm were mounted on the pipe surface diagonally on the opposite sides of the pipe as shown in Fig. 2.7(a). Pipe surfaces were made flat for attaching the transducers. A sonic gel was placed between the transducers and the pipe. As shown in Fig. 2.7(c). In Fig. 2.7(c) the circulating ultrasonic wave inside the SUS pipe is expressed as signal ‘NS’ and the ultrasonic wave traveling airborne of the pipe is expressed as signal ‘AS’. To observe the airborne ultrasonic signal ‘AS’, SAM was pasted on the surface of the SUS pipe as shown in Fig. 2.7(c). Furthermore, 100% N_2 gas was replaced by a 95% N_2+5.0% H_2 gas through a thin pipe inserted into the SUS pipe with a flow rate of 0.5 L/min for 2 hours. Lids were placed on the top and bottom end of the pipe.

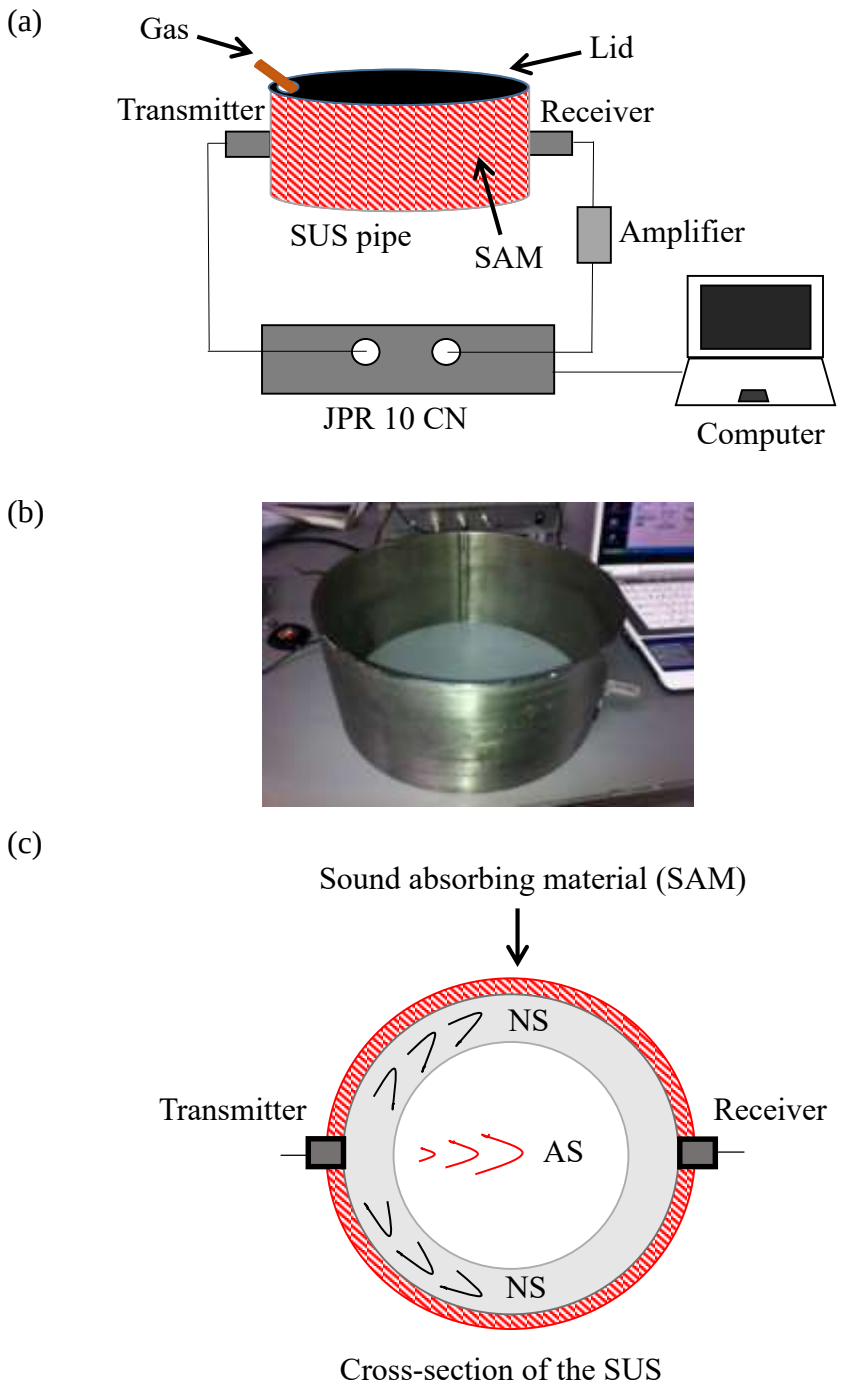

Fig. 2.7. Gas concentration measurement system for stainless steel (SUS) pipe using ultrasound. (a) A schematic diagram of the experimental setup. (b) Photograph of the stainless steel (SUS) pipe. (c) SAM (red shaded portion) is pasted on the surface of the SUS pipe. 'AS' is the airborne ultrasonic signal, and 'NS' is the ultrasonic signal which is circulating inside the SUS pipe itself [19].

2.4. Results and Discussion

2.4.1. Observation of Ultrasonic Signal in Air

An experiment was conducted to observe the airborne signal in the air. Figure 2.8 shows a schematic diagram of the experimental setup. Transmitting and receiving probes were 267 mm apart from each other in the air. The acoustic impedances of the piezo ceramic transmitter and air are given in **Table 2.1**. Ultrasonic signal was transmitted at ceramic-air interface and transmittance of the signal was calculated as 0.004% by using eq. (2.14) from the transmitter to the air. Since the signal was directly transmitted from the transmitter to the air, the airborne signal should be observed in the air even though the transmittance is small. Figure 2.9 shows the experimental result of the received signal amplitude in air. According to the calculation, the airborne signal is observed clearly around 750 to 800 μs in air as shown in Fig. 2.9.

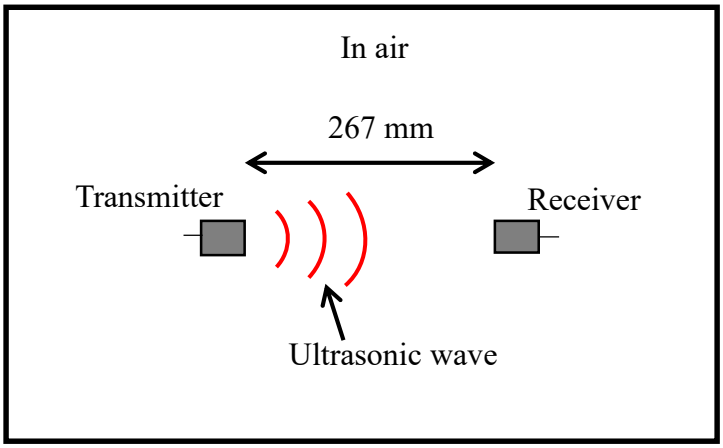

Fig. 2.8. A schematic diagram of the experimental setup for the observation of airborne ultrasonic signal in air.

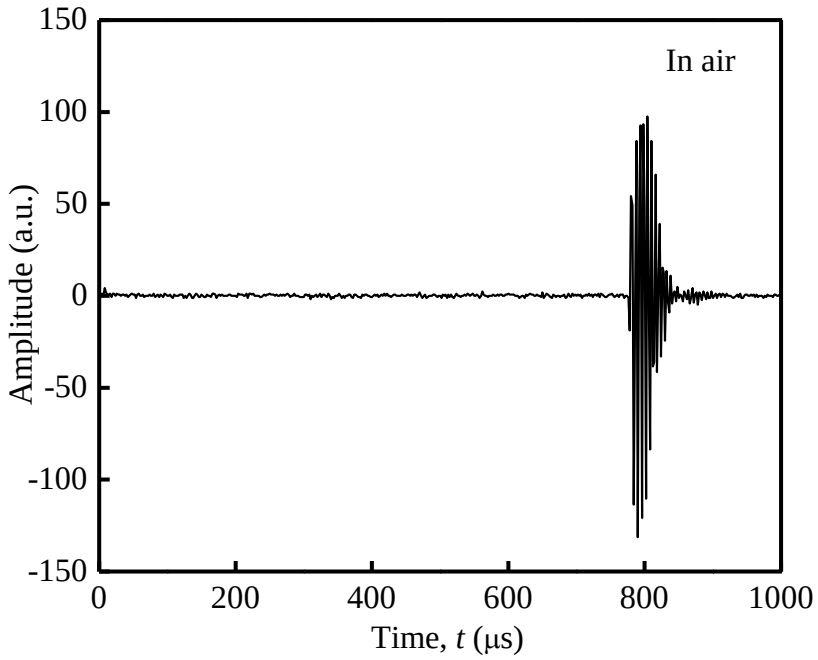

Fig. 2.9. The received signal amplitude of ultrasound passing through the air.

2.4.2. SIMULATION RESULT OF ULTRASONIC WAVE TRAVELING THROUGH A SUS PIPE

To observe the ultrasonic signal propagation in the SUS pipe wall, the signal was visualized by using FDTD simulation method. Figure 2.10 shows the modeling an FDTD simulation results of the two-dimensional sound propagation inside the SUS pipe. Red color represents the high sound pressure of the sound wave. The airborne ultrasonic signal 'AS' is not shown here. An ultrasonic signal pulse is transmitted from a transmitter and divided into two vertical directions in the pipe and propagating upwards and downwards in the pipe as shown in Fig. 2.10(a). One can see the frontends of the traveling signals as well as following reflected signals from the inner pipe surfaces interfering each other. Figure 2.10(b) shows both sound waves reach to the other side of the pipe where the receiver is located. This is when one starts receiving the signals at the receiver at around 100 μs as shown in Fig. 2.12. Figure 2.10(c) shows the signal after passing the receiver position and going back to the original point. One can see the frontends interfering with the other

reflected signals. The two signals keep circulating inside the pipe. After a long time interfering each other, one cannot see the frontends any more as shown in Fig. 2.10(d). FDTD simulation results more or less match with the experimental result of received signal amplitude as shown in Fig. 2.12. FDTD simulation method was also used to find a way to attenuate this ultrasonic wave circulating in the SUS pipe. It may possible to reduce this noise type signal circulating in the SUS pipe by interference.

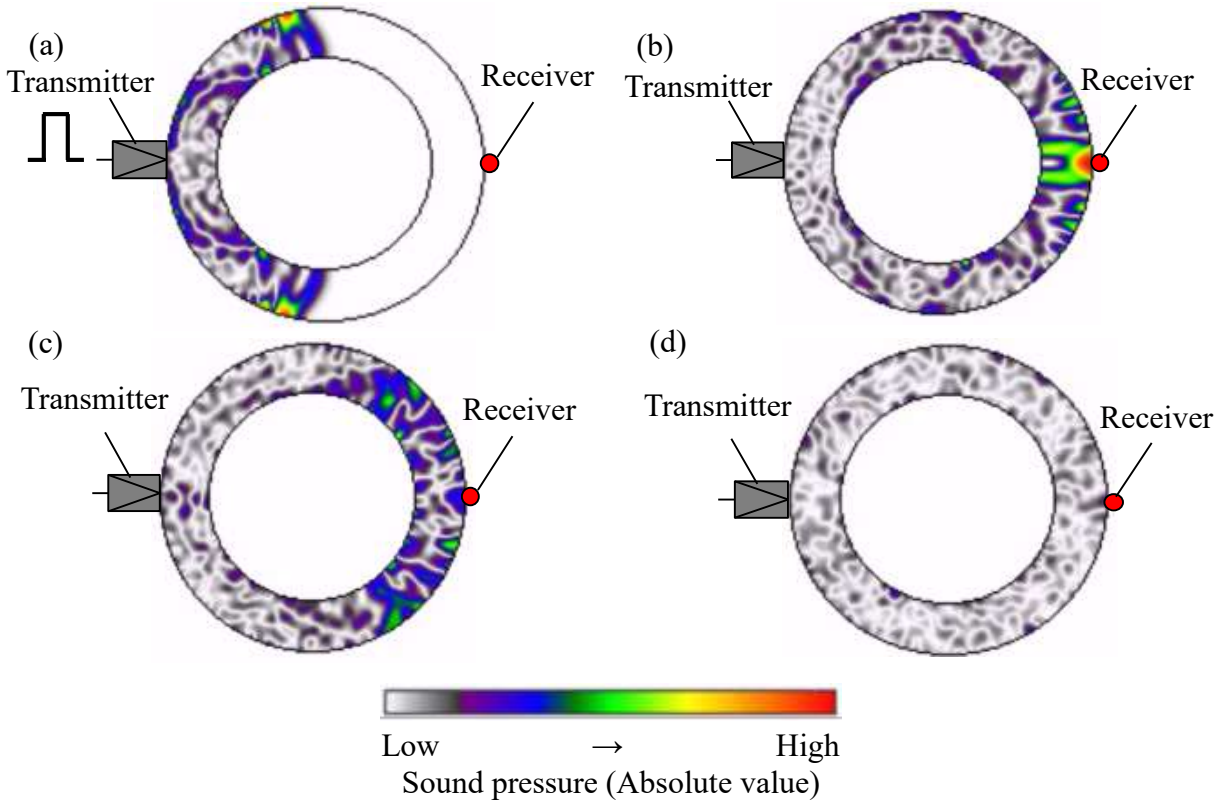

Fig. 2.10. Simulation views of propagating ultrasound inside a SUS pipe using different finite difference-time-domain (FDTD) method. (a) Right after a pulse of ultrasound is emitted from a transducer. (b) Two sound waves are propagating upward and downward reaching to the receiver. (c) Two sound waves are passing the receiver position circulating and interfering with other signals. (d) An echo of a sound circulating after a while and interfering each other [19].

2.4.3. EXPERIMENTAL RESULT OF ULTRASONIC SIGNAL THROUGH A SUS PIPE

An experiment was conducted to observe the propagation of ultrasonic signal through SUS pipe. Figure 2.11 shows a schematic diagram of the experimental setup. A cut SUS pipe having 130 mm in length, 267 mm in inner diameter and a thickness of 4 mm was used for the experiment as showed in Fig. 2.7(b). Transmitter and receiver were attached to the exterior of the SUS pipe. The transducer voltage and gain were set as 10 V and 0 dB, respectively, during this experiment.

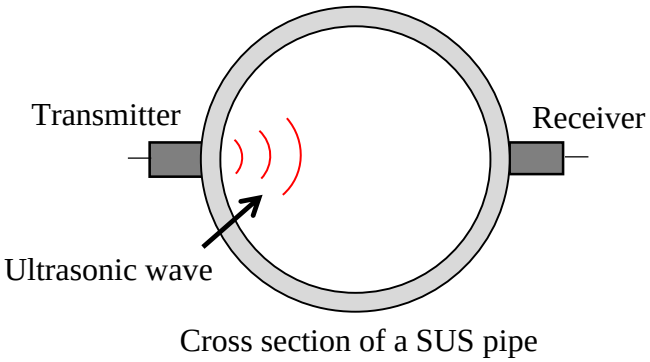

Fig. 2.11. Schematic diagram of the experimental setup for the observation of airborne signal through pipe.

Propagation of sound through a SUS pipe depends on the transmittance of sound from the transmitter to the SUS pipe. The acoustic impedances of the piezo ceramic transmitter, SUS, and air are given in **Table. 2.1**. The transmittance of the signal was calculated as 95.5% by using eq. (2.14) from the transmitter to the SUS pipe. Therefore, almost all the signals are transmitted and strongly circulated in the pipe wall. Furthermore, from the SUS pipe to the air only 0.003% of the signal is transmitted. Since the transmittance of ultrasonic signal from SUS to air is small enough comparing that from the transmitter to SUS, observation of airborne signal will be difficult from the exterior of the SUS pipe. Figure 2.12 shows the experimental result of the received ultrasonic signal through the SUS pipe. As shown in Fig. 2.12, the ultrasonic wave is circulating inside the SUS pipe and last for a long time like in a bell. Propagation of ultrasound wave in SUS pipe was also simulated by the FDTD method that could explain the ultrasound propagation signals in the SUS pipe.

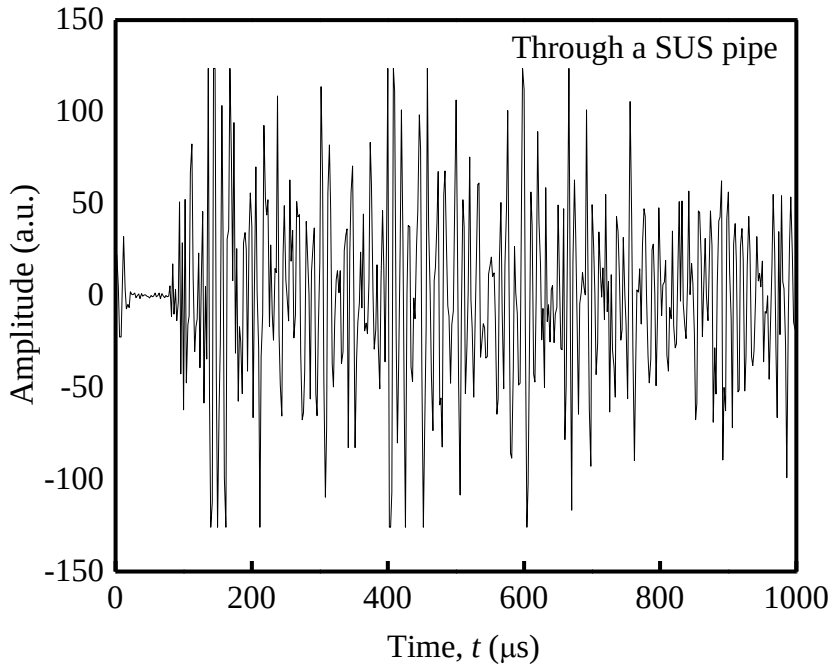

Fig. 2.12. The received signal amplitude of ultrasound passing through a SUS pipe. Transducer voltage and gain were set as 10 V and 0 dB, respectively during this experiment. The observed signal 'NS' is kept circling inside the SUS pipe [19], [20].

2.4.4. NOISE CANCELATION WITH SOUND ABSORBING MATERIAL (SAM)

This section is discussed about a way of noise cancelation of the pipe. Above result shows, that observation of airborne signal is difficult from the exterior of the SUS pipe. However, a SAM was explored, which can reduce the noise signal by pasting on the pipe surface. It is important to reduce the 'NS', which is shown in Fig. 2.7(c) and observe only the airborne signal 'AS' to measure the gas concentration. To observe the airborne signal, it is important to absorb the noise signal 'NS' by pasting the SAM.

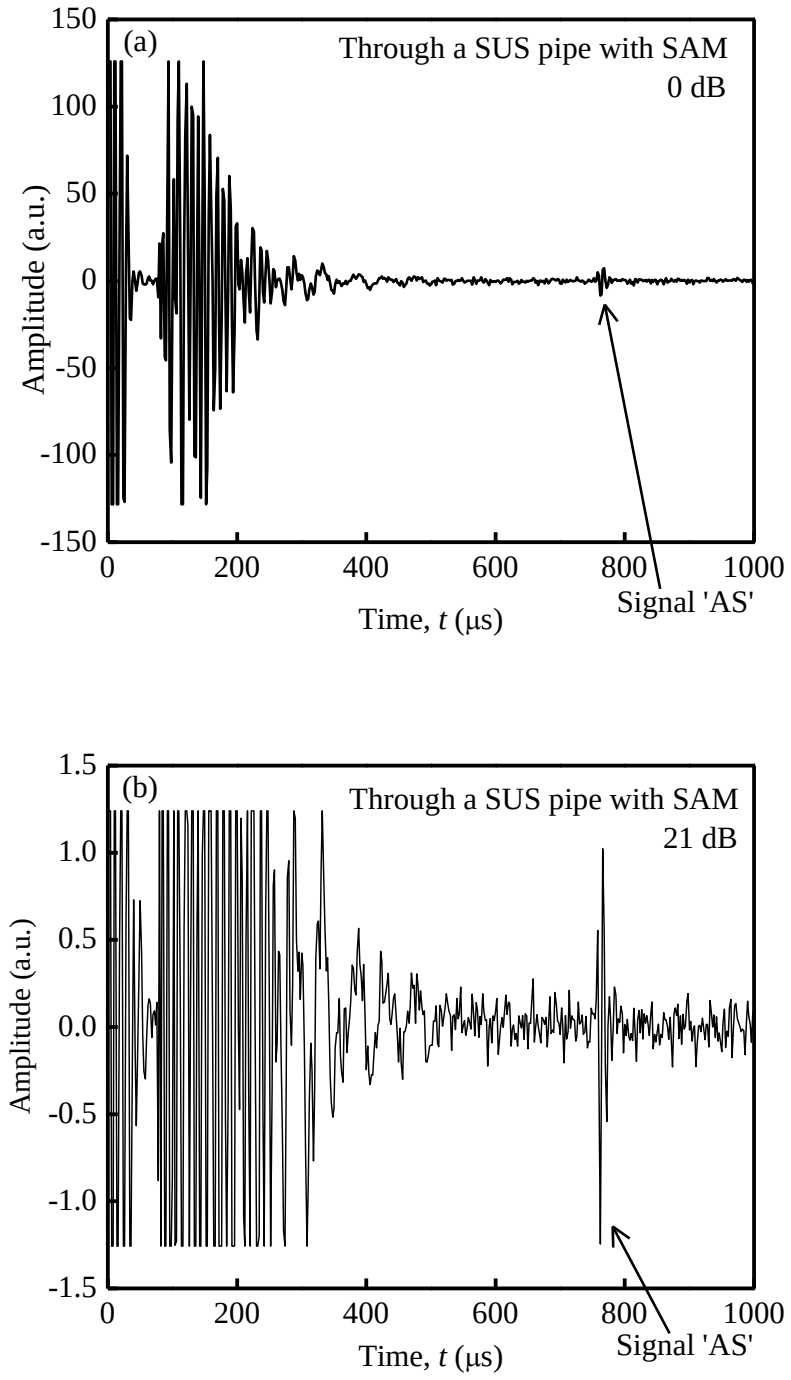

Fig. 2.13. Received signal amplitude of ultrasound after pasting SAM on the pipe surface. The signal ‘AS’, traveling in airborne of the SUS pipe, is observed. The transducer voltage was 300 V and gain were set as (a) 0 dB and (b) 21 dB to observe the enlarged view of signal ‘AS’ [19].

Clay was pasted as a SAM on the surface of the SUS pipe. The acoustic impedances of the piezo ceramic transmitter, SUS, air, and clay are 3×10^7 kg/m^2/s, 4.6×10^7 kg/m^2/s, 4.16×10^2 kg/m^2/s, and 4.4×10^6 kg/m^2/s, respectively. The transmittance of the signal was calculated as 95.5% by using eq. (2.14) from the transmitter to the SUS pipe. Therefore, almost all the signals were transmitted and strongly circulated in the pipe wall as shown in Fig. 2.12. Furthermore, from the SUS pipe to the air, only 0.003% of the signal is transmitted. Since the transmittance of ultrasonic signal from SUS to air is small enough comparing that from the transmitter to SUS, observation of airborne signal will be difficult from the exterior of the SUS pipe. After pasting SAM on the pipe surface, the transmitted signals were calculated according to eq. (2.14) from the transmitter to SAM and SAM to SUS pipe and the values are 44% and 32%, respectively. That means SAM could absorb the noise signal of the pipe and it is possible to observe the airborne signal from the exterior of the SUS pipe. SAM was pasted on the surface of the pipe as shown in Fig. 2.7(c). As a result, the signal 'NS' traveling around the SUS pipe was suppressed, and therefore the signal 'AS' traveling airborne of the pipe can be detected at around 780 μs as shown in Fig. 2.13(a). In Fig. 2.12(a), the transducer voltage and gain were set as 10 V and 0 dB, respectively. Figure 2.13(b) indicates the enlarged view of signal 'AS' To observe the enlarged view of signal 'AS' as shown in Fig. 2.13(b), gain and voltage of a receiver were set as 21 dB and 300 V, respectively. The noise signal was canceled for approximately 50 dB by pasting SAM on the surface of the pipe. In this case, the S/N ratio is approximately 5 dB. This airborne signal 'AS' is used to measure the gas concentration. The signal observed at the earlier traveling time < 400 μs in Figs. 2.13(a) and (b) were due to the signal 'NS' circulating inside the SUS pipe itself. Therefore, by pasting SAM on the surface of the SUS pipe, this signal 'NS' is suppressed, and the airborne signal 'AS' is possible to observe from the exterior of the SUS pipe.

2.4.5. Measurement of Non-flowing Gas Concentration from the Exterior of the SUS Pipe

In the above section, we were able to reduce the noise signal and observe the airborne signal from the exterior of the SUS pipe. In this section, we are conducted an experiment to measure H_2 gas concentration from the exterior of the SUS pipe. For a practical test, 100% N_2 gas was replaced

by 95% N_2+5.0% H_2 gas in a pipe, and the concentration of H_2 gas was measured by using ultrasound. The waveform of the ultrasonic signal was shifted after replacing 95% N_2+5.0% H_2. In Fig. 2.14, red line shows the received ultrasound signal for 100% N_2 gas. The blue line shows the received ultrasound signal for 95% N_2+5.0% H_2 gas which was flown and replacing for 2-hours. From the measurement of Δt, in Fig. 2.15, the H_2 gas concentration was calculated as 4.6% using eq. (2.5). It was estimated that with only 2-hours gas flow replacement, H_2 concentration did not reach to 5.0%.

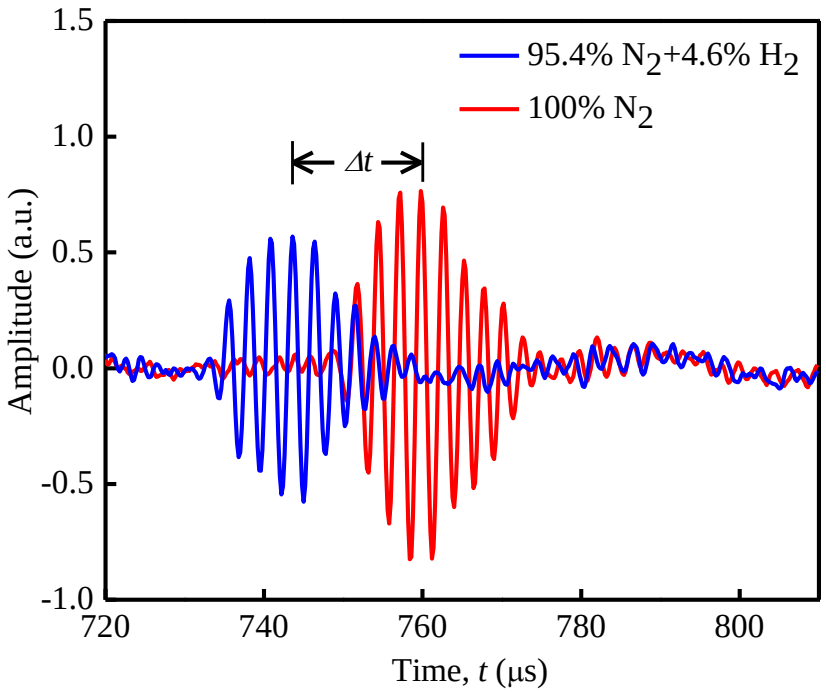

Fig. 2.14. Received signal amplitude of ultrasound for measuring H_2 concentration in N_2 gas. The red line is for 100% N_2 gas, and the blue line is for N_2+H_2 mixed gas. Δt is the sound traveling time difference between 100% N_2 and N_2+H_2 mixed gas [2], [19].

The change of temperature was compensated for the speed of sound, and the H_2 concentration was obtained accurately even if the temperature varied according to eq. (2.9). Since there was no hole in the pipe for measuring the gas concentration and temperature, the temperature was considered to be similar to the temperature of the pipe surface. In this research, temperature variation can be considered and corrected in the calculation using eq. (2.9). In eq. (2.5), it is

assumed that the temperature will not change when H_2 is mixed in N_2. In this experiment, if the temperature changes for 1ºC, Δt becomes approximately 1.5 μs so that the error in gas concentration is about 0.39%. This value is small enough in case of high concentration measurement. The gas concentration is not influenced by the change of pressure, as the pressure does not affect the sound speed [20]. It was shown that the concentration of gas is possible to measure from the exterior of the SUS pipe.

2.4.5.1. MEASUREMENT ERROR DUE TO THE NATURAL SOUND DRIFT

The measurement error due to the drift was studied. Though the gas was in a static state, a small fluctuation of signal was observed during recording. A PVC pipe having the length of 880 mm with the inner diameter of 39 mm and thickness of 2 mm was considered for this experiment. Transmitter and receiver were placed on the exterior of the pipe and signal can pass through the PVC pipe. Since the ends of the pipe were open during measurement, the natural airflow was coming inside the pipe and the fluctuation of the signal was observed. Therefore, the measurement error was calculated. Figure 2.15(a) shows 50 waveforms for the airflow at a speed of 0 m/s. A third peak of the signal is shown in a red square in Fig. 2.15(a) was chosen to calculate the sound traveling time difference Δt. The enlarged view of the third peak is shown in Fig. 2.15(b). The reading of time for measuring the Δt was taken at the intercept of zero intensities of the third wave. Δt was calculated approximately 0.1 μs that is about 0.06% in H_2 concentration due to the natural sound drift.

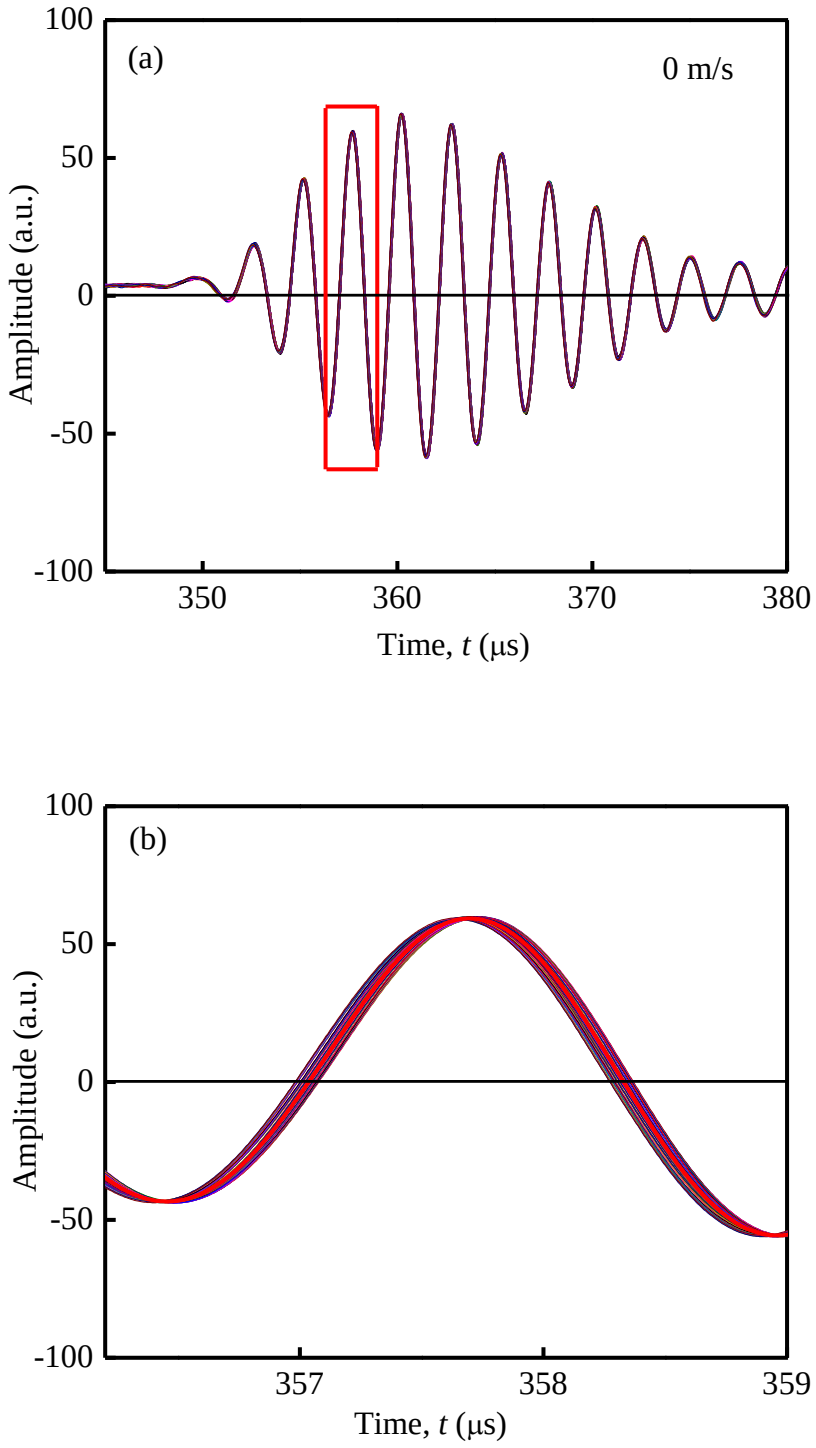

Fig. 2.15. (a) 50 waveforms of the received sound signal at 0 m/s airflow rate. Fluctuation of the signal. (b) An enlarged view of a third peak in (a). A red line is the average of the 50 waveforms.

2.4.6. Noise Cancelation with Two Transmitters

2.4.6.1. Simulation Layout and Results Using Two Transmitters

Figure 2.16 shows the simulation model layouts using and two transmitters having one receiver. The simulated received signal amplitude from one transmitter is shown in Fig. 2.17(a), which is more or less similar to the experimental result as showed in Fig. 2.12. In the simulation, the transmitters were considered having the same amplitudes. Figure 2.17(b) shows the simulated received signal amplitude for the condition of using two transmitters where the ultrasonic waves interfere with each other and cancel out the sound signal 'NS'. It was possible to reduce the noise signal 'NS' above 400 μs using two transmitters. According to this FDTD simulation method, Fig. 2.17(b) shows that signal 'NS' is reduced after 600 to 700 μs by using two transmitters. It was proved by this simulation that it is possible to reduce this noise type signal circulating in the SUS pipe by interference.

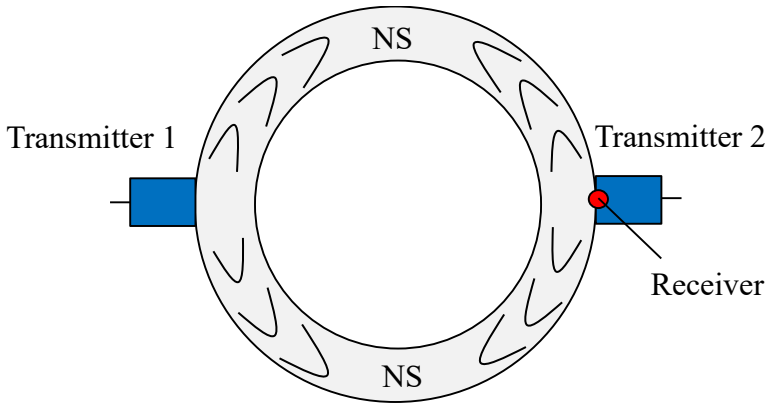

Fig. 2.16. Simulation model layout using two transmitters and one receiver [19].

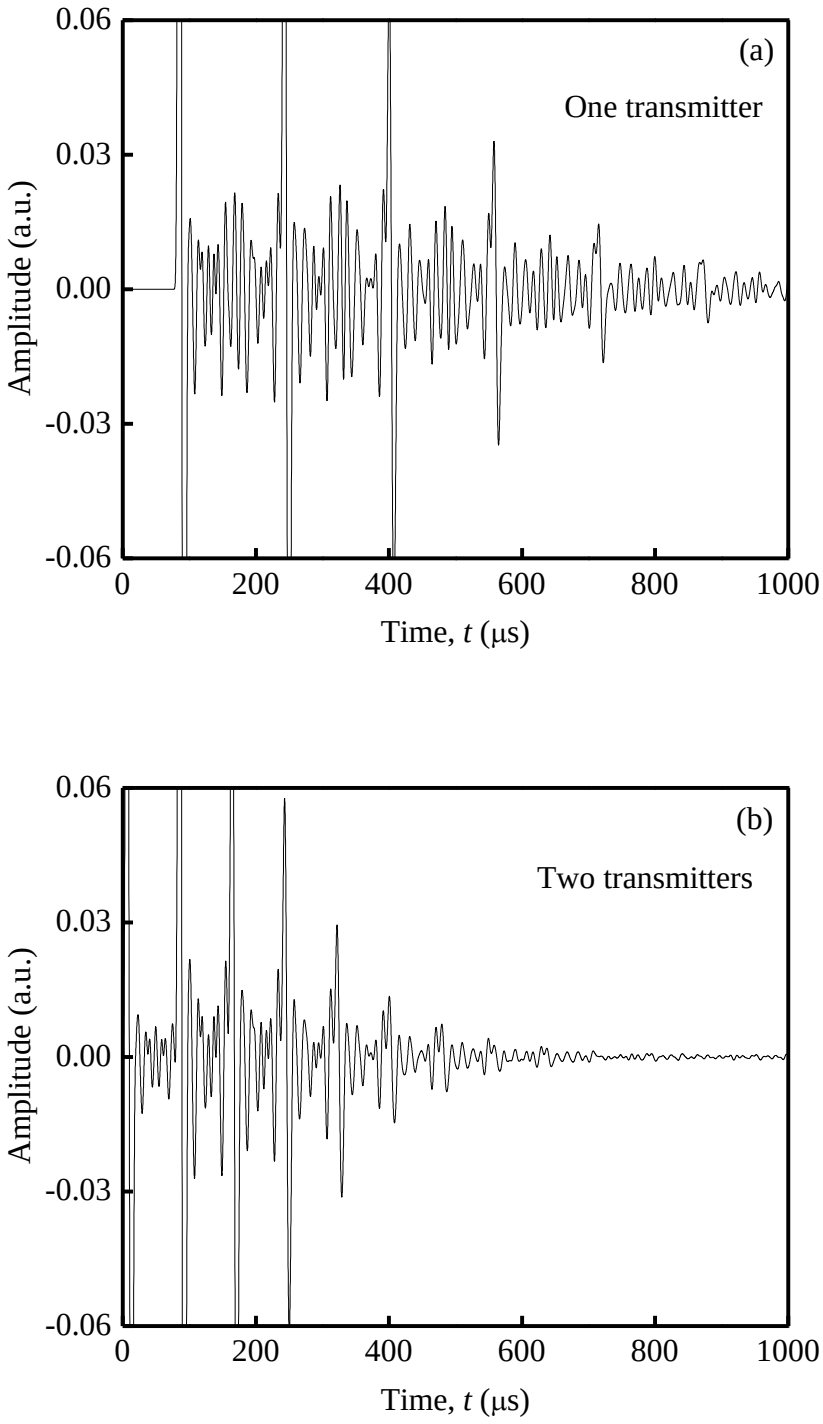

Fig. 2.17. Simulated received ultrasound signal amplitudes for (a) one transmitter condition and (b) two-transmitters condition. Sound waves are interfering each other and decrease after about 400 μs for the two-transmitter condition [19].

2.4.6.2. EXPERIMENTAL RESULT USING TWO TRANSMITTERS

The experimental setup and the result using one transmitter was discussed in section 2.4.3. The received signal amplitude using one transmitter was showed in Fig. 2.12 where the ultrasonic wave was circulating inside the SUS pipe and last for a long time like a bell. In this section, an experiment was conducted using two transmitters to reduce the ultrasonic noise for a practical pipe. Figure 2.18 shows a schematic diagram of the experimental setup to measure the received signal amplitude using two-transmitters. The receiver was attached at the same side of the transmitter 2. Since it is difficult to attach transmitter 2 and receiver exactly at the same position, the receiver was attached at the bottom of transmitter 2.

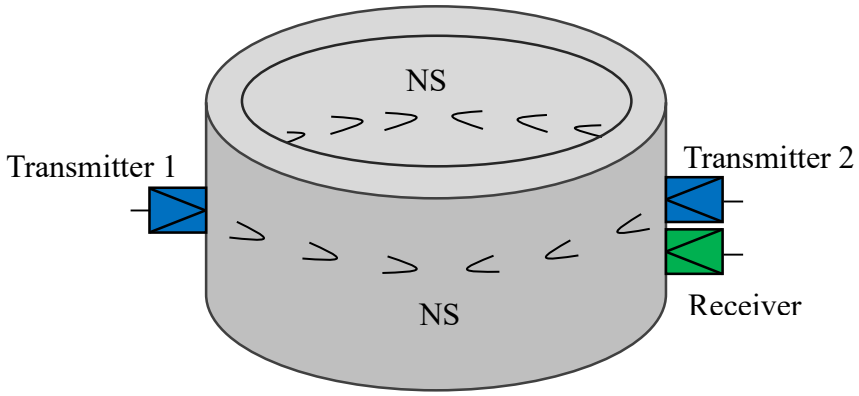

Fig. 2.18. A schematic diagram of the experimental setup using two transmitters and one receiver.

Figure 2.19 shows the experimental received signal amplitude for the condition of using two transmitters where the ultrasonic waves interfere with each other however; the signals do not cancel out the sound signal 'NS'. The result showed in Fig. 2.17(b) by simulation was not achieved in experiment as shown in Fig. 2.19. Signal cancelation using two transmitters is somewhat difficult to achieve in practice. The deviation of experimental result from the simulation might be due the difference of amplitudes of the transmitters. To achieve this the two transmitters' amplitudes and frequencies have to be exactly the same, and this is somewhat difficult to control in practice. The signal cancelation is affected by the temperature change. When the temperature is different, the sound speed will change, and the cancellation will change.

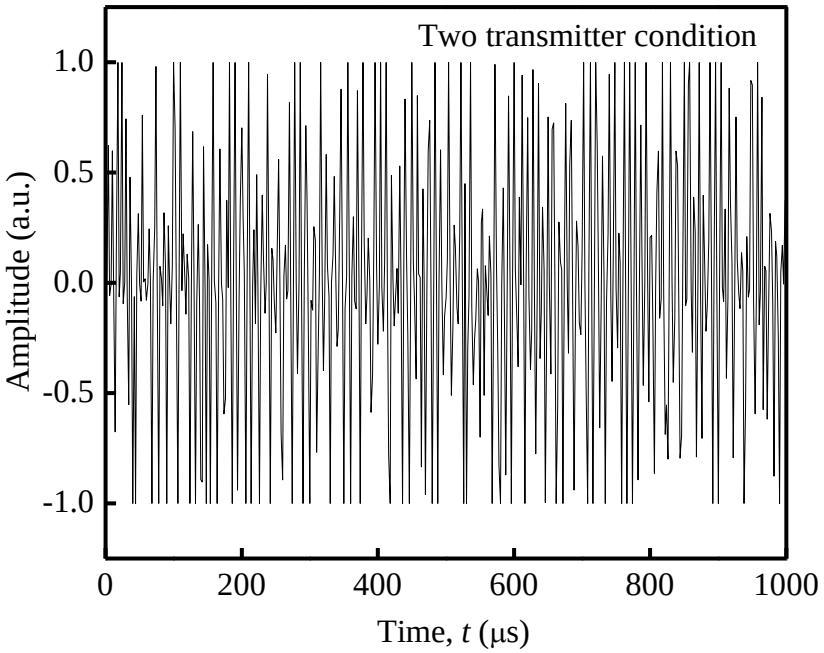

Fig. 2.19. Experimental received ultrasound signal amplitudes for two-transmitter condition. Sound waves are interfering each other however does not decrease after about 400 μs for the two-transmitter condition.

2.4.7. INVESTIGATE THE REASON OF EXPERIMENTAL RESULT DEVIATION FROM THE SIMULATION

The two-transmitters' condition was considered to reduce the signal amplitude on the above section. However, the simulated and experimental results did not match each other. This section is discussed the probable reason of the mismatch in simulation and experimental results.

2.4.7.1. SIGNAL AMPLITUDE OF TRANSMITTERS IN AIR

Variation of signal amplitudes of two different transmitters may one of the reason that signal was not canceled out each other in practice. In section 2.4.6.1, two different transmitters were considered having exactly the same signal amplitudes in the simulation. In this section, the signal

amplitudes of two different transmitters are measured experimentally. Figure 2.20 shows a schematic diagram of the experimental setup of measuring signal amplitudes of transmitter 1 and transmitter 2. Transmitting and receiving probes were placed at a fixed distance apart from each other in the air. The waveforms of transmitter 1 and transmitter 2 were recorded for a certain distance. Figure 2.20(a) shows that transmitter 1 is active and transmitter 2 is inactive while measuring the amplitude of transmitter 1 and Fig. 2.20(b) shows the measurement vice versa.

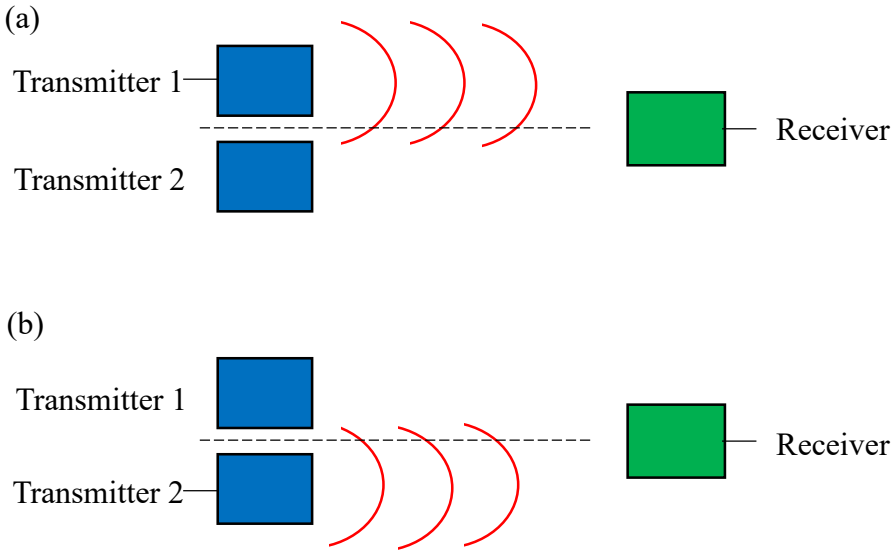

Fig. 2.20. Schematic diagram of the experimental setup of measuring the signal amplitudes of transmitters (a) transmitter 1 is active (b) transmitter 2 is active.

Figure 2.21 shows the experimental waveforms of transmitter 1 and transmitter 2. The blue solid line and the red solid line show the received ultrasound signal for transmitter 1 and transmitter 2, respectively. The experimental result shows the signal amplitude of transmitter 1 is 1.6 times larger than that of the transmitter 2. It was found that due to the variation of the signal amplitudes of the transmitters, the noise signal does not cancel out each other.

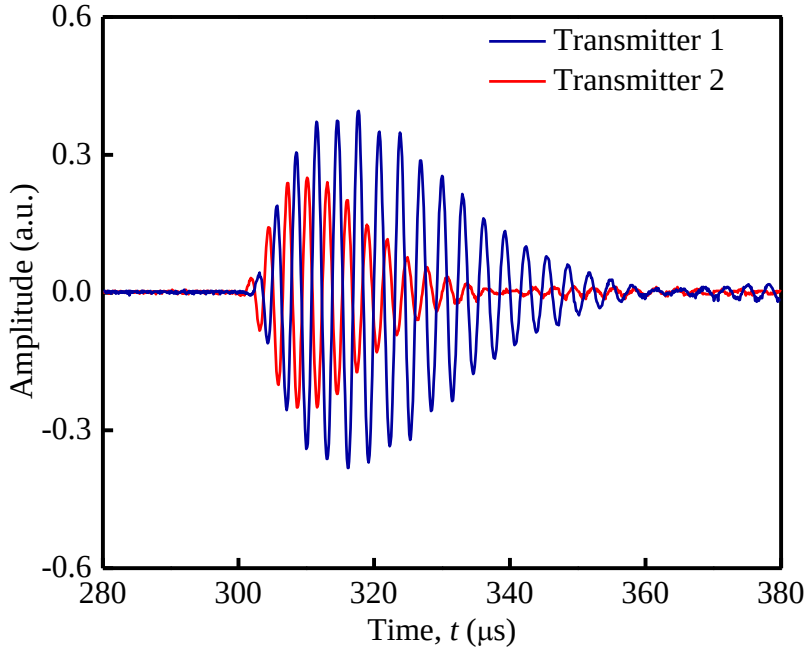

Fig. 2.21. Observation of signal amplitudes of transmitter 1 and transmitter 2 in air.

2.4.7.2. Effect of Welded Pipe to The Signal Propagation

For practical application, we need to consider a pipe having rough surface, non-uniform wall thickness and asymmetric shape. We have investigated how much ultrasonic noise signal can be canceled for a practical pipe. In practice, this pipe was a UOE SUS pipe made from a SUS plate by welding; therefore, in one side of sound propagation path, there was a joint of the SUS material due to the welding as shown in Fig. 2.22(a). Two transmitters' and one receiver layout was considered both in experiment (3D) and in simulation (2D) as shown in Fig. 2.22(a) and Fig. 2.22(b), respectively. Since it is difficult to attach transmitter 2 and receiver exactly at the same position, the receiver was attached below the transmitter 2 for the experiment. The received ultrasound signal amplitude was measured experimentally and also calculated by simulation.

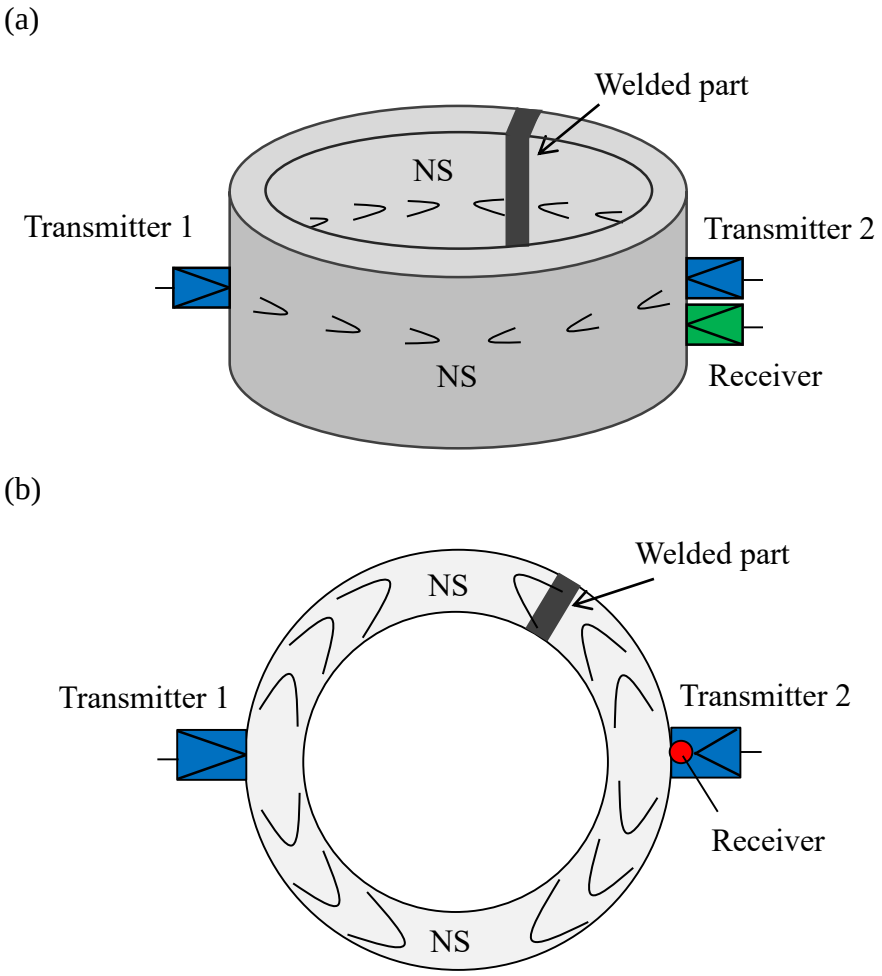

Fig. 2.22. (a) The schematic diagram of the experimental pipe having weld part, (b) Simulation model layout having a welded part. The thick black line shows the welded part of the pipe [19].

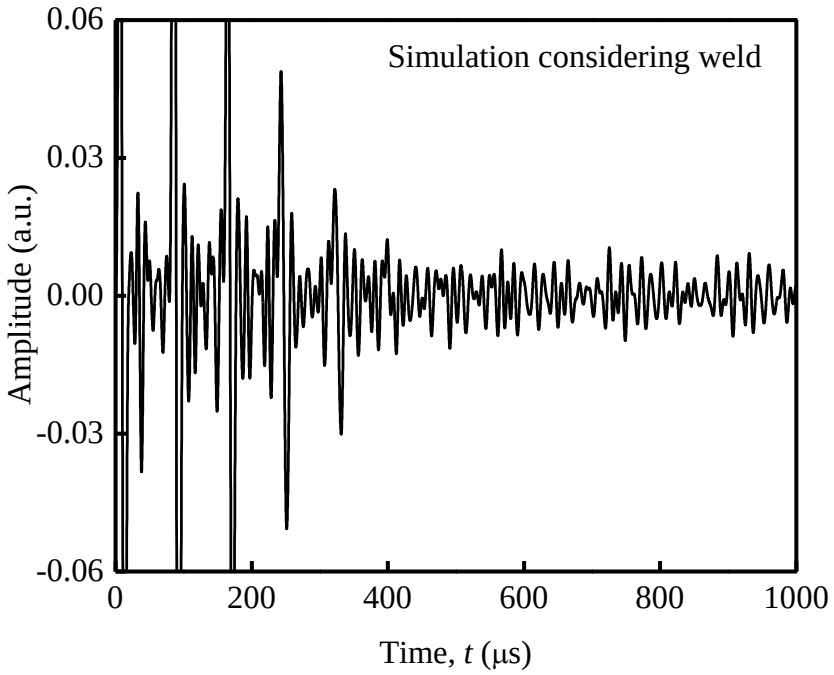

Fig. 2.23. Influence of the weld part on the ultrasonic signal cancelation. Due to the presence of the weld part, noise signal does not cancel each other in simulation result [19].

As shown in Fig. 2.23 the noise cancelation is not as good as in Fig. 2.17(b) when there is a welded part in the pipe. Therefore, it can be concluded that it is rather difficult to cancel the noise signal with two transducers. In practice, a pipe having the uniform material with a smooth surface, symmetric shape and uniform wall thickness are somewhat difficult. In addition, two transducers having exactly the same frequency and signal amplitude are difficult to obtain.

2.5. CONCLUSION

H_2 gas concentration was successfully measured using ultrasound from the exterior of a SUS pipe without making a hole. Two experiments were conducted to reduce the noise signal that is the sound wave circle inside the SUS pipe itself. At first, the airborne ultrasonic signal was able to be observed by pasting the SAM on a SUS pipe surface. SAM could reduce the noise signal significantly. As a result, it was possible to calculate the gas concentration using Δt, the difference

of sound traveling time before and after the gas mixture. Secondly, FDTD simulation was carried out to investigate the noise signal cancellation. In the simulation, it was possible to reduce this noise signal by cancelation using two opposite transmitters; however, it was found that it is not practical after the experiments due to asymmetry in the pipe and two transmitters.

REFERENCES

[1] T. Suzuki, S. Kawabata and T. Tomita, "Present status of hydrogen transport systems utilizing existing natural gas supply infrastructures in Europe and the USA", Institute of Energy Economics, pp. 1-16. 2005.

[2] M. Taskin, G. Utsumi and Y. Kato, "Observation of ultrasound wave from exterior of a metal pipe for flowing gas measurement", Proceeding International Workshop on Piezoelectric Materials and Applications in Actuators (IWPMA 2018), pp. 85, 2018.

[3] S Kočiš and Z. Figura, "Ultrasonic measurements and technologies", London: Chapman & Hall, 1996.

[4] M. Sato, "Numerical formulation of the FDTD method for transient analysis of elastic wave fields in the Y-Z plane of quartz", Japanese Journal of Applied Physics, **vol. 44**, pp. 4490-93, 2005.

[5] M. Sato, "Formulation of the FDTD method for separating the particle velocity vectors of an elastic wave field into longitudinal and shear wave components", Acoustical Science and Technology, **vol. 25**, pp. 382-85, 2004.

[6] H. Fukuoka, J. Jung, M. Inoue, H. Fujita and Y. Kato, "Absolute concentration measurement for hydrogen", Energy Procedia, **vol. 29**, pp. 283-90, 2012.

[7] M. Sonoyama, H. Fujita and Y. Kato, "Application of ultrasonic to a hydrogen sensor", 2010 IEEE Sensors, No. 3, pp. 2141-2144, 2010.

[8] N. Feather, "An Introduction to the physics of vibration and waves", Chicago: Edinburgh University Press, 1963.

[9] G S K Wong, "Speed of sound in standard air", The Journal of the Acoustical Society of America, **vol. 79**, pp. 1359-66, 1986.

[10] J. Jung, M. Sonoyama, H. Fujita, M. Inoue and Y. Kato, "The novel hydrogen sensor using ultrasonic", International Conference on Hydrogen Production (ICH2P-11), 160 ELE, pp 1-8, 2011.

[11] M. Taskin and Y. Kato, “Instant gas concentration measurement using ultrasound from exterior of a pipe”, IEEE Sensors Journal, **vol. 19**, no. 11, pp. 4017-4024, 2019. DOI: 10.1109/JSEN.2019.2897736.

[12] J. C. Vyas, V. R. Katti, S. K. Gupta and J. V. Yakhmi, “A non-invasive ultrasonic gas sensor for binary gas mixtures”, Sensors and Actuators B, **vol. 115**, pp. 28-32, 2006.

[13] M. Taskin, T. Kido, M. Inoue and Y. Kato, “Methane detection in dirflow using ultrasound from exterior of the ventilation pipe”, in Proceeding of International Symposium in Mine Ventilation (SIVM 2018), pp. 177-184, 2018.

[14] B. S. Hoyle, “Process tomography using ultrasonic sensors”, Measurement Science and Technology, **vol. 7**, pp. 7 272–80, 1996.

[15] H. J. Pain, “The physics of vibrations and waves”, Chichester: Wiley, 1985.

[16] S. Yee, “Numerical solution of initial boundary value problems involving Maxwell’s equations in isotropic media”, IEEE Transactions on Antennas and Propagation, **vol. 14**, pp. 302-307, 1966.

[17] J. G. Maloney and K E Cummings, “Adaptation of FDTD techniques to acoustic modeling”, 11th Annual Review of Progress in Applied Computational Electromagnetics, Monterey, CA, **vol. 2**, pp. 724-31, 1995.

[18] T. Sakuma, S. Sakamoto and T. Otsuru, “Computational simulation in architectural and environmental acoustics”, Japan, Springer; 2014.

[19] M. Taskin, G. Utsumi and Y. Kato, “Observation of ultrasonic signal and measurement of H_2 concentration from the exterior of a metal pipe”, International Journal of Hydrogen Energy, 2019. (Accepted)

[20] O. Cramer, “The variation of the specific heat ratio and the speed of sound in air with temperature pressure humidity and CO_2 concentration”, Journal of the Acoustical Society of America, **vol. 93**, pp. 2510-2516, 1993.

CHAPTER 3

MEASUREMENT OF FLOWING GAS CONCENTRATION FROM THE EXTERIOR OF A PIPE

3.1. INTRODUCTION

This chapter mainly focuses on the flowing H_2 gas concentration measurement using ultrasound from-exterior of the pipe. Concentration of flowing H_2 gas was measured for the first time from the exterior of the pipe, which was more challenging that measuring non-flowing gas concentration. The principle of gas concentration measurement is same as described in Chapter. 2. Drilling a hole in the pipe to extract the gases is not necessary for the gas concentration measurement. In this study, the concentration of H_2 gas in the air was measured accurately while the air was flowing inside the pipe. Various airflow speeds were examined, and it was estimated that it is possible to measure the gas concentration for up to about 60 m/s of the airflow rate. The response time for measuring gas concentration was less than 0.1 s. For the practical test, an experiment was conducted to replace air with H_2 gas in a SUS pipe.

3.2. PRINCIPLE

3.2.1. DIVERGENCE ANGLE OF THE TRANSMITTER

A transmitter produces a sound field in front. The energy in the beam spread out as it propagates through the material. The phenomenon is usually referred as beam spread. Figure 3.1 gives a simplified view of a sound beam for a transmitter. Beam spread for a flat piston source transmitter is a function of the distance between width of the transmitter (r), transmitter frequency (f), and the sound velocity (v) in the medium through which the sound is traveling. Equation (3.1) can be used to calculate the beam divergence angle, β [1]. This angle represents a measure from the center of the acoustic axis to the point where the sound pressure has decreased by one half to the side of the acoustic axis.

$$\sin\beta = \frac{0.61v}{rf} \tag{3.1}$$

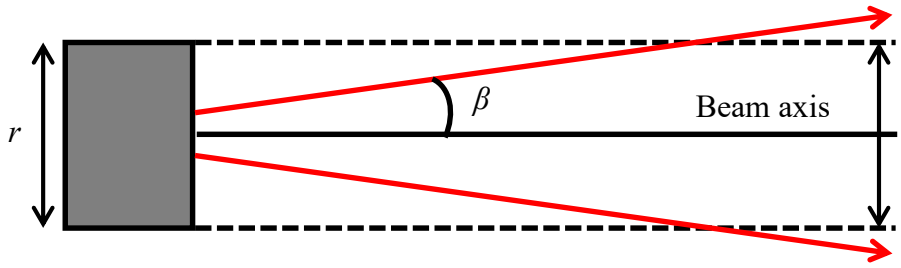

Fig. 3.1. Divergence angle of the transmitter.

3.2.2. Oblique Incidence of Ultrasonic Wave at Interface

The propagation of longitudinal and transverse waves in solid were described in section. 1.3.2. of Chapter 1. When a sound wave in a gas arrives at the boundary between the gas and another medium, which have different physical properties, it is partially or totally reflected. During the process of reflection, both the amplitude and phase of the wave are changed in general. Sometimes a part of the sound wave penetrates this boundary and propagates behind it with a different sound velocity and in a different direction. This latter process is called 'refraction'. As with reflection, both the phase and the amplitude differ from those of the primary wave.

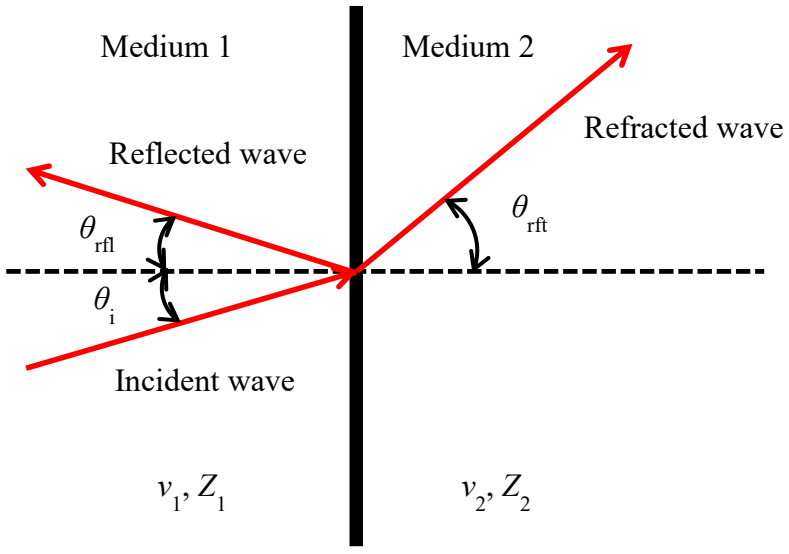

Fig. 3.2. Reflection and refraction at the boundary between two media.

In the following, assuming the extension of the boundary to be unlimited. Let θ_i be the angle between its normal and the direction of the incident wave as depicted in Fig. 3.2 (left side). The sound velocity of incident wave is v_1 and impedance is Z_1. When the sound wave incident on the boundary some part reflects in the same medium with the angle of reflection equals the angle of incidence. If the 'wall' is the boundary interface against another medium with sound v_2 and characteristic impedance Z_2, a third wave appears the 'refracted' wave (see Fig. 3.2, right side). For the angle θ_{rft} of refraction, the law becomes as expressed in eq. (3.2):

$$\frac{\sin\theta_{rft}}{\sin\theta_i} = \frac{v_2}{v_1} \tag{3.2}$$

Which is known in optics as 'Snell's law'. In this case, reflection coefficient is expressed as in eq. (3.3) [2]:

$$\text{Reflection coefficient, } R_A = \left(\frac{Z_2\cos\theta_i - Z_1\cos\theta_{rft}}{Z_1\cos\theta_{rft} + Z_1\cos\theta_i} \right) \tag{3.3}$$

The amplitude of the refracted wave divided by that of the incident wave is the 'transmission coefficient', which is expressed as in eq. (3.4) [2]:

$$\text{Transmission coefficient, } T_A = \frac{2Z_2\cos\theta_i}{Z_1\cos\theta_{rft} + Z_2\cos\theta_i} \tag{3.4}$$

The intensity is proportional to the square of the amplitude. Therefore, the intensities of the reflected (R_p) and transmitted (T_p) waves at an interface of two materials can be described as in eqs. (3.5), and (3.6), respectively:

$$R_p = \left(\frac{Z_2\cos\theta_i - Z_1\cos\theta_{rft}}{Z_1\cos\theta_{rft} + Z_2\cos\theta_i} \right)^2 \tag{3.5}$$

$$T_p = \frac{4Z_1Z_2\cos\theta_i\cos\theta_{rft}}{\left(Z_1\cos\theta_{rft} + Z_2\cos\theta_i\right)^2} \tag{3.6}$$

Here the phenomenon of 'total reflection' is introduced. If $v_2 > v_1$, the refraction angle is larger than the angle of incidence. Since θ_i can never exceed 90°, there is a maximum angle of incidence, the limiting angle of total reflection

$$\theta_i = \arcsin\left(\frac{v_1}{v_2} \right) \tag{3.7}$$

up to which regular refraction according to eq. (3.2) can occur.

3.2.3. General Characteristics of Pipe Flow

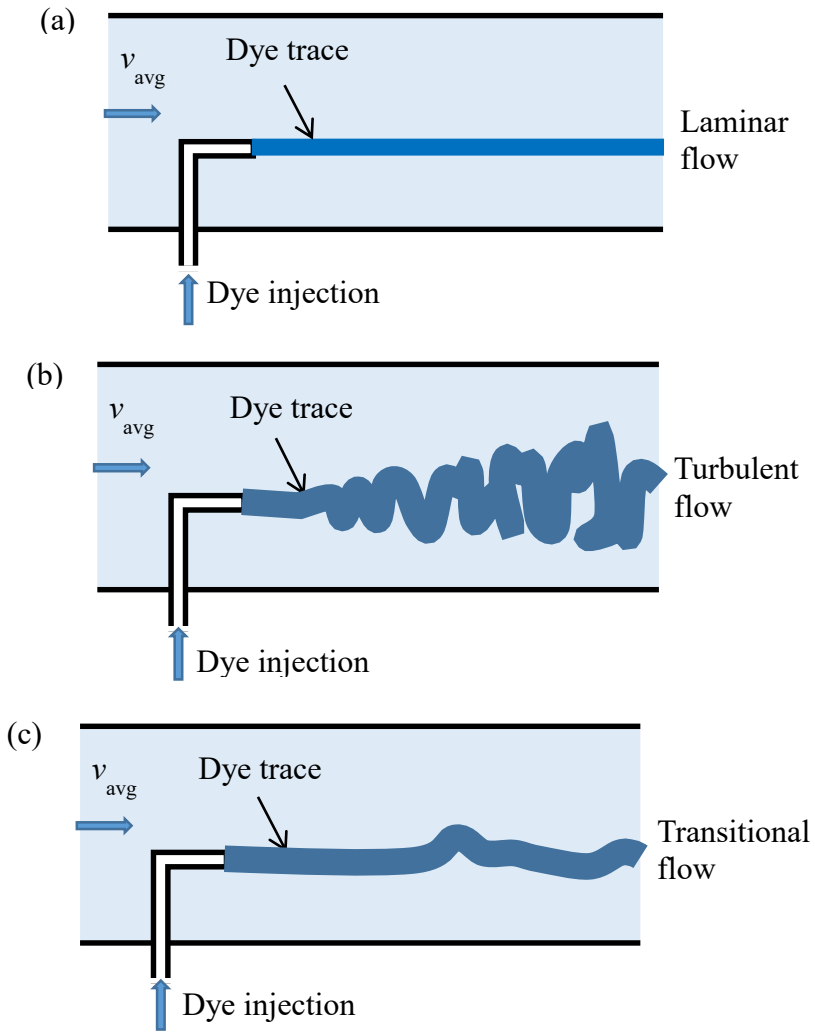

Fig. 3.3. The behavior of colored fluid injected into the flow in (a) laminar, (b) transitional and (c) turbulent flows in a pipe.

The nature of the streak-line formed by injecting the dye depends on the fluid velocity.

- When the fluid is moving slowest, get a well-defined streak-line as shown in Fig. 3.3(a). This flow situation is called laminar flow. The laminar flow has a constant velocity, which is smallest.

- When the fluid is moving faster, get an irregular streak-line, which blurs and spreads the dye out as shown in Fig. 3.3(b). The streak-line also fluctuates randomly with time. This is called turbulent flow. The turbulent flow has a fluctuating velocity about some mean value. The flow rate is largest.

- When the fluid is moving at an intermediate velocity, there are irregularities in the streak-line, but the streak-line is still well defined as shown in Fig. 3.3(c) is called transitional flow. The transitional flow has a mostly constant velocity with the occasional fluctuation.

The transition from laminar to turbulent flow depends on the geometry, surface roughness, flow velocity, surface temperature, and type of fluid, among other things. After exhaustive experiments in the 1880s, Osborne Reynolds discovered that the flow regime depends mainly on the ratio of inertial forces to viscous forces in the fluid. This ratio is called the Reynolds number, Re and is expressed for internal flow in a circular pipe as expressed in eq. (3.8) [3].

$$\text{Re}=\frac{\text{Inertial forces}}{\text{Viscous forces}}=\frac{v_{avg}L}{\upsilon}=\frac{Dv_{avg}L}{\mu} \tag{3.8}$$

where, $v_{avg}=\frac{\text{maximum speed of flow(m/s)}}{2}=\frac{v_{\max}}{2}$ is the average flow velocity (m/s), L is the diameter of the pipe (m), D is the density of the fluid, υ is the kinematic viscosity of the fluid (m^2/s) and μ is the dynamic viscosity of the fluid (Pa·s).

Under most practical conditions, the flow in a circular pipe is laminar for $\text{Re} \leq 2300$, turbulent for $\text{Re} \geq 4000$, and transitional in between. That is,

$\text{Re} \leq 2300$	laminar flow
$2300 \leq \text{Re} \leq 4000$	transitional flow
$\text{Re} \geq 4000$	turbulent flow

3.3. Experimental Setup for the Measurement of Flowing H_2 Gas Concentration

The specimen gases were flown in a PVC pipe that was placed horizontally. Figure 3.4(a) shows the photograph of the experimental apparatus. Length of the pipe was 880 mm with the inner diameter of 39 mm and PVC thickness of 2 mm. The ultrasonic signal can pass through the PVC pipe so that the gas concentration in the pipe can be measured from outside of the pipe. A blower was used to control the airflow speed flowing inside the pipe as shown in Fig. 3.4 (b). The flow rate of the blower is controlled by frequency, and the speed of flow according to the frequency is shown in **Table 3.1**. The airflow speeds were measured at the exit of the pipe were set at 20, 25, 30, 35, and 39 m/s. In the experiment, maximum speed of flow was used 39 m/s.

Table 3.1: Speed of flow according to the blower frequency.

Frequency (Hz)	0	16	31.7	45	60
Speed of flow (m/s)	0	10	20	30	39

About 30 ml of hydrogen gas was injected manually, within about 0.1 s into the airflow using a glass syringe through a 1/4 in. diam. and 5 cm length pipe, which exit was placed at the center of the PVC pipe diameter as shown in Fig. 3.4(c). As the airflow speed increases and ultrasound propagation becomes oblique, the transducer starts detecting the longitudinal and transverse waveforms or the mixture of both waveforms. Therefore, the receiver has to be move downstream according to the airflow speed and placed orthogonally to the pipe axis.

Figure 3.4(c) shows a schematic diagram of the experimental setup of the pipe and a traveling signal. The ultrasonic transmitter Tx was mounted near the exit of the pipe. The position of the receiver Rx was shifted downstream to detect the maximum signal amplitude as shown in Fig. 3.4(c). Two piezo ceramic transmitting and receiving probes having the surface area of 20 mm x 15 mm were mounted on the pipe surface diagonally on the opposite sides of the pipe as shown in Fig. 3.4(c). A sonic gel was used between transducers and the pipe.

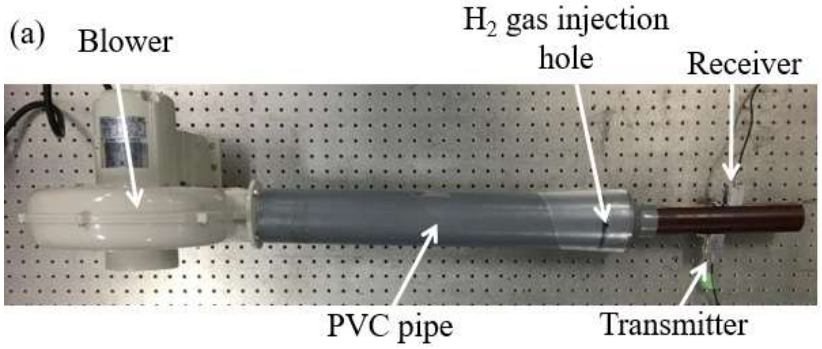

(b)

(c)

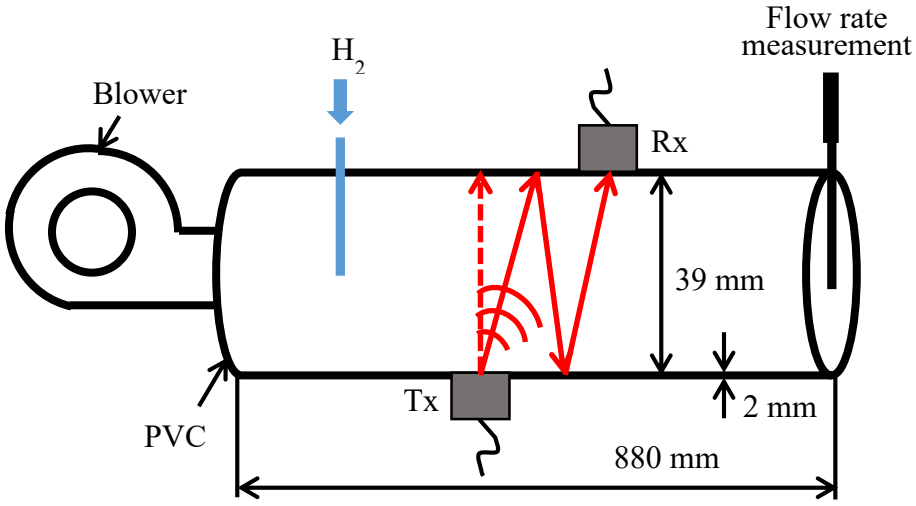

Fig. 3.4. (a) Photograph of the experimental apparatus [4] (b) Photograph of the blower, and (c) Schematic diagram of experimental setup and image of ultrasonic wave propagation in red with respect to airflow inside the pipe.

A JPR-10CN pulsar receiver Japan Probe Co. LTD was used as an ultrasonic generator. During the experiment, the frequency and the voltage were fixed at 400 kHz and 60 V, respectively. The sampling time was as short as 0.08 s. The width of one pulse was 2 μs. During the experiment, temperature, humidity, and air pressure were about 300 K, 55% and 1 atm., respectively. Since different transducers were used to transmit and receive the ultrasound, there was no interference of reflected signal from the transmitter. Since the inner surface of the PVC pipe is smooth, there is no need to consider diffraction phenomena when the sound is reflected inside the pipe. When the sound incident from air to the PVC pipe obliquely, both the longitudinal and transverse waves need to be considered in the PVC pipe. The effect of longitudinal and transverse waves will be discussed later. The other alternative sound paths that connect the two transducers passing exclusively inside the PVC pipe walls is the sound circle around the PVC pipe itself. However, this circulating signal appears earlier than the airborne signal passing through the PVC pipe traveling inside the PVC pipe walls. This experimental result will be shown later.

3.4. Results and Discussion

3.4.1. Divergence Angle of the Transmitter

The divergence angle was measured experimentally. The received ultrasound signal amplitude was measured experimentally by moving the receiver position. Figure 3.5(a) shows the schematic diagram of measuring the divergence angle. In this experiment, the air was in steady state.

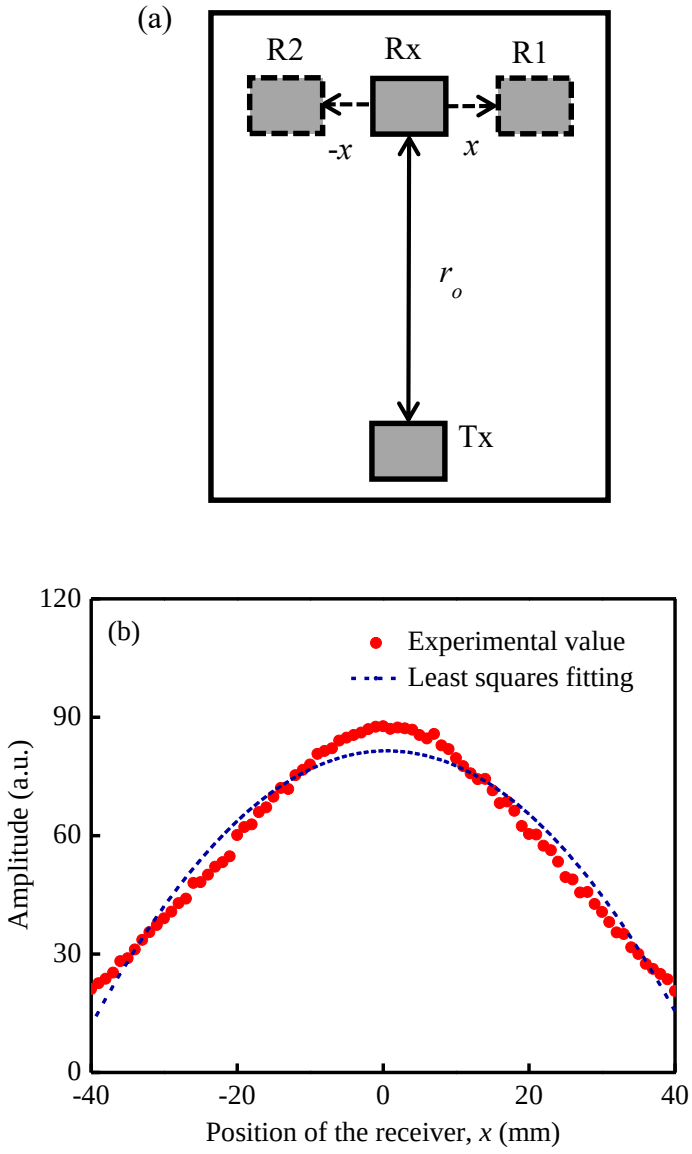

Fig. 3.5. (a) Schematic diagram of the experimental setup of measuring divergence angle. (b) Variation in the amplitude of the received ultrasonic signal with position x of the receiver in still airflow.

Transmitter, Tx and receiver, Rx were placed r_o = 1000 mm apart from each other. The receiver was moved from x = 0 mm to R1 and R2. The distance between Rx and R1 was considered as $+x$ and the distance between Rx and R2 was considered as $-x$. 50 waveforms of the received signal was recorded for each mm of shifted receiver. The average amplitude of each 50 waveforms

was calculated. Figure 3.5(b) shows the results of the sound signal spread with the received amplitude at each shifted receiver position x as shown in Fig. 3.11(a) for the 0 m/s speed of airflow. Maximum amplitude is observed at the position of around x = 0 mm according to the least-squares fitting with a dashed line. At x = 40 mm, the amplitude of the received signal becomes half. β can be calculated using (3.9).

$$\beta = \tan^{-1} \frac{x}{r_o} \tag{3.9}$$

The measured value of β becomes 2.3°. In this experiment, the transmitter was used having the frequency, f = 400 kHz, radius, r = 10 mm, and speed of sound in air, v =343 m/s, β is roughly calculated as about 3º using eq. (3.1). The experimental value and the theoretical value matched relatively close to each other. Hence, it was assumed that the sound was not spreading much through the experiment and considered the signal as a ray.

3.4.2. OBSERVATION OF ULTRASONIC SIGNAL IN AIR

An experiment was conducted to compare the ultrasonic signal in air and through PVC pipe. Figure 3.6(a) shows the schematic diagram of the experimental setup. As shown in Fig. 3.6(a), transmitter, Tx and receiver, Rx were placed 39 mm apart from each other in air which is same distance of the pipe inner diameter. The waveform of the ultrasonic signal passing through the air is shown in Fig. 3.6(b). The second signal around 350 μs is the signal reflected twice at the transducer surface for Fig 3.6(b). Air was steady in this experiment. The transmitting and receiving probes are having the surface area of 20 mm x 15 mm. As the surface area of the transducers are large enough, the signal can reflect many times at the transducer surface.

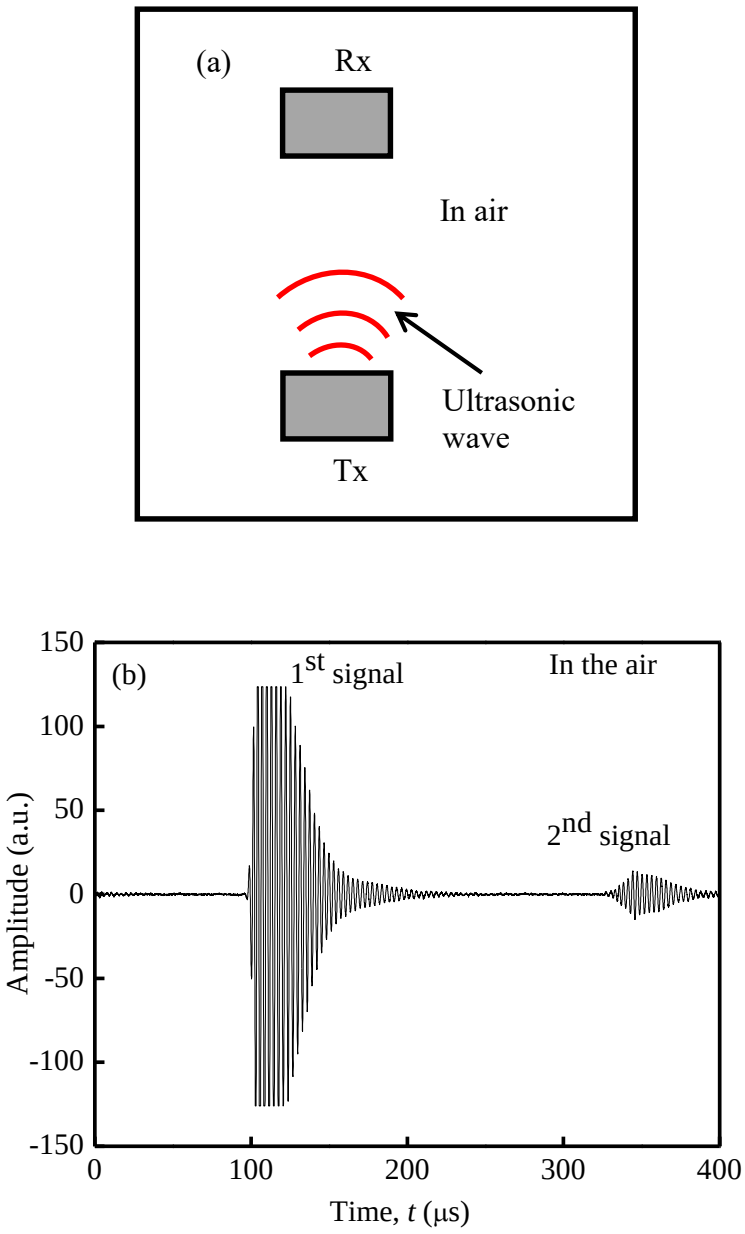

Fig. 3.6. (a) Schematic diagram of the experimental setup to observe the ultrasonic signal in air. (b) The received signal amplitude of ultrasound passing in air.

3.4.3. OBSERVATION OF ULTRASONIC SIGNAL THROUGH A PVC PIPE

An experiment was conducted to observe the ultrasonic signal through the PVC pipe. Transmitter, Tx and receiver, Rx were mounted on the exterior of the pipe surface diagonally on the opposite sides of the pipe as shown in Fig. 3.7(a).

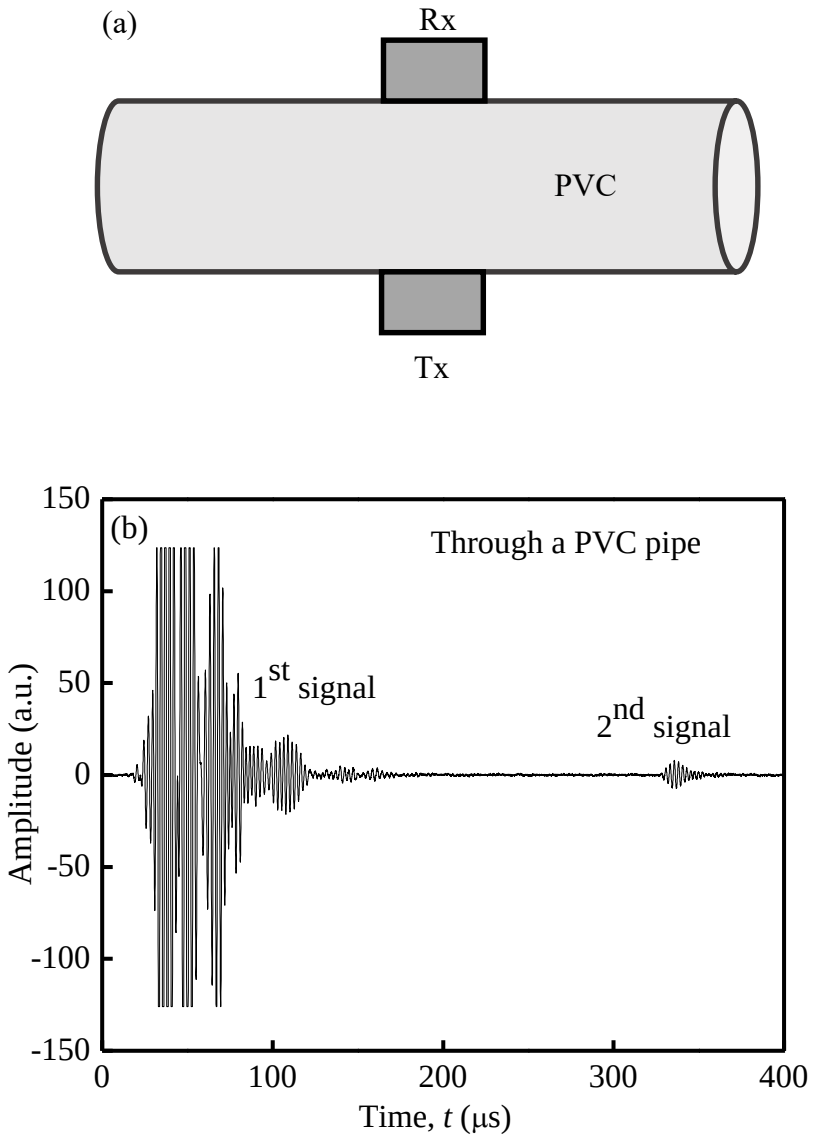

Fig. 3.7. (a) Schematic diagram of the experimental setup to observe the ultrasonic signal through a PVC pipe. (b) The received signal amplitude of ultrasound passing through the PVC pipe [4].

Figure 3.7(b) shows the received signal of the ultrasonic signal passing through both the PVC pipe and the air. In this experiment, the transmitted pulse emission time was set as 0.0 μs. The first signal around 110 μs is the direct signal from the transducer in Fig. 3.7(b). The second signal around 350 μs is the signal reflected twice at the PVC pipe surface as it was explained in Fig. 3.4(b). The noise like signal observed earlier than the first signal is due to the ultrasound circulating

around the PVC pipe material itself. Since the second signal has less interference from the noise earlier than 100 μs, it was used for the measurement and calculation of gas concentration.

3.4.4. CONCENTRATION OF H_2 GAS IN DIFFERENT AIRFLOW

For a practical test, H_2 gas was injected instantly into an air flowing pipe and measured with the ultrasound. As shown in Figs. 3.8 rapid increase in Δt for a period of about 0.3 s was observed due to sudden change in speed of sound after instant injection of H_2. Figures 3.8(a), 3.8(b), 3.8(c), and 3.8(d) show the measured Δt and the calculated H_2 concentration for the airflow speed of 20, 25, 35, and 39 m/s, respectively. The H_2 gas concentration was calculated from eq. (2.5) using the Δt. As shown in Figs. 3.8 horizontal axis, the ultrasonic signal was recorded for about 3 s before and after the H_2 gas injection. The readings of the traveling time in air and in the mixture of air and hydrogen were taken manually at the intercept of zero amplitudes. The difference between the traveling time before and after H_2 mixing was read manually as Δt. Although the background noise increases with the increase of airflow speed as seen in Figs. 3.8(a) – 3.8(d), Δt that is the H_2 gas concentrations of each peak are about the same. This result shows the accuracy of the measurement method of H_2 gas concentration by the ultrasound. For example, $\Delta t = 4.7$ μs corresponds to about 1.2% of H_2 gas concentration, which can be observed from Figs. 3.8.

The response time of measuring gas concentration variation is as fast as 0.1 s from the exterior of the pipe. Humidity does not affect much to the H_2 concentration measurement at room temperature. Therefore, the effect of humidity can be neglected for practical use. The change of temperature was compensated for the speed of sound, and the H_2 concentration was obtained accurately even if the temperature varied [5], [6]. The gas concentration is not influenced by the change of pressure, as the pressure does not affect the sound speed [7].

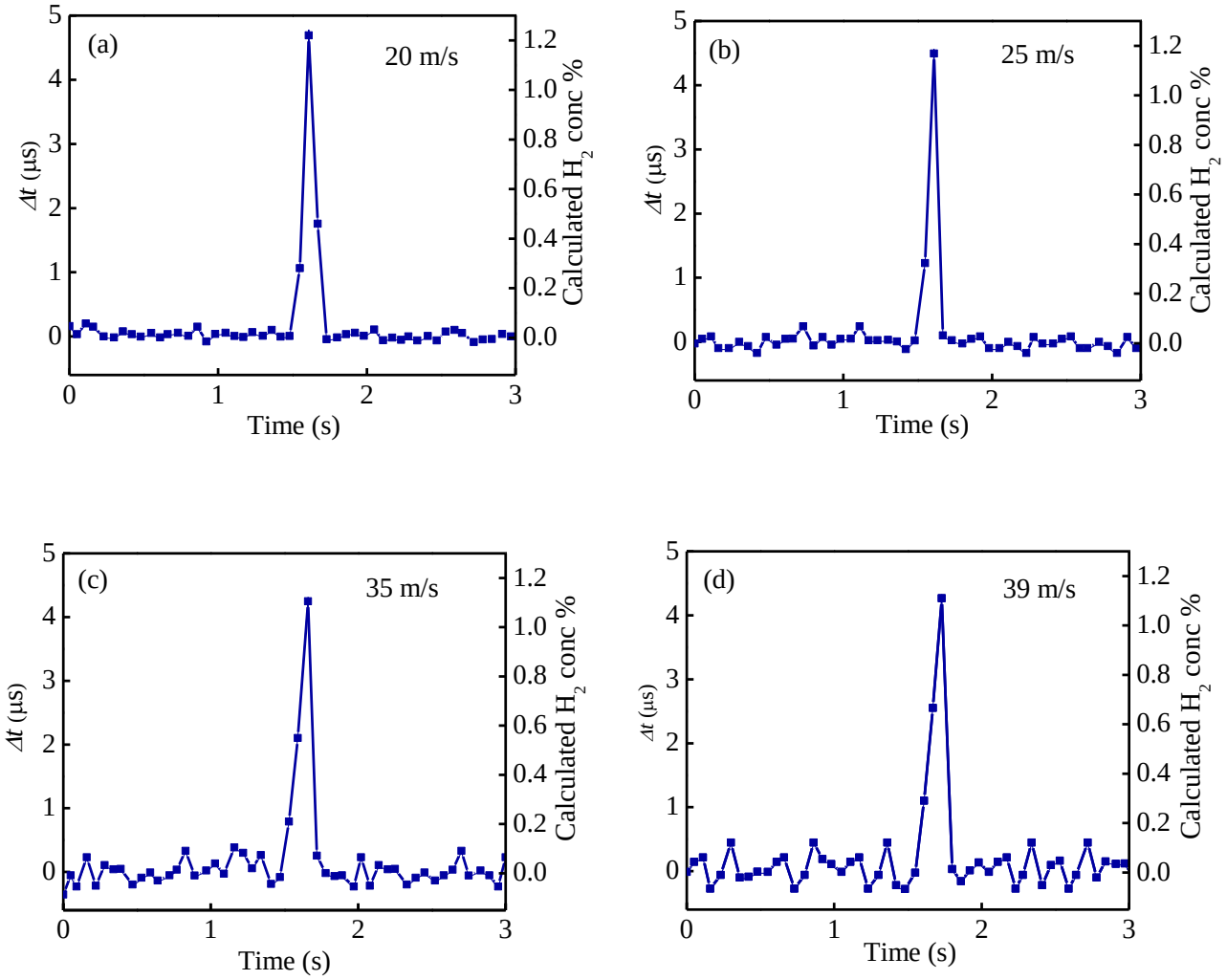

Fig. 3.8. Measured Δt and calculated H_2 concentration from Δt for (a) 20 m/s, (b) 25 m/s, (c) 35 m/s, and (d) 39 m/s airflow rate. The horizontal axis shows the ultrasonic signal recording time during the H_2 injection [4].

3.4.5. Influence of Signal Fluctuation on Gas Concentration

In this section, we have investigated the influence of signal fluctuation on the gas concentration. The blower creates a turbulent flow, which influences the measurement error of the ultrasonic signal. The error of the gas concentration was measured for four different speeds. Figure 3.9 shows 50 waveforms for the airflow at a speed of 39 m/s, and the waves are not stable due to

the turbulent flow. A third peak of the signal shown in a red square in Fig. 3.9 was chosen to calculate the sound traveling time difference Δt. Figures 3.10(a), 3.10(b), 3.10(c), and 3.10(d) show 50 waveforms for the airflow at a speed of 10, 20, 30, and 39 m/s, respectively. Figures 3.10 show that fluctuation of waveforms increase according to the airflow speed. The average of 50 waveforms was calculated and shown in a thick red line of Fig. 3.10(d). The reading of time for measuring the Δt was taken at the intercept of zero intensities of the third wave.

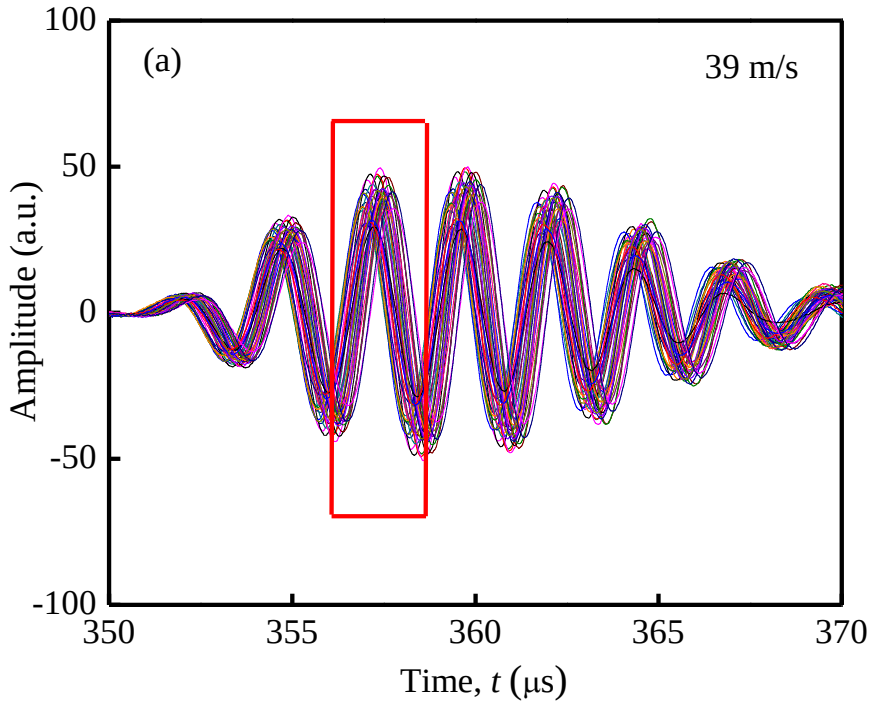

Fig. 3.9. 50 waveforms of the received sound signal at 39 m/s airflow rate. Fluctuation of the signal is due to turbulent flow [4].

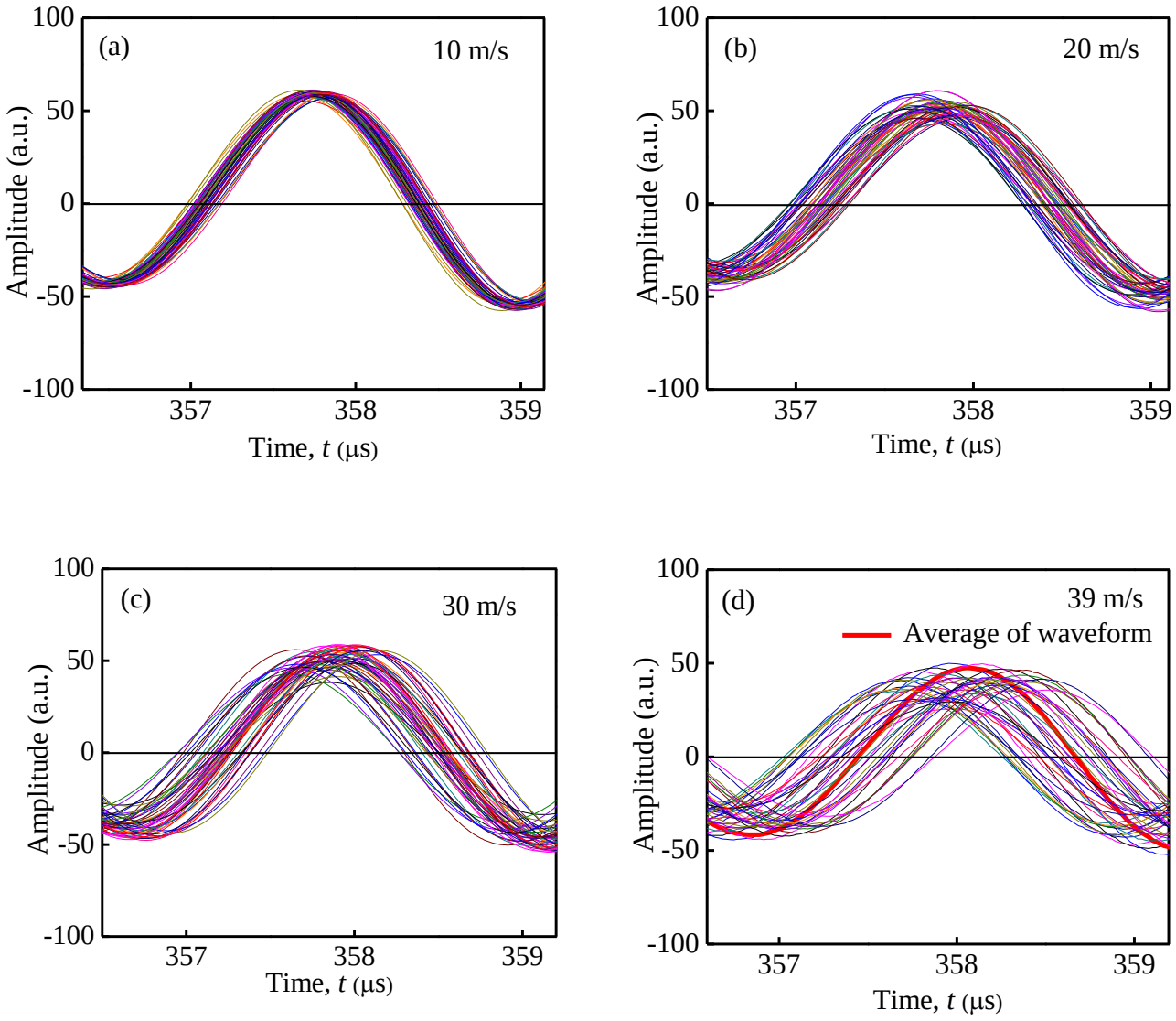

Fig. 3.10. An enlarged view of a third peak in (a) 10 m/s, (b) 20 m/s, (c) 30 m/s, and (d) 39 m/s speed of airflow. A thick red line in (d) is the average of the 50 waveforms [4].

As described above, the error of Δt was measured by reading minimum and maximum sound traveling time of the 50 waveforms recorded for each flow rate. Figure 3.11 shows this error in Δt with various airflow rate. The readings of the sound traveling time were taken at the intercept of zero intensities of the third wave as shown in Figs. 3.10. Noise error is approximately proportional to the airflow rate. The H_2 gas concentration in the right axis is the converted from the Δt error

values using eq. (2.5). For example, for the airflow rate of 39 m/s, the error of Δt is approximately 0.54 μs that is about 0.32% in H_2 concentration.

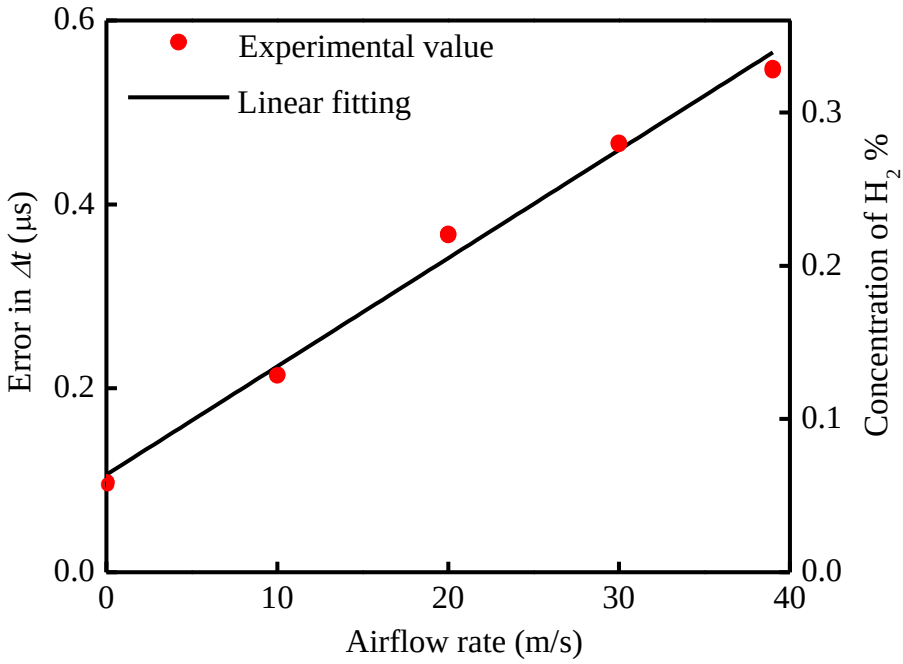

Fig. 3.11. The error of Δt and its conversion to hydrogen gas concentration versus airflow rate [4].

3.4.6. Relation Between Reynolds Number and Error in ΔT

The Reynolds numbers for different speeds of flow were calculated using eq. (3.8). These numbers are shown in **Table 3.2**. Since the diameter of the pipe and the kinematic viscosity coefficient are constant, in this experiment, only the speed of flow is variable. According to **Table 3.2**, as the speed of flow increases, turbulence increases. Figure 3.12 shows this error in Δt with Reynolds number. Since the kinematic viscosity coefficient and the speed of flow cannot be changed in many cases, the diameter of the pipe can be changed to achieve less error in Δt.

Table 3.2: Flow type according to the Reynolds number, *Re*.

Speed of flow (m/s)	**Diameter of the pipe (m)**	**Kinematic viscosity (m^2/s)**	**Reynolds number, *Re***	**Flow type**
0	0.039	1.51×10^{-5}	0	Laminar
10			12913	Turbulent
20			25827	Turbulent
30			38741	Turbulent
39			51655	Turbulent

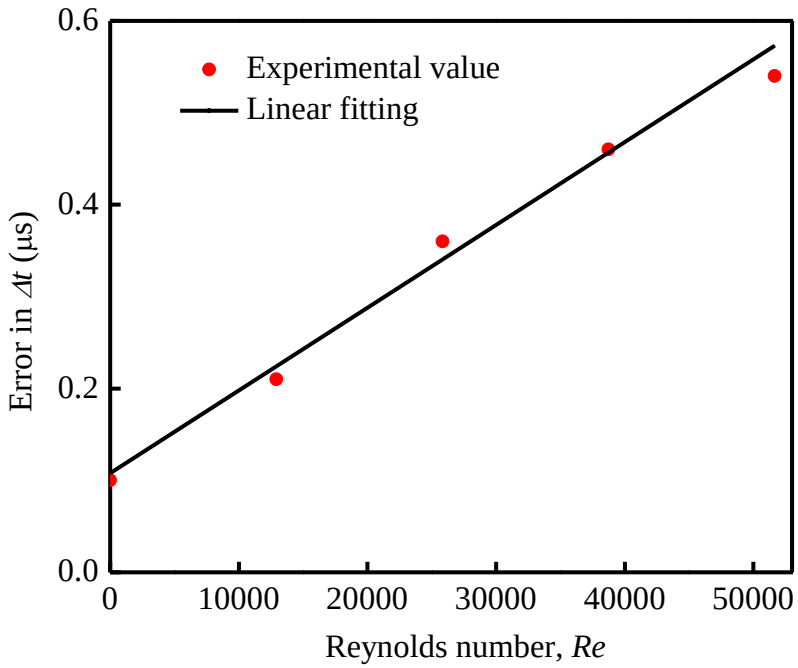

Fig. 3.12. The error in Δt according to Reynolds number, *Re*.

3.4.7. POSITION OF THE RECEIVER

We have investigated how much the ultrasound signal drifts towards downstream of the airflow. The sound traveling distance from Tx to Rx was determined by using eq. (3.10) [2]:

$$3x_a + x_p = 3l_o \frac{v_a}{v} + \left(d^2 - d_o^2\right)^{1/2} \tag{3.10}$$

where, as shown in Fig. 3.13, l_o is the inner diameter, and d_o is the thickness of the PVC pipe. l is the propagation length of the ultrasonic wave in airborne of the pipe. d is the propagation length inside of the PVC pipe. v_a is the air flow velocity in the pipe and v is the speed of sound in the air. θ_1 is the angle between the axis along a pipe diameter and the ultrasound propagation direction flowing downstream. θ_2 is refracted angle from air to PVC pipe. θ_3 is refracted angle from PVC to the transducer.

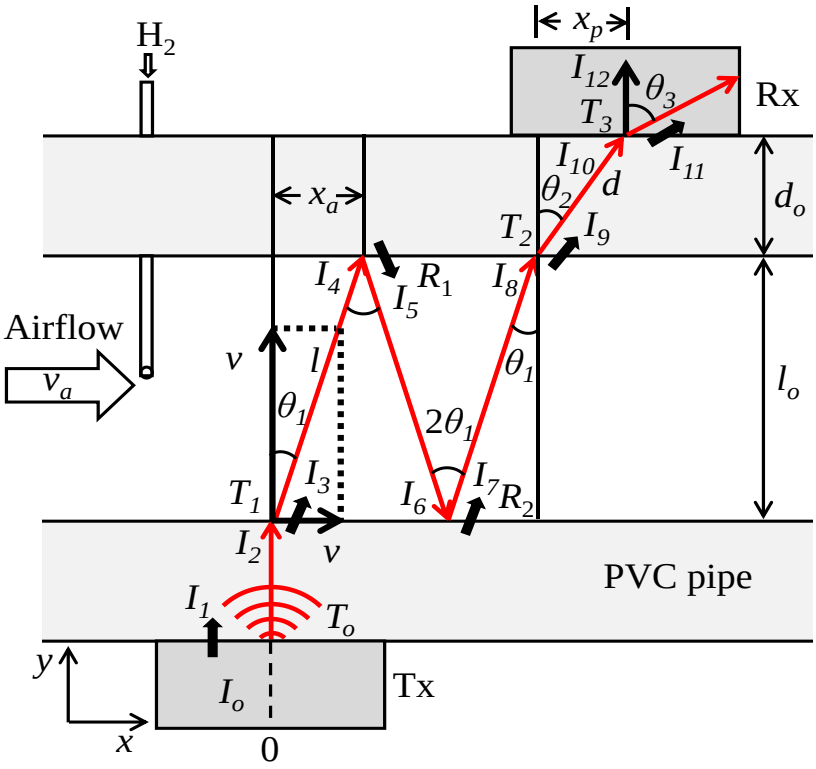

Fig. 3.13. Schematic diagram of experimental setup and image of ultrasonic wave propagation in red with respect to airflow inside the pipe [4], [8].

x_a is determined by the airflow speed as shown in eq. (3.11) [4].

$$\tan\theta_1 = \frac{v_a}{v} = \frac{x_a}{l_o} \tag{3.11}$$

$(3x_a+x_p)$ is the position of the receiver after the second reflection of the sound signal passing through the airflow and the PVC pipe. Since the sound travels faster in solid compared with that in the gas, the time for which the ultrasonic wave propagates in the PVC pipe can be ignored. Therefore, the thickness of the pipe may not be necessary to consider. The sound traveling time

through the airborne of the pipe and the PVC pipe are calculated as 114 μs and 0.85 μs, respectively. As shown in Fig. 3.13, red arrows represent the traveling sound that attenuates while passing through the medium. Black arrows on the two different interfaces represent the reflection or transmission of sound at the interface.

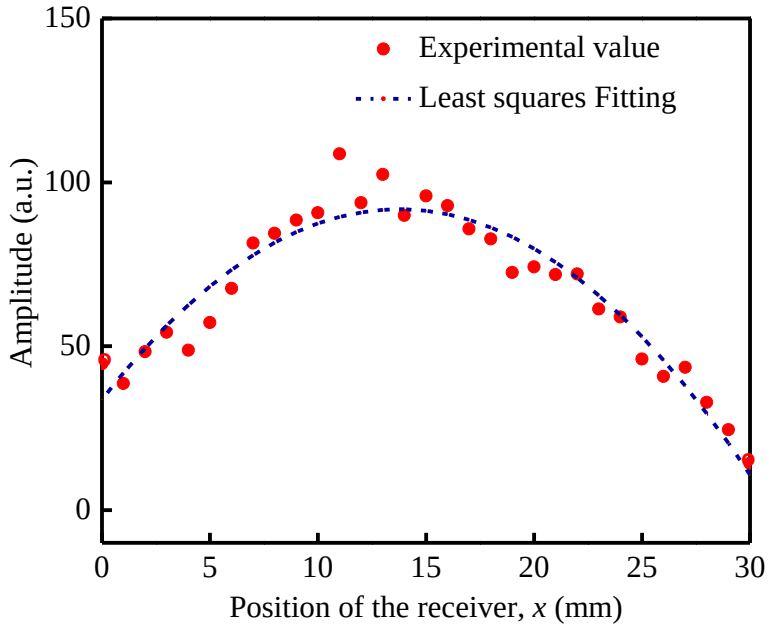

Fig. 3.14. Variation in the amplitude of the received ultrasonic signal with position x of the receiver at 39 m/s airflow [4].

Figure 3.14 shows the results of this sound drift with the received amplitude at each shifted receiver position x (see Fig. 3.13) for the 39 m/s speed of airflow. The receiver was moved from x = 0 mm position to 30 mm towards downstream and 50 waveforms of the received signal was recorded for each mm shifted of receiver position. The average amplitude of each 50 waveforms was calculated. Due to the airflow in a pipe, the transmitted ultrasound was drifted downstream for a distance of $(3x_a+x_p)$ as showed in Fig. 3.13. Maximum amplitude is observed at the position of around x =14 mm according to the least-squares fitting with a dashed line. The theoretical value of receiver position was calculated as x=13.4 mm by using (3.10) for the 39 m/s airflow. This theoretical value and experimental value matched relatively close to each other.

3.4.8. LIMIT SPEEDS OF AIRFLOW

In this section, the limit of the airflow speed was investigated. In this experiment, since the divergence angle, β is small enough and the distance between the transmitter and the receiver is short as 39 mm, the ultrasonic sound wave can be considered like a ray. Since the speed of the airflow increases, the ultrasound signal drifts towards downstream of the airflow. Limit of airflow speeds were calculated, that is ultrasonic signal does not reach to the receiver due to the internal reflection at the PVC/receiver interface. Figure 3.14 shows the experimental and theoretical values of the amplitude of ultrasound at the receiver versus the airflow rate in the pipe. The calculation of the received ultrasonic intensity I_{12} is expressed in eq. (3.12) [4] (the derivation is shown in Appendix A).

$$I_{12} = I_o \frac{256 \times Z_a^2 Z_t^2 Z_P^4 \cos\theta_1 \cos^2\theta_2 \cos^2\theta_3}{\left(Z_a + Z_P\right)^2 \left(Z_P + Z_t\right)^2 \left(Z_t \cos\theta_2 + Z_P \cos\theta_3\right)^2} \times \frac{\left(Z_a \cos\theta_2 - Z_P \cos\theta_1\right)^4}{\left(Z_a \cos\theta_2 + Z_P \cos\theta_1\right)^6} \times e^{-\left(\alpha_P \cdot d_o + 3\alpha_a + \alpha_P \cdot d\right)} \tag{3.12}$$

where, Z_a, Z_p, and Z_t are the acoustic impedances of air, PVC and transducer ceramic, respectively. The acoustic impedance is the product of sound velocity and density of the medium. α_p, and α_a are the attenuation coefficients of the PVC and the air, respectively. The longitudinal and transverse waves propagate in a solid with different velocities [9]. Speed of sound and attenuation coefficient of PVC are given in **Table. 3.3**.

Table 3.3: Speed of sound and attenuation coefficient of PVC

Medium	**Speed of sound (m/s) [10]**		**Attenuation coefficient (dB/mm) [11]**	
	Longitudinal wave	**Transverse wave**	**Longitudinal wave**	**Transverse wave**
PVC	2330	1070	0.2	0.12

The attenuation coefficient of the air is about 0.007 dB/mm [2] at around 400 kHz, and the influence of this value is negligibly small with the change of humidity. As shown in Fig. 3.15, the transverse wave traveling in the pipe material is not detected under 5 m/s airflow rate since the wave does not give pressure to the transducer. However, as the airflow increases θ_3 increases (see Fig. 3.13), a component of the transverse wave starts increasing, and the pressure to the transducer

appears. It is calculated that when about θ_3>9.7º, the receiver starts detecting the transverse wave of the PVC pipe.

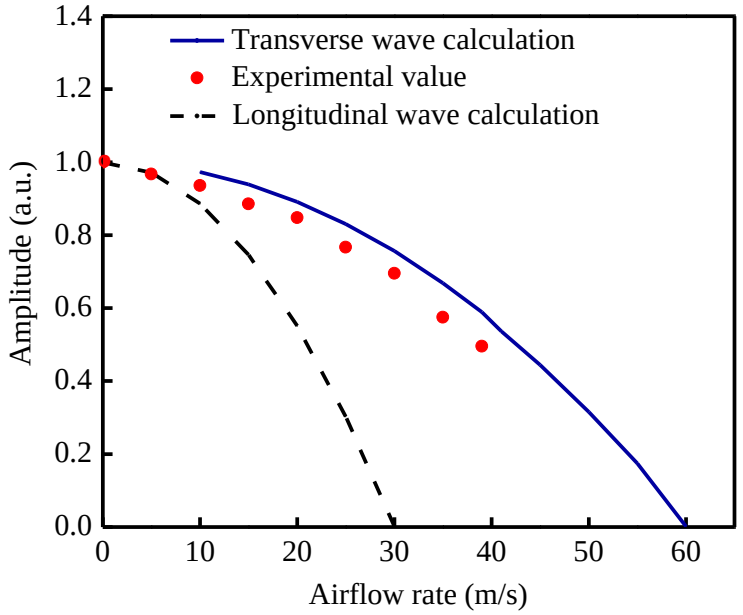

Fig. 3.15. Experimental and theoretical amplitude of the received ultrasonic signal versus airflow rate in the pipe [4], [8].

As it is known that when the longitudinal acoustic wave travels in the gas phase and propagates into the solid phase obliquely, it separates into both the longitudinal and transverse wave. According to this phenomenon, the limit of detecting ultrasound wave in the high-speed airflow was investigated. As the oblique angle increases the y-axis component (see Fig. 3.13) of sound amplitude in increases, therefore, the transverse wave in the PVC pipe can be detected. As shown in Fig. 3.15, at low airflow rate below 5 m/s the experimental data (red dotted line) match well with the calculated longitudinal wave curve (black dashed line). However, as the airflow rate increases the experimental data shift toward a calculated transverse wave curve (blue solid line). This deviation may occur due to the mixed observation of the longitudinal and transverse wave as the refracted angle θ_2 and θ_3 increase (see Fig. 3.13). As the airflow rate increases the angle of θ_1 increases due to the drift and thus θ_2 reaches the critical angle, therefore no more signal is detected at the receiver. For the experimental data, the intensity of the received signal is slightly smaller than that of the theoretical values of the transverse wave for the airflow of more than 10 m/s. This

deviation might be because of mixed propagation of the longitudinal and transverse wave in the PVC pipe and the ceramic of the receiver. The limits of measurement were calculated as 30 m/s and 60 m/s airflow for longitudinal and transverse wave, respectively as shown in Fig. 3.15.

3.4.8. REPLACEMENT OF AIR WITH H_2

We have conducted an experiment to replace the air with H_2 Gas. Figure 3.16(a) shows a schematic diagram of the experimental setup to measure the flowing H_2 gas concentration by using ultrasound from the exterior of the aluminum (Al) pipe. About 2000 mm long hollow square aluminum pipe having the width of 36 mm and a thickness of 4 mm was placed horizontally. Two piezo ceramic transmitting and receiving probes were mounted on the pipe surface diagonally on the opposite sides of the pipe as shown in Fig. 3.16(a). A sonic gel was placed between the transducers and the pipe. Figure 3.16(b) shows the front view of the pipe end. During the experiment, the frequency and the voltage were fixed at 400 kHz. Since the signal was circulating inside the SUS pipe, SAM was pasted on the surface of the SUS pipe to observe the airborne ultrasonic signal from the exterior of the pipe. Furthermore, air was replaced by H_2 using mass flow meter with a flow rate of 5 L/min for 10 minutes.

For a practical test, air was replaced by 100% H_2 gas in a SUS pipe, and the concentration of H_2 gas was measured by using ultrasound. Since the speed of sound in H_2 is faster than that in the air, the ultrasonic signal traveling time is shorter in H_2 than that in air after replacing to 100% H_2. From the measurement of Δt, H_2 gas concentration was calculated as 99.6% using eq. (2.5). It was estimated that with only 10-minutes gas flow replacement, H_2 concentration did not reach to 100%. A thermocouple was placed inside the pipe to measure the temperature. The change of temperature was compensated for the speed of sound using eq. (2.6), and the H_2 concentration was obtained accurately even if the temperature is varied by using eq. (2.9) [12]. The gas concentration is not influenced by the change of pressure, as the pressure does not affect the sound speed [7]. It was shown that the concentration of flowing gas is possible to measure from the exterior of the SUS pipe.

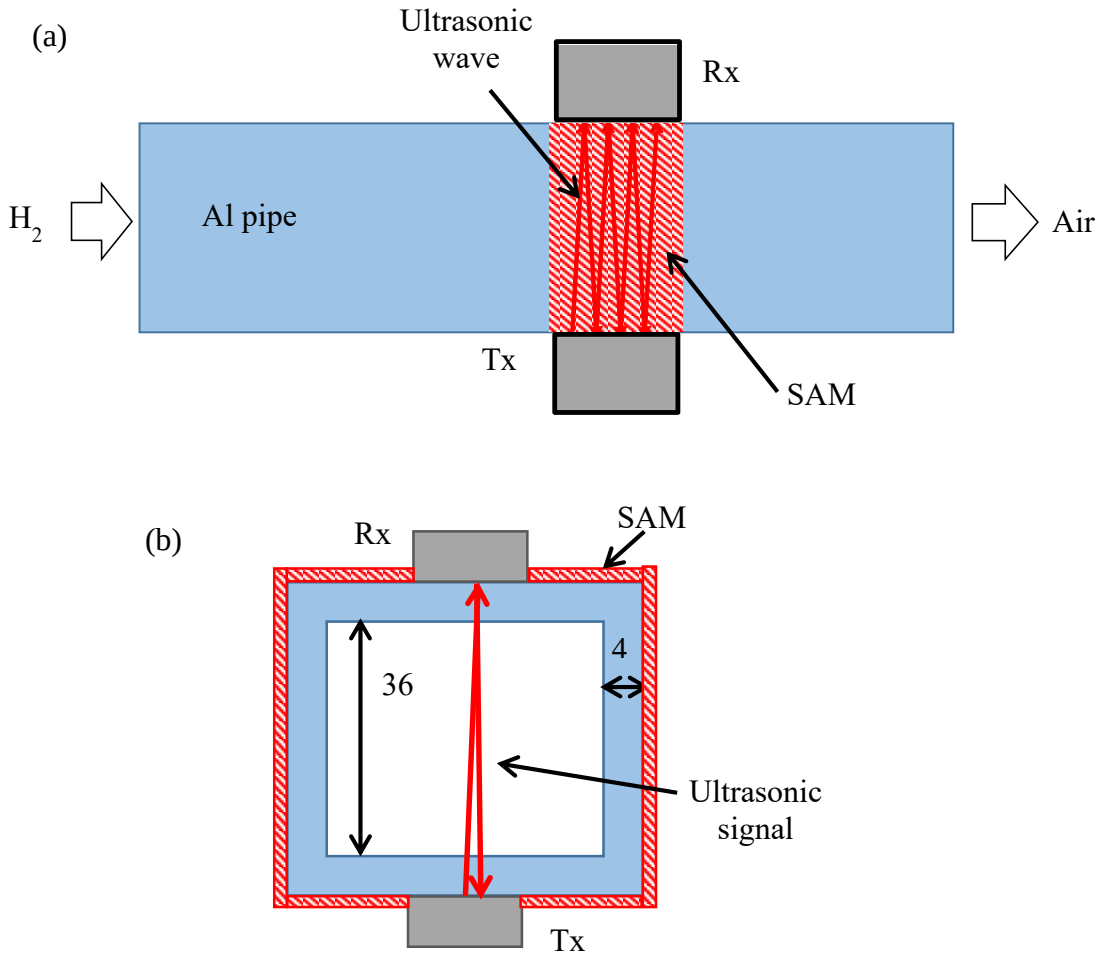

Fig. 3.16. A schematic diagram of the experimental setup to replace air with H_2. (a) Side view of the pipe where SAM is pasted on the surface of the Al pipe. Red arrows are ultrasonic signals. (b) Front view of the pipe end showing width and pipe thickness.

3.5. CONCLUSION

This Chapter shows that it was possible to measure the gas concentration instantly from the exterior of a pipe without making any hole. The speed measurement method by ultrasound was used to find the concentration of H_2 gas in a flowing air of up to 39 m/s. The concentration of H_2 gas can be measured accurately for different airflow speed. The maximum error in the hydrogen concentration at 39 m/s flow was about 0.32% due to turbulence of the airflow. The response time

of measuring the gas concentration was less than 0.1 s. The limit speeds for airflow were calculated as 30 m/s and 60 m/s for longitudinal and transverse wave, respectively.

APPENDIX

Derivation of (3.12):

As shown in Fig. 12 ultrasonic sound wave generated from the transmitter Tx with an intensity I_o goes through the PVC pipe and reaches the air medium inside of the pipe with lower intensity. I_o decreases due to the transmittance T_o at the transmitter/PVC interface [13].

$$I_1 = I_o T_o \tag{A.1}$$

$$T_o = \frac{4 Z_p Z_t}{\left(Z_p + Z_t \right)^2} \tag{A.2}$$

where, Z_p and Z_t are the acoustic impedances of PVC and transducer ceramic, respectively.

The decrease in intensity in the PVC follows Beer-Lambert law. I_2 can be expressed as [14]:

$$I_2 = I_1 e^{-\alpha_p \cdot d_o} \tag{A.3}$$

where, α_p is the attenuation coefficient of the PVC. d_o is the thickness of the PVC pipe.

The decrease in intensity at the PVC/air interface I_3 is:

$$I_3 = I_2 T_1 \tag{A.4}$$

where, the transmittance T_1 for normal incidence sound at PVC/air interface is

$$T_1 = \frac{4 Z_a Z_p}{\left(Z_a + Z_p \right)^2} \tag{A.5}$$

where, Z_a is the acoustic impedance of the air.

The I_3 decreases by the attenuation in the air and I_4 will be

$$I_4 = I_3 e^{-\alpha_a \cdot l} \tag{A.6}$$

where, l is the propagation length of the ultrasonic wave in airborne of the pipe.

The intensity of I_4 decreases by reflectance at PVC/air interface and I_5 will be

$$I_5 = I_4 R_1 \tag{A.7}$$

where, R_1 is the reflectance with an oblique incidence angle of sound at the PVC/air interface expressed as [2]

$$R_1 = \left(\frac{Z_a \cos\theta_2 - Z_p \cos\theta_1}{Z_a \cos\theta_2 + Z_p \cos\theta_1} \right)^2 \tag{A.8}$$

where, θ_1 is the angle between the axis along a pipe diameter and the ultrasound propagation direction flowing downstream. θ_2 is the refracted angle from air to PVC pipe.

The sound intensity is decreased by the attenuation of sound in the air and by the reflection at the PVC surface (R_1 and R_2) as well and shown as I_6, I_7, and I_8.

Intensity I_8 decreases by the transmittance at the air-PVC interface; therefore, I_9 becomes:

$$I_9 = I_8 T_2 \tag{A.9}$$

where, T_2 is the transmittance with an oblique incidence angle of sound at the air/PVC interface expressed as [2]

$$T_2 = \frac{4 Z_p Z_a \cos\theta_1 \cos\theta_2}{\left(Z_a \cos\theta_2 + Z_p \cos\theta_1 \right)^2} \tag{A.10}$$

Intensity I_9 decreases by the attenuation in the PVC; therefore, I_{10} becomes

$$I_{10} = I_9 e^{-\alpha_p \cdot d} \tag{A.11}$$

where, d is the propagation length inside the PVC pipe.

Intensity I_{10} decreases by the transmittance at the air-PVC interface; therefore, I_{11} becomes:

$$I_{11} = I_{10} T_3 \tag{A.12}$$

where, T_3 is the transmittance for oblique angle incidence of sound at the PVC/transducer interface expressed as

$$T_3 = \frac{4 Z_t Z_P \cos\theta_2 \cos\theta_3}{\left(Z_t \cos\theta_2 + Z_p \cos\theta_3 \right)^2} \tag{A.13}$$

where, θ_3 is the refracted angle from PVC to the transducer. $\vec{y}$ component of the received signal intensity I_{12} is expressed as

$$I_{12} = I_{11} \cos\theta_3 \tag{A.14}$$

Using (A.1) to (A.13) into (A.14), the intensity I_{12} becomes:

$$I_{12} = I_o \frac{256 \times Z_a^2 Z_t^2 Z_P^4 \cos\theta_1 \cos^2\theta_2 \cos^2\theta_3}{\left(Z_a + Z_P \right)^2 \left(Z_P + Z_t \right)^2 \left(Z_t \cos\theta_2 + Z_P \cos\theta_3 \right)^2} \times \frac{\left(Z_a \cos\theta_2 - Z_P \cos\theta_1 \right)^4}{\left(Z_a \cos\theta_2 + Z_P \cos\theta_1 \right)^6} \times e^{-\left(\alpha_P \cdot d_o + 3\alpha_a + \alpha_P \cdot d \right)} \tag{A.15}$$

REFERENCES

[1] J. Krautkrämer and H. Krautkrämer, “Ultrasonic testing of materials”, New York: Springer-Verlag, 1983.

[2] H. Kuttruff, “Ultrasonics: fundamentals and applications”, London: Elsevier, 1991.

[3] W. S. Janna, “Introduction to fluid mechanics”, 3rd ed. Bos-ton: PWS-Kent, 1993.

[4] M. Taskin and Y. Kato, “Instant gas concentration measurement using ultrasound from exterior of a pipe”, IEEE Sensors Journal, **vol. 19**, no.11, pp. 4017-4024, 2019. DOI: 10.1109/JSEN.2019.2897736.

[5] H. Fukuoka, J. Jung, M. Inoue, H. Fujita and Y. Kato, “Absolute concentration measurement for hydrogen”, Energy Procedia, **vol. 29**, pp. 283-290, 2012.

[6] M. Sonoyama, H. Fujita and Y. Kato, “Application of ultrasonic to a hydrogen sensor”, 2010 IEEE Sensors, No. 3, pp. 2141-2144, 2010.

[7] O. Cramer, “The variation of the specific heat ratio and the speed of sound in air with temperature pressure humidity and CO_2 concentration”, Journal of the Acoustical Society of America”, **vol. 93**, pp. 2510-2516, 1993.

[8] M. Taskin, T. Kido and Y. Kato, “Flowing H_2 gas concentration measurement using ultrasound from exterior of the pipe”, IEEE Xplore, 2018, in Proceeding of IEEE Sensors 2018, pp. 983-985, 2018. DOI: 10.1109/ICSENS.2018.8589539.

[9] S. Kočiš and Z. Figura, “Ultrasonic measurements and technologies”, London: Chapman & Hall, 1996.

[10] J. E. Mark, “Physical properties of polymers handbook”, New York: American Institute of Physics, 1996.

[11] B. B. Kolupaev, V. V. Klepko, E. V. Lebedev, V. V. Levchuk, Yu. R. Maksimtsev and B. S. Kolupaev, “The absorption of ultrasonic waves in modified polyvinyl chloride”, International Polymer Science and Technology, **vol. 42**, pp. 12-15, 2015.

[12] M. Taskin, T. Kido, M. Inoue and Y. Kato, “Methane detection in airflow using ultrasound from exterior of the ventilation pipe”, in Proceeding of International Symposium in Mine Ventilation (SIVM 2018), pp. 177-184, 2018.

[13] H. J. Pain, “The physics of vibrations and waves”, Chichester: John Wiley & Sons Ltd, 1985.

[14] D. H. Towne, “Wave phenomena”, New York: Dover, 1988.

CHAPTER 4

PROPAGATION OF ULTRASOUND THROUGH TWO-LAYER GAS FLOW

4.1. INTRODUCTION

This chapter mainly focuses on the ultrasonic signal propagation through air-H_2-air gas flow. Previous chapters showed the concentration of H_2 gas mixed in the flowing air could be measured from the exterior of the pipe [1]-[4]. In this chapter, the relation between gas concentration and the loss of received signal intensity due to signal propagation through two-layer of gas separated by two interfaces is studied. The severe intensity degradation of signal was observed while the signal was propagating through the air-H_2-air two-layer gas flowing system. Different concentrations of flowing H_2 gas were measured using ultrasound from the exterior of the pipe, and it was calculated that the intensity was decreased with increasing H_2 concentration. However, this experiment is not enough to explain the intensity degradation. To investigate the intensity degradation, Schlieren photography was taken to visualize the H_2 gas motion after the injection into the flowing air of 2 m/s. It was observed that high concentration H_2 gas was flowing in the middle of the airflow without quick diffusion into the air. A 2D air-H_2-air gas flow model was considered where 100% H_2 gas was flowing in the middle of the airflow, and the gas layers were separated by two fluctuated interfaces. According to the calculation using this model, only limited conditions of the signals can reach to the receiver due to the refraction at the fluctuating air-H_2-air gas interfaces while propagating. It was found that the receiver could hardly detect the transmitted signals. So far, the ultrasonic propagation in gas-liquid [5], liquid-liquid [6], and liquid-solid [7] two-phase flows have already been studied; however, the ultrasonic propagation in two gas-gas (air-H_2) layers has not yet been studied.

4.2. PRINCIPLE OF CLASSICAL ABSORPTION COEFFICIENT

The intensity loss of the signal may depends on the absorption and transmission of sound in gasses. Considering heat conductivity and viscosity, the absorption of sound in a gas can be calculated by Stokes-Kirchhoff's equation [8]. This absorption due to heat conductivity and viscosity is usually called the classical absorption.

Absorption coefficient due to viscosity can be calculated as in eq. (4.1) [9]:

$$\alpha_{vis} = \frac{8}{3}\frac{\pi^2 f^2 \eta}{Dv^3} \tag{4.1}$$

where, f is the frequency (Hz), D is the density of the gas (kg/m^3), v is the speed of sound (m/s), and η is the viscosity (kg/(m·s)).

The absorption coefficient associated with heat conduction can be calculated as in eq. (4.2) [9]:

$$\alpha_{hc} = \frac{2\pi^2 f^2}{Dv^3}\frac{k-1}{C_p}\chi \tag{4.2}$$

where, k is the specific heat ratio, C_p is the specific heat at constant pressure (J/(kg·K)), and χ is the coefficient of heat conductivity (W/(m·K)).

When the absorption is small, it is possible to assume that viscous and thermal conduction losses act independently in producing attenuation of sound. This means that the combined classical absorption coefficient is the sum of viscosity and heat conduction coefficient as given in eq. (4.3) [9]:

$$\alpha_{classical} = \frac{2\pi^2 f^2}{Dv^3}\left[\frac{4}{3}\eta + \frac{k-1}{C_p}\chi\right] \tag{4.3}$$

The amplitude is visually represented by the vertical distance between the maximum of the ultrasonic signal, and the equilibrium value. As shown in Fig. 4.1, the amplitudes of ultrasonic signals before and after H_2 mixture in the air were obtained manually by reading the highest amplitudes as A_o, and A, respectively. The intensity ratio was calculated by squaring the ratio of the amplitudes as expressed in eq. (4.4):

$$\text{Intensiy ratio} = \frac{I}{I_o} = \frac{A^2}{A_o^2} \tag{4.4}$$

where, I_o and I are the intensities of air and, H_2 mixed air, respectively.

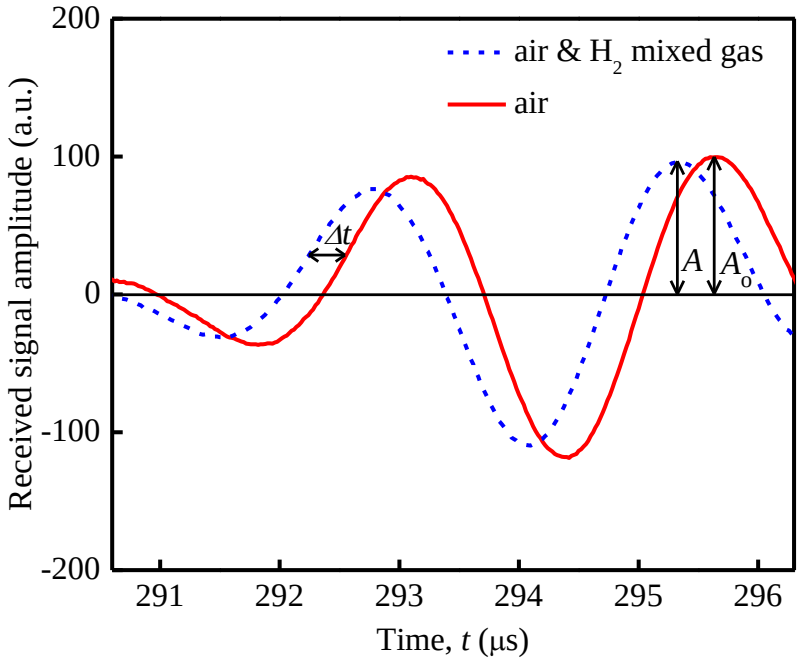

Fig. 4.1. The amplitude of received ultrasonic signal traveling in the air and the mixture of the air and H_2. The amplitudes of air and H_2 mixed air are expressed as A_o, and A, respectively. Δt is the sound traveling time difference between air and the mixture of air, and H_2 [10].

4.3. Experimental Setup

4.3.1. Absorption of Sound in H_2 Gas for Different Concentrations

An experiment was conducted to investigate the absorption of sound for different H_2 gas concentration. Figures 4.2(a), and 4.2(b) show the schematic diagram and the photograph of the experimental setup, respectively. As shown in Fig. 4.2, the ultrasonic transducers, and a commercial H_2 sensor (Cosmos-XP-3140-H_2) were placed into an acrylic pipe. The concentration of H_2 gas was changed from 0% to 100% with mass flow meter, and the amplitude of the received signal was recorded by an oscilloscope.

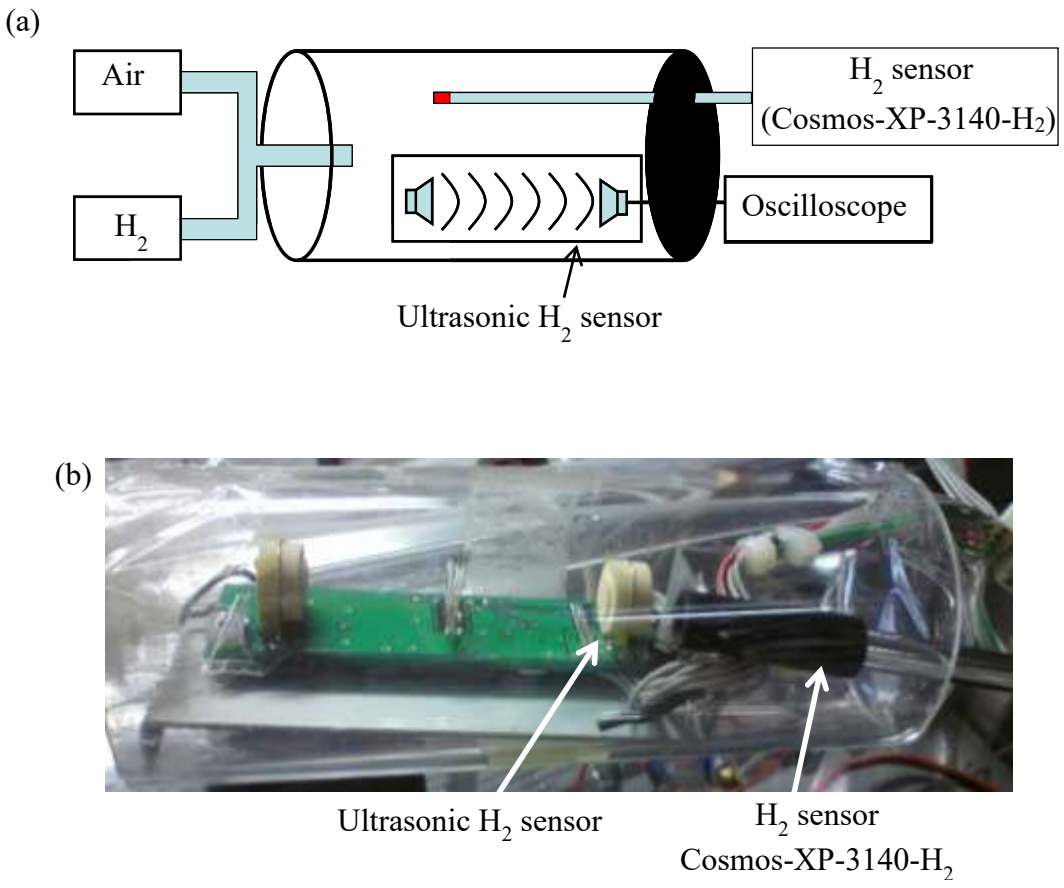

Fig. 4.2. Measurement of the amplitude of sound in H_2 mixed air at different concentrations. (a) Schematic diagram, (b) Photograph of the experimental setup.

4.3.2. MEASUREMENT OF GAS CONCENTRATION

This experimental setup is to measure the H_2 gas concentration by using ultrasound from the exterior of an acrylic pipe. In this experiment, an acrylic transparent square pipe having the length 1000 mm, width 100 mm, height 110 mm, and pipe thickness of 4 mm was placed horizontally. Figure 4.3 shows the schematic diagram of the experimental apparatus for measuring H_2 concentration. The ultrasonic signal can pass through the acrylic pipe so that the gas concentration in the pipe can be measured from the exterior of the pipe. By using a blower, airflow speed was set at 2 m/s, which was measured at the exit of the pipe. About 30 ml of H_2 gas was injected manually by a glass syringe, within about 0.1 s into the airflow through a 1/4 in. diam., and 50 mm length pipe, which exit, was placed at the center of the acrylic pipe diameter as shown in Fig. 4.3. Two piezo ceramic transmitting and receiving probes having the surface area of 20 mm x 15 mm

were mounted diagonally on the surface of the pipe as shown in Fig. 4.3. Transducers were mounted at various distances at L_o = 20, 110, and 190 mm, from the H_2 gas injection hole. A sonic gel was used between transducers and the pipe. The divergence angle, β of the transducer was roughly calculated and confirmed by the experiment as about 3º [2]. Since β is small enough and the distance between the transmitter and the receiver is short as 100 mm, the ultrasonic sound wave was considered as a ray. A JPR-10CN pulsar receiver manufactured by Japan Probe Co. LTD was used as an ultrasonic generator. During the experiment, the frequency and the voltage were fixed at 400 kHz and 60 V, respectively. The sampling time was as short as 0.08 s. The width of one pulse was 2 μs. The temperature, humidity, and air pressure were about 295 K, 55% and 1 atm., respectively during the experiment.

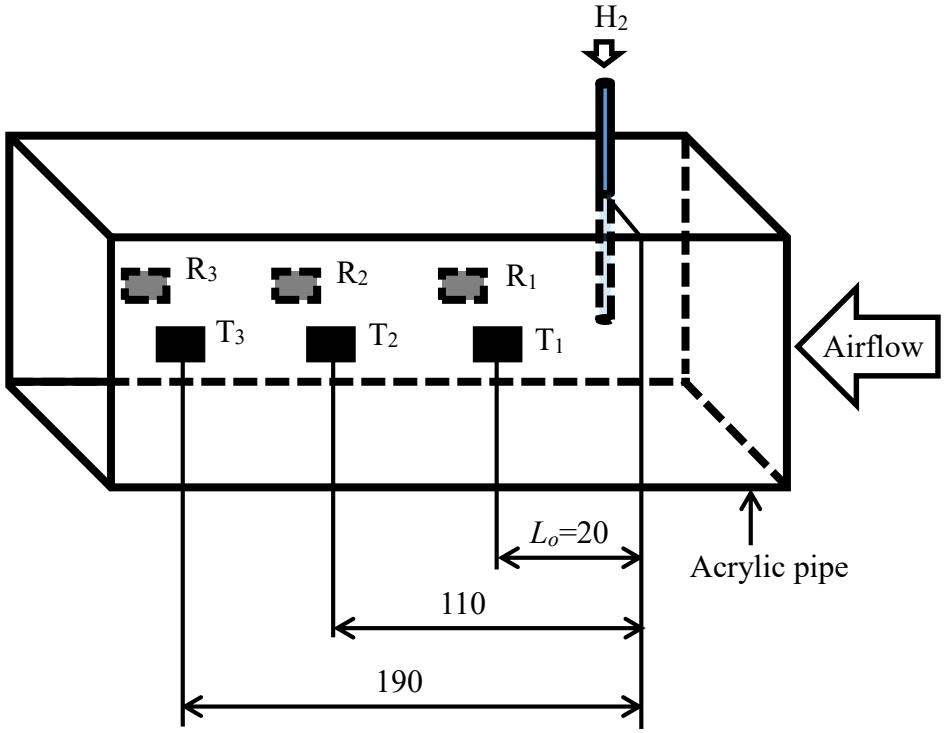

Fig. 4.3. Schematic diagram of the experimental setup and the distance from the H_2 injection hole to the transducers are L_o=20, 110, and 190 mm [10].

4.3.3. SCHLIEREN PHOTOGRAPHY

The experimental setup of Schlieren photography to visualize the mixing phenomena when H_2 is injected into the flowing air in the acrylic pipe is shown in Fig. 4.4. Two large Schlieren parabolic mirrors having 200 mm in diameter, with a focal length of 2035 mm were mounted on adjustable heavy base stands. The acrylic pipe was horizontally paced between the mirrors as shown in Fig. 4.4. A diameter of 1 mm pinhole was placed beside the parabolic mirror 2. A white LED light was used behind the pinhole as a light source. In this experiment, a camera, shutter speeds up to 1/2000 s was used which was placed behind a 1 mm slit. H_2 gas was injected into 2 m/s speed of airflow and H_2 was visualized by using Schlieren photography for various distances from the gas injection hole that is L_o = 0-70 mm, 70-140 mm, and 140-210 mm, respectively.

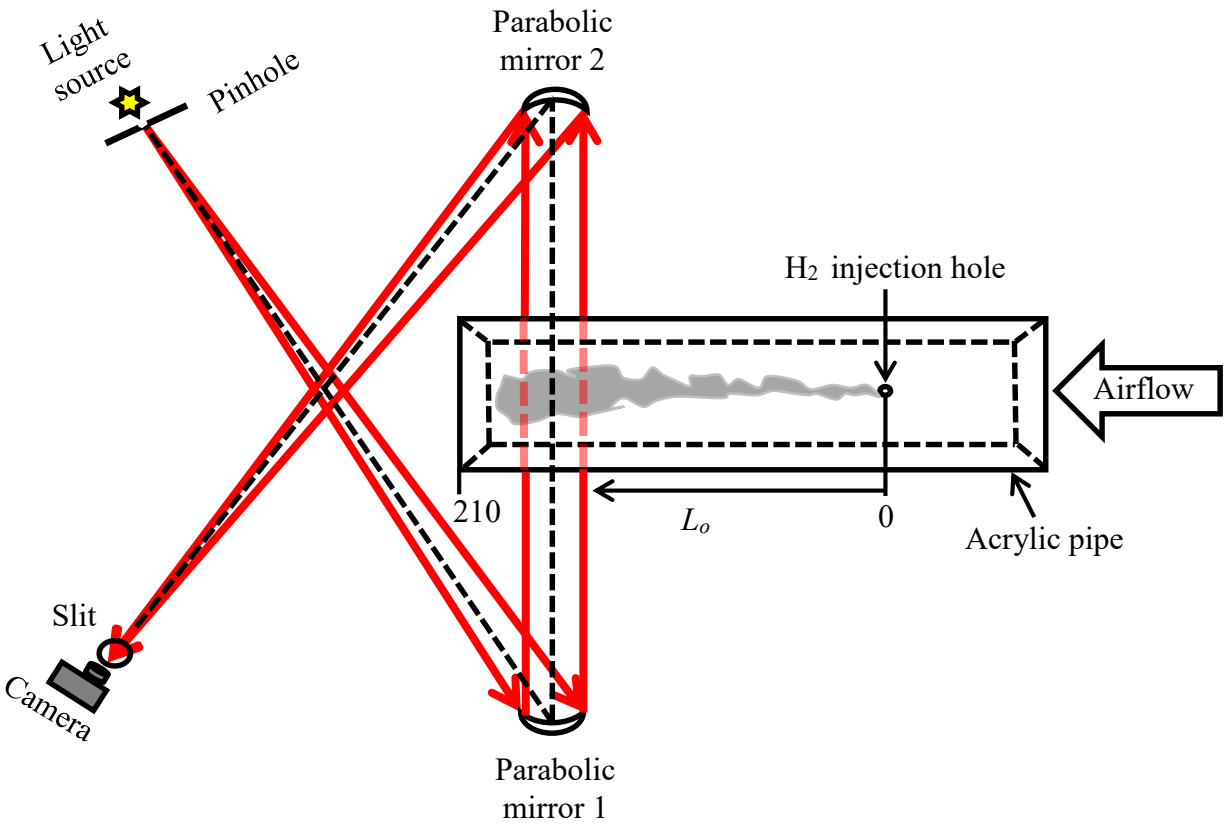

Fig. 4.4. Schematic diagram of taking Schlieren photography to visualize H_2 mixed in the air [10].

4.4. Results and Discussion

4.4.1. Absorption of Sound for Different H_2 Concentrations

For the practical measurement, H_2 gas was mixed in the air in different concentrations uniformly, and the intensities of the signals were measured. Figures 4.5 show the amplitude of received signal for different H_2 concentrations. The concentration of H_2 was changed for each 10% from 0% to 100% and the amplitude of received signal was recorded for each 10% of H_2. Figures 4.5(a) - 4.5(k) show the received signal amplitudes of 0% - 100% H_2 concentration. The amplitude of received signal is decreasing with increasing H_2 concentration as shown in Fig. 4.5.

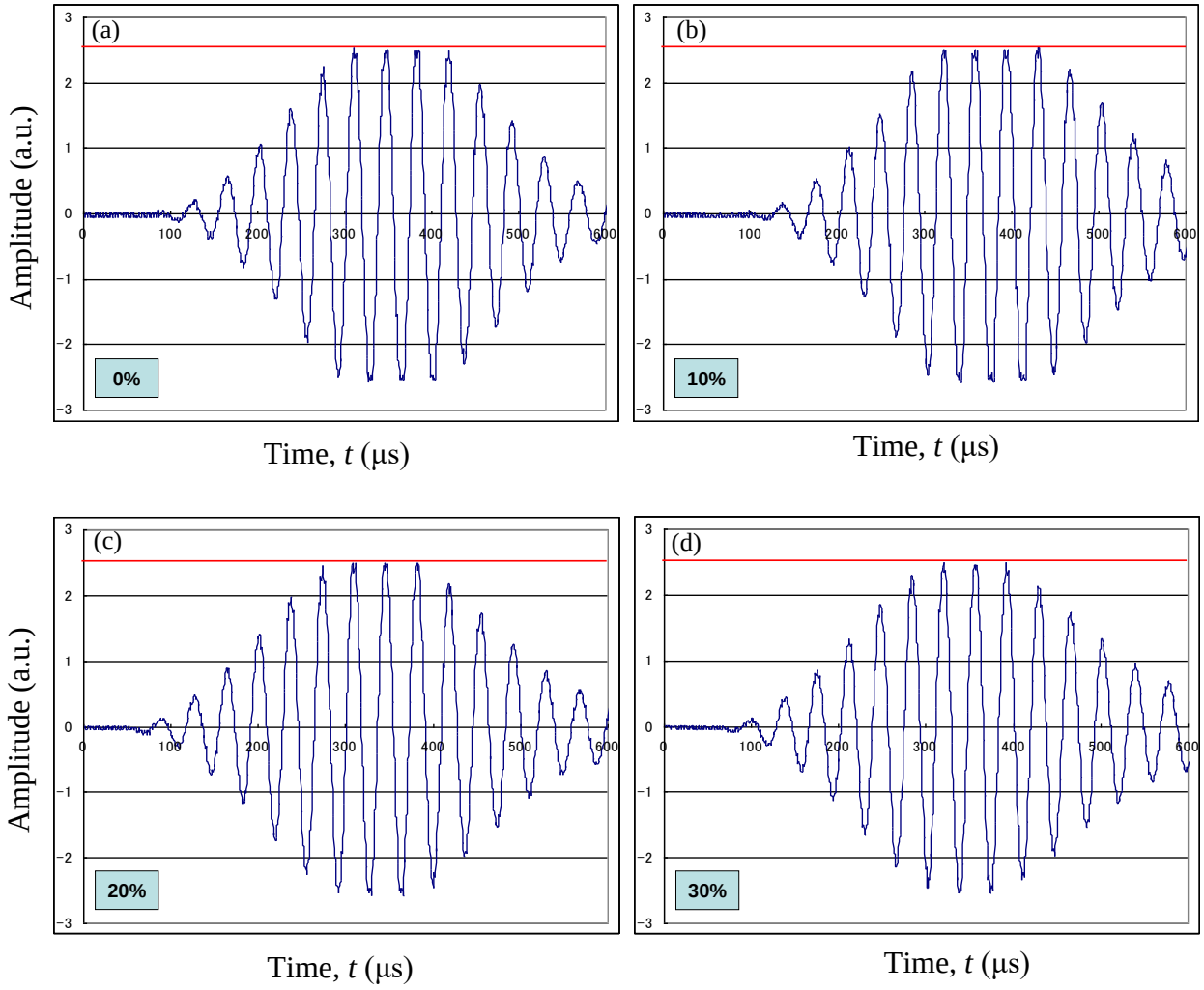

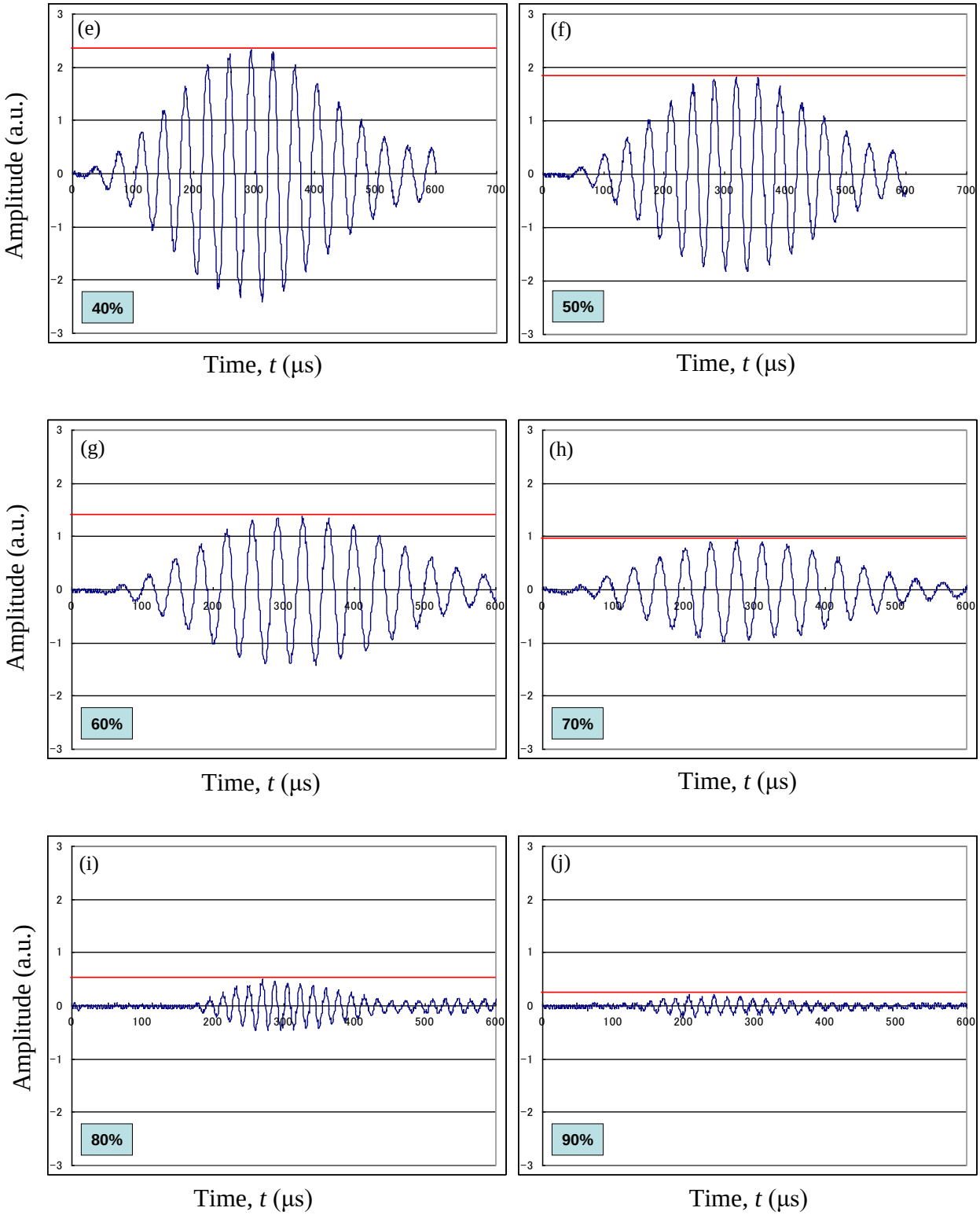
(e)
40%
(f)
50%
(g)
60%
(h)
70%
(i)
80%
(j)
90%
Amplitude (a.u.)
Time, t (μs)

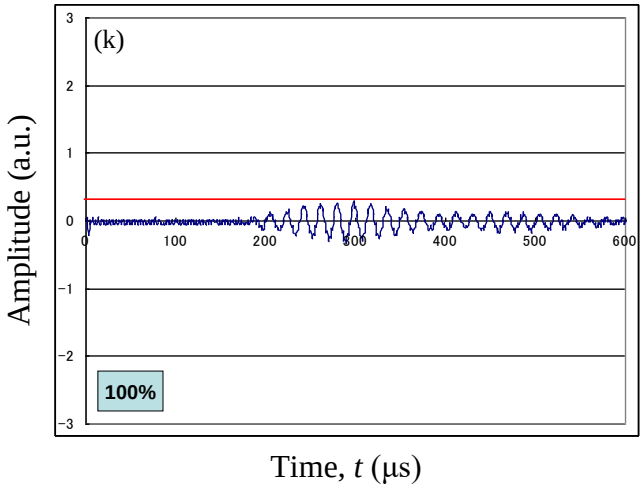

Fig. 4.5 Received signal amplitude for different concentrations of H_2 gas. (a) - (k) show the received signal amplitudes of 0% - 100% H_2 concentration for each 10% change of H_2.

Figure 4.6 shows the intensity ratio of the received signals for different concentrations of H_2 gas mixed in the air. As shown in Fig. 4.6, only 7% of the signal is transmitted to the receiver in case of 100% H_2. When the H_2 concentrations are about 2 or 3%, there should be almost no attenuation. This result conflict with that in Figs. 4.5(a´), 4.5(b´), and 4.5(c´). According to these results, it appears that this intensity ratio decreasing does not only depend on the H_2 concentration.

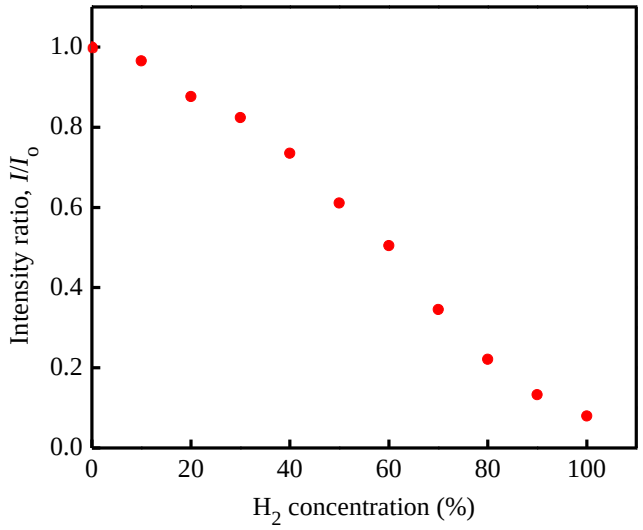

Fig 4.6. Ultrasound receiver intensity ratio with respect to the various H_2 concentration where H_2 is mixed with the air uniformly. Intensity of ultrasonic signal decreases with increasing the concentration of H_2 gas in uniform H_2 gas mixture [10].

4.4.2. INTENSITY LOSS OF RECEIVED SIGNAL DUE TO AIR AND H_2 TWO-LAYER GAS FLOW

H_2 gas was injected into an air flowing pipe, and the concentrations were measured using ultrasound in various distances from the H_2 injection hole. After instant injection of H_2, a rapid increase in Δt was observed due to the sudden change in the speed of sound as shown in Figs. 4.7(a), 4.7(b), and 4.7(c). Figures 4.7(a), 4.7(b), and 4.7(c) show the measured Δt and the calculated H_2 concentration for L_o = 20, 110, and 190 mm, respectively. H_2 gas concentration was calculated from eq. (2.5) using the Δt. As shown in the horizontal axis of Figs. 4.7(a), 4.7(b), and 4.7(c), the ultrasonic signal was recorded for about 3 s after the H_2 injection. As shown in Figs. 4.7(a), 4.7(b), and 4.7(c), the peak height is getting smaller as the value L_o increases. The highest value of Δt = 6.0 μs, which corresponds to about 4.8% of H_2 concentration was measured for L_o = 20 mm as shown in Fig. 4.7(a). As shown in Fig. 4.7(b), and Fig. 4.7(c), with the increasing value of L_o = 110 mm, and 190 mm, the highest value of Δt are decreased to 4.7 μs, and 3.7 μs, respectively which corresponds to about 3.7%, and 3.1% of H_2 concentration, respectively. These results show that H_2 is diluted as the value of L_o increases.

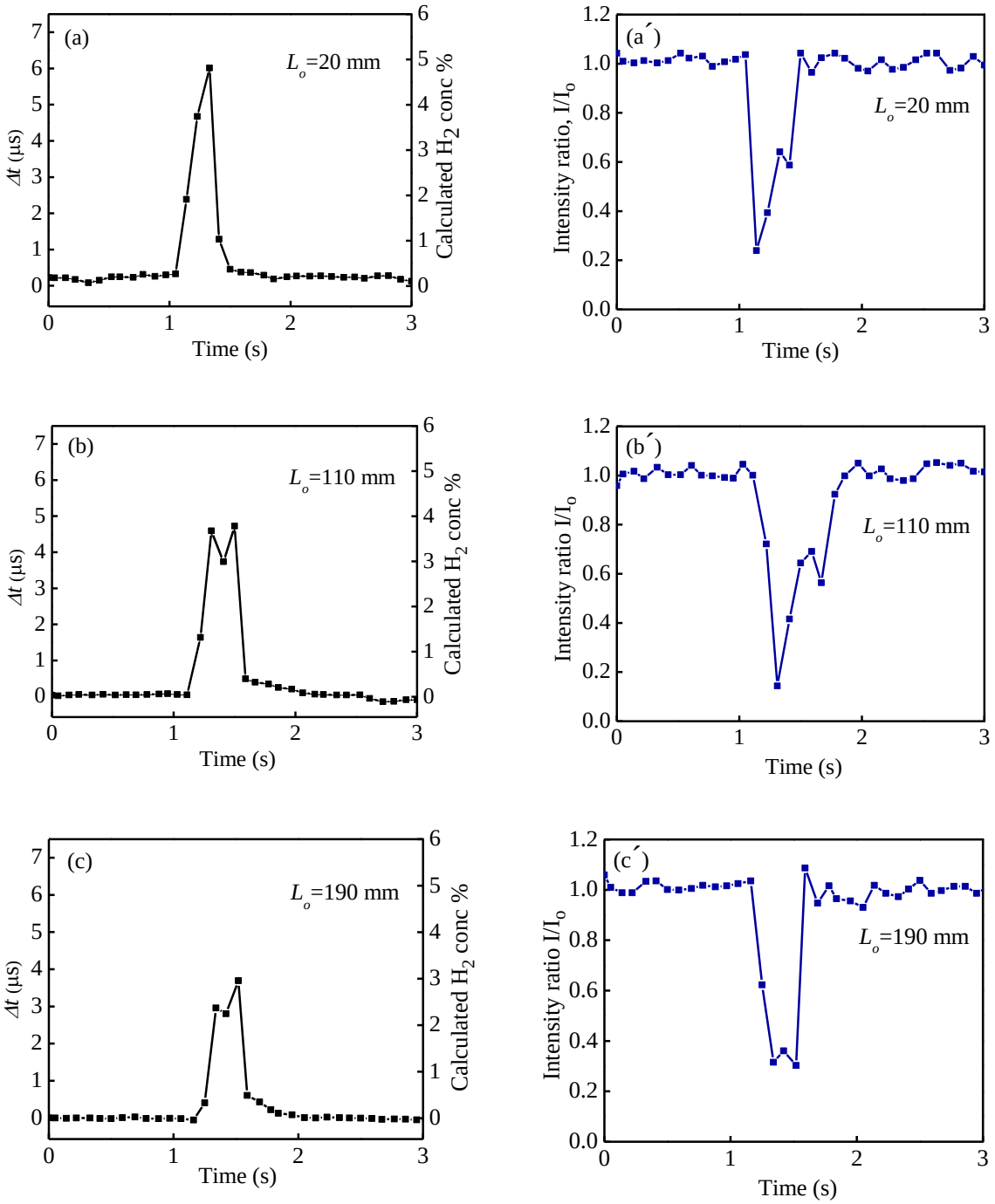

Fig. 4.7. Measured Δt and calculated H_2 concentration from Δt which are measured at (a) L_o=20 mm, (b) L_o=110 mm, and (c) L_o=190 mm from the H_2 gas injection hole. The horizontal axis shows the ultrasonic signal recording time during the H_2 injection. Ultrasound receiver intensity ratio measured at (a´) L_o=2 mm, (b´) L_o=110 mm, and (c´) L_o=190 [10] mm.

A loss of receiving signal intensity was observed when the H_2 gas was injected into the airflow. The intensity ratios of received ultrasonic signals while injecting H_2 in the airflow are shown in Figs. 4.7(a´), 4.7(b´), and 4.7(c´). The amplitudes of ultrasonic signals before and after H_2 mixed in the air were obtained manually by reading the highest amplitudes as A_o and A, respectively (see Fig. 4.1 for example). As shown in Figs. 4.7(a´), 4.7(b´), and 4.7(c´), the intensity ratio I/I_o, which was calculated by squaring the ratio of amplitudes decreases rapidly after injecting H_2. For example, as shown in Fig. 4.7(a´), considering the lowest intensity ratio point (time $\approx$ 1.1s, corresponding H_2 concentration is about 4.8%), only 25% signal can be transmitted to the receiver compared with the pure air case. For L_o = 110 mm, and 190 mm, according to Figs. 4.7(b´) and 4.7(c´), only 14% and 30% of the signal can be transmitted, respectively. These values correspond to H_2 concentrations of only 3.6% and 3.1% as showed in Figs. 4.7(b) and 4.7(c), respectively. To investigate the reason of intensity ratio becoming quite low even with a small amount of H_2 concentration, the transmittance of signal from air to H_2 was calculated theoretically and measured experimentally. By using eq. (2.10) (see Table 2.1), the acoustic impedances of air and H_2 are calculated as 416 kg/m^2/s, and 116 kg/m^2/s, respectively.

4.4.3. VISUALIZATION OF H_2 GAS USING SCHLIEREN PHOTOGRAPHY

It is assumed that the injection of H_2 gas in airflow does not make a uniform mixture. The signal intensity may lose due to the non-uniform mixture of H_2 with air. To confirm this assumption, Schlieren photography was used to visualize the gas mixing phenomena. Three different positions from the gas injection hole were chosen to visualize H_2 gas. Schlieren photographs were taken at L_o = 0-70 mm, 70-140 mm, and 140-210 mm. H_2 gas was injected into the airflow at the center of the pipe diameter, and the interfaces between air and H_2 were observed. As shown in Fig. 4.8(a), the interfaces between air and H_2 are observed clearly for L_o = 0-70 mm. However, as L_o increases, the interfaces are observed rather blurry as shown in Figs. 4.8(b), and 4.8(c). These results confirm that H_2 is diluted in the air with the increasing value of L_o. It is also confirmed that H_2 gas was not mixed uniformly in air, and the intensity of the ultrasonic signal may lose while passing through the interfaces of H_2 and air.

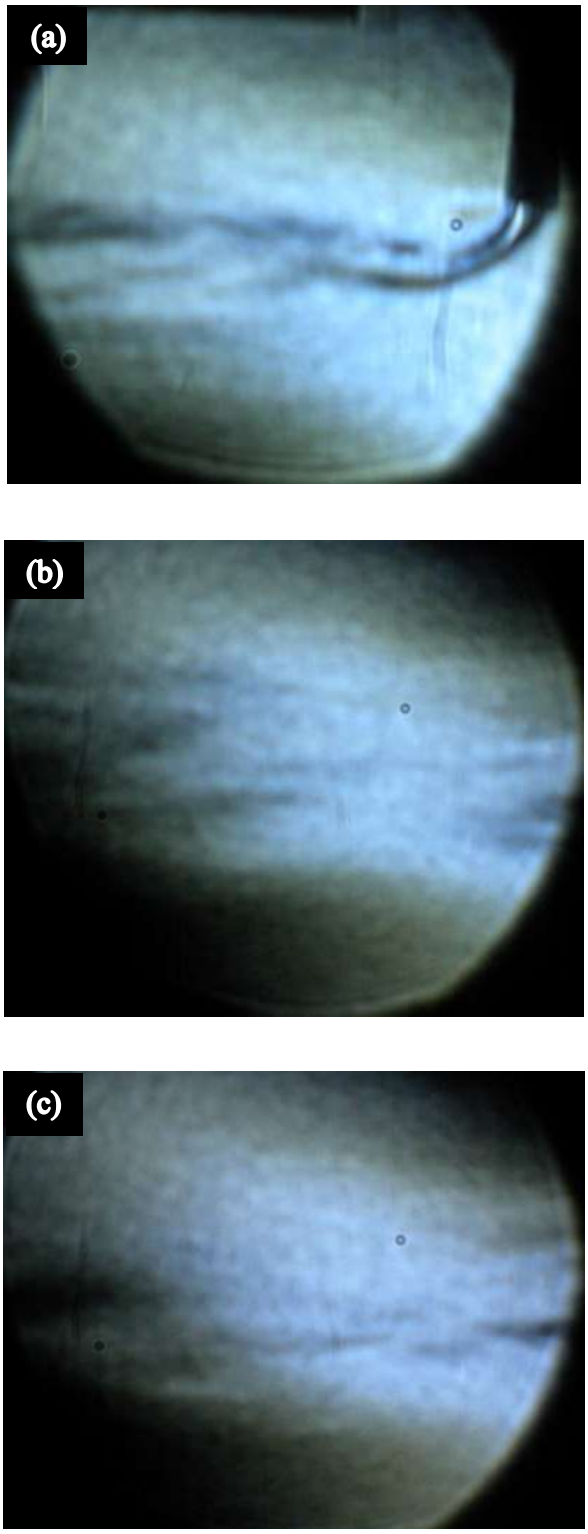

Fig. 4.8. Visualization of H_2 gas by using Schlieren photography (a) L_o=0-70 mm, (b) L_o=70 140 mm, and L_o=140-210 mm distance from the H_2 injection hole. H_2-air fluctuated interfaces are observed [10].

4.4.4. ULTRASOUND PROPAGATION THROUGH AIR-H_2-AIR TWO-LAYER MODEL

We have considered a 2D model having air-H_2-air two layer interfaces in order to calculate the ultrasound propagation. At 1 atm. pressure and 20ºC temperature, the speed of sound in air and H_2 are 343 m/s and 1304 m/s, respectively. The refraction of sound at interfaces is calculated using Snell's law. The geometric configuration for the signal propagation and interfaces is provided in Fig. 4.9. Figure 4.9 is a model of two gas layers having two fluctuated interfaces.

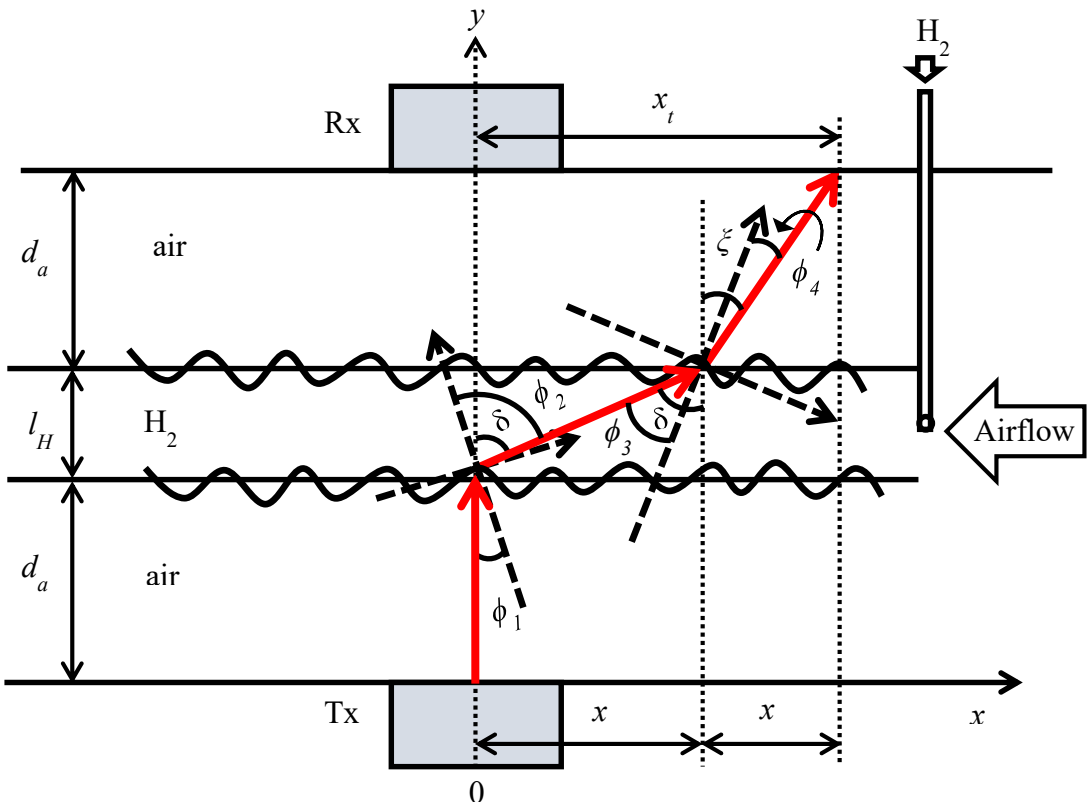

Fig. 4.9. The proposed 2D model having fluctuated interfaces of air-H_2-air two-layer gas flow system. Red lines show the sound propagation direction. ϕ_1 and ϕ_3 are the incident angles towards the fluctuated interfaces from air and H_2 side, respectively. ϕ_2 and ϕ_4 are the refracted signal angles at the H_2 and air interfaces [10].

The model is considered that air-H_2-air two-layer gas is flowing inside a pipe. Transmitter Tx and receiver Rx are placed at the position $x = 0$ and orthogonal to the pipe surface as shown in Fig 4.9. In this model, it is assumed that 100% of H_2 gas is flowing in the middle of airflow. Since the air-H_2-air interfaces are fluctuated, the average thicknesses of the air and H_2 gas layers are assumed

as d_a, and l_H, respectively. The thickness ratio of each gas layers in the air-H_2-air system is considered as 2:1:2. Red arrows indicate the propagation of the sound wave. First and second refractions are occurred at air-H_2 and H_2-air interfaces, respectively. At first, the ultrasonic signal incidents on the air-H_2 curved interface with an angle of ϕ_1, and then refracted into the H_2 medium with a refraction angle of ϕ_2. Not all the signals passing through air layer can reach to the H_2 layer, since the speed of sound in air is lower than that of the H_2, total reflection will occur for some signals. As ϕ_1 increases and reaches the critical angle; therefore, the values of $-15.2^o < \phi_1 < +15.2^o$ were used for the calculation. The incident angle ϕ_1 is considered for both positive and negative values in the calculation. Then the refracted signal incidents on the H_2-air interface with the incident angle of ϕ_3. Then the signal is refracted with an angle of ϕ_4 at the H_2-air interface. All the signals passing through H_2 gas layer can reach to the air layer since the speed of sound in H_2 is larger than that of the air, and total reflection does not occur. The positive and negative values of ϕ_3 are also considered. x_t that is the distance between the center of Rx and the signal arrival position is determined by using eq. (4.5) and (4.6):

$$x_t = x_1 \pm x_2 \tag{4.5}$$

$$x_1 = l_H \cdot \tan\delta, \quad \text{and} \quad x_2 = d_a \cdot \tan\xi \tag{4.6}$$

where, x_1 is the distance between first and second refraction points, and x_2 is the distance between the second and third refraction points. δ is the angle between the first refracted wave and y-axis. ξ is the angle between the second refracted wave and y-axis at second refraction point.

4.4.5. LIMIT ANGLES OF TRANSMITTED SIGNAL

Using Snell's law, it was found that ϕ_1 is limited to $-15.2^o \leq \phi_1 \leq 15.2^o$, due to the total reflection. Figure 4.10(a) shows the calculated values of x_t vs. ϕ_3 with different values of ϕ_1. Figure 4.10(b) is the enlarged view of Fig. 4.10(a). Since the width of the receiver is 20 mm, signals can be only received for the values at $-10 \text{ mm} \leq x_t \leq 10 \text{ mm}$ as shown between red lines in Fig. 4.10(b). For example, according to Fig. 4.10(b), ϕ_1 is limited to only about $-12^o \leq \phi_1 \leq 12^o$, and when $\phi_1 = 0^o$, the signal can be detected only for the case when about $-20^o \leq \phi_3 \leq 20^o$. In practice, the gas layers are not limited to two-layer as shown in Figure 4.9. The signal might not be observed due to having many interfaces in the gas mixture.

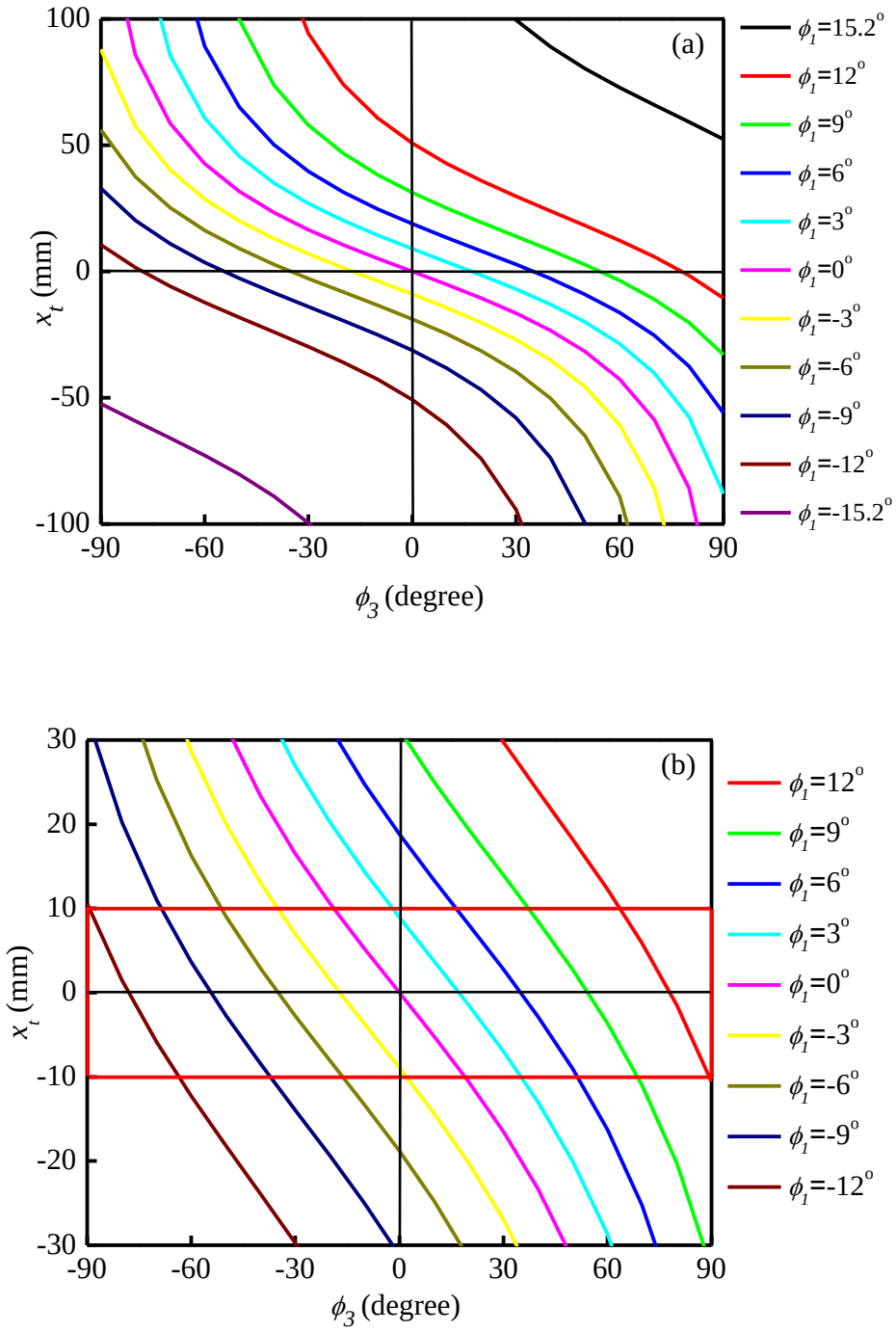

Fig. 4.10. (a) ϕ_3 dependence to the theoretical value of x_t. ϕ_1 was calculated and found that for the value of -15.2°≤ϕ_1 ≤ 15.2°, the signals could be reaches to the receiver side. (b) Enlarge view of Fig. 4.10(a) where the red box shows that the signal can be received at-10 mm $\leq x_t \leq 10$ mm [10].

For the fluctuated interface condition, it is unlikely that the transmitted signal can reach to the receiver. These phenomena can occur only when the sound signal is propagating without spreading. Since the divergence angle of the transmitter signal is as sharp as 3º, loss of signal was observed. The loss of received signal intensity could be solved by using a transmitter having a larger angle of divergence.

4.5. CONCLUSION

The ultrasonic signal propagation through the 'air-H_2-air' two-layer gas flowing system was studied. The degradation of intensity was observed while sound propagation through air-H_2-air two-layer gas flowing system. Different concentrations of flowing H_2 gas were measured using ultrasound from the exterior of the pipe, and it was calculated that the intensity degradation of signal did not simply depend on the H_2 concentration.

To investigate the intensity degradation, 100% H_2 gas was injected into the airflow pipe and two fluctuated interfaces (air-H_2 and H_2-air) were observed using Schlieren photography. By using ultrasound measurement, H_2 concentration was calculated for about only 3-5%, thus the ultrasound intensity should not degrade. However, the experimental results showed the received intensity degraded to about 10-20%.

The intensity loss of the ultrasonic signal was calculated by calculating the refraction of sound in two fluctuating interfaces. According to the refracted angle calculation, only the signals having the incidence angle towards the first fluctuating interface (air -> H_2) of about $-12^o \leq \phi_1 \leq 12^o$ and with the incidence angle towards the second fluctuating interface (H_2 -> air) of about $-20^o \leq \phi_3 \leq 20^o$ can transmit to the receiver. Therefore, only a part of the signals with specific incident angles was received. It can be concluded that the intensity loss of ultrasonic signal propagation through two fluctuated interfaces of air-H_2 two-layer gas flow was due to the refraction at the interfaces.

REFERENCES

[1] M. Taskin, T. Kido and Y. Kato, "Flowing H_2 gas concentration measurement using ultrasound from exterior of the pipe", IEEE Xplore, 2018, in Proceeding of IEEE Sensors 2018, pp. 983-985, 2018. DOI: 10.1109/ICSENS.2018.8589539.

[2] M. Taskin and Y. Kato, "Instant gas concentration measurement using ultrasound from exterior of a pipe", IEEE Sensors Journal, **vol. 19**, no.11, pp. 4017-4024, 2019.

[3] M. Taskin, G. Utsumi and Y. Kato, "Observation of ultrasound wave from exterior of a metal pipe for flowing gas measurement", in Proceeding of International Workshop on Piezoelectric Materials and Applications in Actuators (IWPMA 2018), pp. 85, 2018.

[4] M. Taskin, G. Utsumi and Y. Kato, "Observation of ultrasonic signal and measurement of H_2 concentration from the exterior of a metal pipe", International Journal of Hydrogen Energy, 2019. (Accepted).

[5] B. M. Abbagoni and H. Yeung, "Non-invasive classification of gas–liquid two-phase horizontal flow regimes using an ultrasonic Doppler sensor and a neural network", Measurement Science and Technology, **vol. 27**, pp. 084002, 2016.

[6] X. Dong, C. Tan, Y. Yuan and F. Dong, "Oil–water two-phase flow velocity measurement with continuous wave ultrasound Doppler", Chemical Engineering Science, **vol. 135**, pp. 165 2015.

[7] E. I. Tanahashi, T. A. Paiva, R. D. M. Carvalho, O. J. Venturini, F. A. Grangeiro, A. C. Bannart and V. C. Bizotto, "Application of the ultrasonic technique for monitoring intermittent liquid-gas and liquid-solid flows", in Proceeding of 7th North American Conference on Multiphase Technology, pp. 125-139, 2010.

[8] E. S. Stewart, "Dispersion of the velocity and anomalous absorption of sound in hydrogen", Physical Review Journals, **vol. 69**, pp. 632-640, 1946.

[9] L. E. Kinsler, A. R. Frey, A. B. Coppens and J. V. Sanders, "Fundamentals of acoustics", New York: John Wiley & Sons, 1982.

[10] M. Taskin, T. Kido, M. Inoue and Y. Kato, “Ultrasound propagation in two-layer gas flow”, International Journal of Hydrogen Energy, 2019. (Accepted).

CHAPTER 5

CONCLUSIONS AND FUTURE WORK

5.1. CONCLUSIONS

The purpose of this dissertation is to measure of H_2 gas concentration in a pipe using ultrasound. The gas concentration was measured from the exterior of the pipe without making a hole in the pipe. Since gas is not extracted for the measurement, there is no risk of explosion, which is a unique and attractive advantage of this ultrasonic gas sensor. This research focuses measuring both the non-flowing and flowing gas. Different kinds of pipe material were used to observe the airborne signal from the exterior of the pipe. The concentration of gas is measured based on the speed of sound variation in various gasses, this method is simple comparing with other sensors. I have summarized the experimental results obtained during my PhD tenure as below:

At first, non-flowing H_2 gas concentration was measured from the exterior of the SUS pipe. Since the noise signal was circling inside the SUS pipe surface itself, the airborne signal was difficult to observe from the exterior of the pipe. Two experiments were conducted to reduce the noise signal. One of them was pasting SAM on the SUS pipe surface and the airborne signal was observed. As a result, the concentration of H_2 gas was successfully measured. Two transmitters condition was applied to cancel the noise signal. FDTD simulation method revealed that it is possible to cancel the noise signal circulating in the pipe by using two transmitters having exactly the same frequencies and amplitudes, however it was difficult in practical test.

Next, the flowing H_2 gas concentration was measured instantly from the exterior of the pipe, which was more challenging than measuring non-flowing gas concentration. The concentration of H_2 gas was measured based on speed variation of the ultrasound traveling inside the pipe. H_2 gas was flowing inside a PVC pipe and the concentration of H_2 gas was measured accurately up to 39 m/s. Since the PVC pipe was used for this experiment, the airborne signal was clearly observed. The response time of measuring the gas concentration was fast as less than 0.1 s. Due to the fluctuation of waveform, the maximum error in the H_2 gas concentration at 39 m/s flow was

calculated about 0.32%. Since longitudinal and transverse waves can propagate through the solid, the limit speeds of flow were calculated as 30 m/s and 60 m/s for longitudinal and transverse wave, respectively.

In the above experiment, the large ultrasonic signal intensity degradation was observed while H_2 gas was mixed into the airflow. Hence, the ultrasonic signal propagation passing through the 'air-H_2-air' two-layer gas flowing model system was studied. It was proved that the intensity loss did not depend on the average concentration of H_2 gas. A Schlieren photography experiment was conducted to study the relation between intensity loss and the H_2 gas concentration. 100% H_2 gas was injected into the middle of the air flowing pipe; therefore, two fluctuated interfaces (air-H_2 and H_2-air) were observed using Schlieren photography. Comparing with the photograph, a 2D 'air-H_2-air' model was considered having two fluctuated interfaces. According to the refracted angle calculation, only the signals having the incidence angle towards the first fluctuating interface (air -> H_2) of about $-12^o \leq \phi_1 \leq 12^o$ and with the incidence angle towards the second fluctuating interface (H_2 -> air) of about $-20^o \leq \phi_3 \leq 20^o$ can transmit to the receiver. Therefore, only a part of the signals with specific incident angles was received. It can be concluded that the intensity loss of ultrasonic signal propagation through two fluctuated interfaces of air-H_2 two-layer gas flow was due to the refraction at the interfaces.

This research is related to the rapid growth of H_2 based society. For example, this ultrasonic sensor can be applied to the H_2 based Tokyo Olympic village. This sensor is also applied to the concentration measurement of other explosive gasses, such as measurement of methane (CH_4) gas concentration in the mine ventilation. Therefore, it can be concluded that this study is critically significant for introducing as accurate as well as instant measurement of gas concentration using ultrasound from the exterior of the pipe (different pipe materials) without making a hole.

5.2. FUTURE WORK

The research work described in this dissertation can be very interesting and challenging possible future research directions in ultrasonic gas sensor applications. In this dissertation, the concentration of non-flowing and flowing H_2 gas was measured and the propagation of ultrasonic signal through air-H_2-air was discussed. Based on this research work, some future works are suggested:

1) The principle of measuring H_2 gas concentration is highly accurate. Since this principle is applied to the gasses having the same heat capacity ratio, it is not applicable for the gasses having different heat capacity ratio. The principle of measuring gas concentration having different heat capacity ratio was derived roughly. Hence, the principle needs to improve to measure other gas concentrations. Further research is required to measure other gas concentrations.

2) This is the first time that noise signal was reduced by using SAM on the surface of a metal pipe. It is important to explore another way to cancel the noise signal to observe the airborne signal from the exterior of the pipe.

3) In this research, the concentration of H_2 gas was measured only when the pipe was placed horizontally. However, the pipe is bent and somewhere vertical in practice. Further research is required to investigate the dangerous places that are difficult to replace the gas and the efficiency of the replacement methods.

4) In this study, the propagation of ultrasound was studied only for the air-H_2 layer. Study of sound propagation through other gasses such as He will give the proper idea about the loss of sound intensity.

LIST OF PUBLICATIONS

❖ Journals/Transactions/Letters

1. **M. Taskin** and Y. Kato, "Instant gas concentration measurement using ultrasound from exterior of a pipe", IEEE Sensors Journal, **vol. 19**, no. 11, pp. 4017-4024, 2019.

2. **M. Taskin**, G. Utsumi and Y. Kato, "Observation of ultrasonic signal and measurement of H_2 concentration from the exterior of a metal pipe", International Journal of Hydrogen Energy, 2019. (Accepted).

3. **M. Taskin**, T. Kido, M. Inoue and Y. Kato, "Ultrasound propagation in two-layer gas flow", International Journal of Hydrogen Energy, 2019. (Under review).

❖ Conference/Proceedings

1. Y. Kato, H. Fukuoka, **M. Taskin** and Akitoshi Matsuda, "Oxygen concentration measurement in the air by using ultrasonic", The International Conference on Advanced Materials Science and Engineering (AMSE 2019), 22-25, March, Chengdu, China, 2019.

2. **M. Taskin**, T. Kido, M. Inoue and Y. Kato, "Methane detection in airflow using ultrasound from exterior of the ventilation pipe", in Proceeding of International Symposium in Mine Ventilation (SIVM 2018), 21-22 November, Santiago, Chile, pp. 177-184, 2018.

3. **M. Taskin**, T. Kido, M. Inoue and Y. Kato, "Ultrasonic Flow Meter for Mine Ventilation", in Proceeding of International Symposium in Mine Ventilation (SIVM 2018), 21-22, November, Santiago, Chile, pp. 291-296, 2018.

4. **M. Taskin**, T. Kido and Y. Kato, "Flowing H_2 gas concentration measurement using ultrasound from exterior of the pipe", IEEE Xplore, 2018, in Proceeding of IEEE Sensors 2018, pp. 983-985, 2018. DOI: 10.1109/ICSENS.2018.8589539.

5. **M. Taskin**, G. Utsumi Y. Kato, "Observation of ultrasound wave from exterior of a metal pipe for flowing gas measurement", in Proceeding of International Workshop on Piezoelectric Materials and Applications in Actuators (IWPMA 2018), 11-14, September, Kobe, Japan, pp. 85, 2018.

ACKNOWLEDGEMENT

Alhamdulillah……

All praise to the Almighty ALLAH (SWT), the Most Magnificent, that by His will, I am able to successfully complete my Ph.D. thesis as part of the requirements for Ph.D. study in the Graduate School of Integrated Frontier Sciences (IFS), Kyushu University.

I wish to express my deepest sense of gratitude and appreciation to my honorable supervisor, Professor Yoshimine KATO for his constructive guidance, logistic philosophy and encouragement throughout the whole investigation of my present work. I am very much pleased to be the research student of an excellent supervisor because his inspiration and dedication always gave me a lot of strength and motivation to continue the research even in some of the hardest days of my Ph.D. life.

Also, it is my great pleasure to show my great gratitude to Professor Shigeto OKADA and Professor Ken-ichi ABE, examiners of my dissertation. Thanks a lot for spending their precious time on the reading of my detestation and providing valuable suggestions to improve the quality of the thesis. I also like to give my thanks to Professor Masahiro INOUE for his cooperation during my experimental study and valuable suggestions.

Moreover, my thanks for the different staffs of the Kyushu University for their sincere help and cordial cooperation in this three years. I also wish to express my gratefulness to all lab mates due to their help and support that made my Japanese life became very convenient and comfortable.

To my family, I cannot say in words how lucky I am to constantly receive encouragement and prayers from you. The memory of my father Md. Solaiman, is always a great source of inspiration for me. My mother Anowara Begum, and two sisters, thank you very much for your continuous love and support. I am deeply grateful to my husband Kazi Sarwar Uddin for his patience, support, care, and stay together in Japan. Not to forget, my beloved children Muaz Sarwar and Zunairah Sarwar who fill this journey with joy and happiness.

Financial support was graciously provided throughout the study period in Kyushu University by the Japanese government with prestigious Monbukagakusho (MEXT) scholarship. Travel grant was gratefully provided by Marubun Foundation, Japan.

The Author
(Mahjabin Taskin)